POLITECNICO DI MILANO
School of Industrial and Information Engineering
Department of Aerospace Science and Technology

MODULAR DESIGN AND STRUCTURAL ANALYSIS OF A TROLLEY PART OF A MECHANICAL GROUND SUPPORT EQUIPMENT FOR SPACE APPLICATION

Master of Science in Space Engineering

Advisor: Prof. Riccardo Vescovini
Company tutor: Ing. Riccardo Corsini

Candidate:
Silvia Malagoli
Matr. 905208

Academic Year 2019-2020

Abstract

Trolleys represent the main structure of a mechanical ground support equipment, which has the purpose of integrating, testing and transporting satellites or parts of them. The function of trolleys is to allow the assembling of payloads and satellites, rotating them or keeping them in position.
In this thesis, the modular design of a mechanical trolley per space application is carried out. Trolleys of different dimensions are designed to allow the mounting of payloads of various sizes and masses. The preliminary design of main and rotating frames is conducted starting from a beam model of the structure. Flanges and screws sizing is based on verification criteria defined by NASA. A 3D model of different trolleys is built through the software for product 3D CAD design Catia V5.
After this initial design phase, the structure is verified through finite element analysis. This analysis is carried out through the use of the solver for Finite Element Analysis MSC Nastran. The pre and post-processing software Patran allows building the finite element model, setting up the analysis and displaying the results. The finite element model is presented and the mesh created is described. The checks, necessary to ensure consistent results, are exposed and verified. They are carried out at different times, both before and after the analysis, and on different parts, like finite elements and output files. The analysis of the stresses on each element of the structure allows detecting critical issues to modify the components and improve the initial design.

Sommario

I telai rappresentano la struttura principale di un mechanical ground support equipment, il quale ha lo scopo di integrare, testare e trasportare satelliti o parti di questi. La funzione dei telai consiste nel permettere l'assemblaggio di strumenti e satelliti, ruotandoli o mantenendoli in posizione.
In questa tesi è svolta la progettazione modulare di un telaio meccanico per applicazione spaziale. Sono progettati telai di diverse dimensioni per consentire il montaggio di payload di differenti grandezze e masse. Il dimensionamento preliminare della struttura principale e di quella rotante è eseguito partendo da un modello a travi della struttura. Il dimensionamento di flange e viti è basato sui criteri di verifica definiti dalla NASA. Un modello 3D dei diversi telai è costruito grazie al software di progettazione 3D CAD parametrico Catia V5.
Dopo questa fase iniziale di progettazione, la struttura è verificata attraverso un'analisi ad elementi finiti. Questa analisi è realizzata tramite l'uso del solutore per analisi ad elementi finiti MSC Nastran. Il software di pre e post-elaborazione Patran permette di costruire il modello ad elementi finiti, di preparare l'analisi e di visualizzare i risultati. Il modello ad elementi finiti è presentato e la mesh realizzata è descritta. I controlli, necessari per assicurarsi risultati coerenti, sono esposti e verificati. Questi sono effettuati in diversi momenti, sia prima che dopo l'analisi, e su diverse parti, come elementi finiti e output file. L'analisi degli sforzi su ogni elemento della struttura permettere di rilevare le criticità per modificare le componenti e migliorare il progetto iniziale.

Acknowledgements

I would like to thank my advisor, Professor R. Vescovini, for his support, helpfulness and for transmitting me the passion for structural mechanics. I would also like to thank my company tutor, Ing. R. Corsini, for the opportunity he gave me.

Thanks to all the colleagues of Highftech Engineering, for coffee breaks, for teachings and, in particular, for cakes. I never thought I would find such a friendly team in a working environment.

I am so glad to have reached this goal because it means that I survived Milano, Politecnico and flatmates. The years I spent here would have been much more boring without the people I met at university. I would like to thank my guys, Simone, Lorenzo, Marco and Francesco, for making every moment spent together fun, even if constantly testing my patience. Thanks to the first person I met at Polimi, Elena, a wonderful friend who always cheers me up by telling me her misadventures. Thanks to Chiara, the most sporty and energetic person I know, for sharing stories and thoughts in the many trips to and from Politecnico.

Thanks to my friends from Modena, Sara, Monica and Giorgia, who shown me that it is not important to see each other every day to maintain a special relationship.
Thanks to my lifelong friend, Greta, for all the laughs and the support she has given me over the years.

Thanks to Marco, for all the things he explained to me, for all the times he helped and supported me, but above all for putting up with me during these challenging months.

Finally, I would like to thank my family for all the support: my parents, Barbara and Andrea, which have encouraged me to go beyond my limits since I was a child, Alessandro, who is the best brother I could ever want, and my grandma, Maura, that gives me so much love and food.

Contents

List of Figures

List of Tables

Acronyms

Table 1: Acronyms

Acronym	Definition
AIT	Assembly, Integration and Testing
BC	Boundary Condition
CAD	Computer-Aided Design
CoG	Center of Gravity
CPU	Central Processing Unit
DOF	Degree Of Freedom
EGSE	Electrical Ground Support Equipment
EU	European Union
FE	Finite Element
FEA	Finite Element Analysis
FEM	Finite Element Method
GPWG	Grid Point Weight Generator
HFT	Highftech Engineering Srl
MGSE	Mechanical Ground Support Equipment
MoS	Margin of Safety
MPC	Multi-Point Constraint
NASA	National Aeronautics and Space Administration
S/C	Spacecraft
UM	Unit of Measurement

Chapter 1

Introduction

1.1 Overview

The manufacturing of satellites and International Space Station modules is done using particular mechanical and electrical support equipment for movement, integration, testing and transportation. These equipments are called MGSE (Mechanical Ground Support Equipment) and EGSE (Electrical Ground Support Equipment). Regarding MGSE, there are a lot of different kinds of devices that have to accomplish several functions. Spacecraft transportation from integration sites to launch sites can be performed via road, ship and air transportation, but always in safe mode and clean condition. This is done by spacecraft transport and storage containers, that assure protection from environmental conditions and shocks. MGSE shall support satellite or payload during assembly, integration and testing (AIT) activities. During mechanical integration activities, they hold in position, for example vertical or horizontal, the payload, or adjust its height. To allow movement, the equipment can have swivel castors, while screw jacks permit to unload castors and level the payload. For instance, MGSEs are used for the integration of the components of the propulsion system, for the offline preparation of tanks, for support and weight the spacecraft during refuel operations.
The lifting structures allow to lift the satellite using crane and move or install it on a different MGSE or on test supports or adapters. Adapters are used to connect the spacecraft with other MGSEs, to hold it in position during the measurements, or to connect it to test machines. MGSEs for testing can be built in a way that allows simulating the effective position that an instrument has on the S/C. Some MGSEs, like scaffolding or specific platform, help access to the payload. Others simulate 0g condition in space in the facility, and still others deploy sensible equipment like panels, radiators or booms, which are connected to the S/C.
Another type of MGSE, the one that will be designed in this thesis, is the multipurpose trolley. It supports the spacecraft, or dedicated modulus, during horizontal or vertical integration. It provides a table capable of tilting and rotating the spacecraft.
All these types of equipment shall respect customers' requirements and also safety regulations. For example, tilt and rotation shall not be possible simultaneously in multipurpose trolley. In addition to this, a trolley can be required to transfer the flight hardware from the container into the precision clean area. It will need to meet the stringent cleanliness and planetary protection requirements of the cleanroom whilst providing an element of mobility over the cleanroom floor. A dummy mass, representing a mass with the same center of gravity of the spacecraft, is useful to perform proof tests and check the integrity and characteristics of MGSEs.

Two examples of multipurpose trolley realized by Highftech Engineering Srl are described below. They have been designed taking into account the applicable national safety standards and EU directives in order to guarantee the safe and reliable use of each item.
Trolley 1, reported in Fig. 1.1a, shall support the flight hardware during integration and functional testing activities. It is composed of two parts: the main frame and the rotating frame. It has the capability to provide a full rotation in both senses of the instrument around one axis. The rotating frame can be blocked only at 0° and 180°, as can be seen in Fig. 1.1b, and when the access to the instrument is safe and easy. There are two different versions: a tall version that allows access to the instrument upper part when the bridge is blocked at 180° and a short version that permits working at a comfortable height during instrument integration. This trolley has swivel casters, adjustable jacks, but also four hoisting points and a forklift interface, shown in orange in Fig. 1.1.

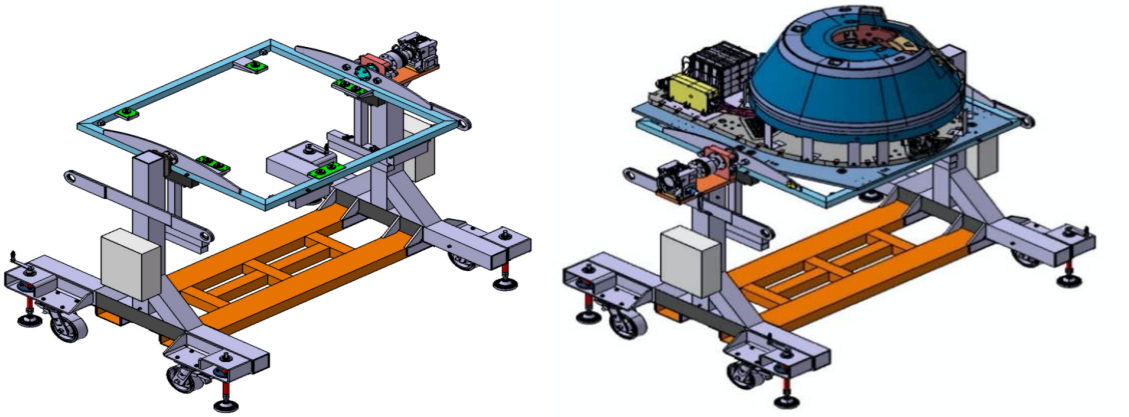

(a) Trolley 1

(b) Trolley 1 with instrument and bridge blocked at 0°

Figure 1.1: Trolley 1 by HFT

Trolley 2 is reported in Fig. 1.2a and shall support the AIT activities at the instrument level. It ensures an operational life of 20 years because no limited life items are used and the materials have limited risk of corrosion and degradation. Also, this trolley consists of two metallic frames, a fixed one and a rotating one. It has a rotating capability of 360° clockwise and counterclockwise directions, but in this case, the bridge can be blocked every 45° with two blocking pins. Swivel casters allow movement inside the facility, while screw jacks allow leveling the trolley. In Fig. 1.2a, two sets of balancing masses are reported in brown, they help to perform better balancing, maintaining the center of gravity of the rotating instrument as close as possible to the rotation axis in any configuration. The interface between bridge and instrument is made of a set of plates fixed to the rotating frame. Fig. 1.2b shows four columns in light blue, which are able to maintain the instrument at a comfortable height and to maintain also the space between the two frames, which lets the operator to work around the sides of the payload.

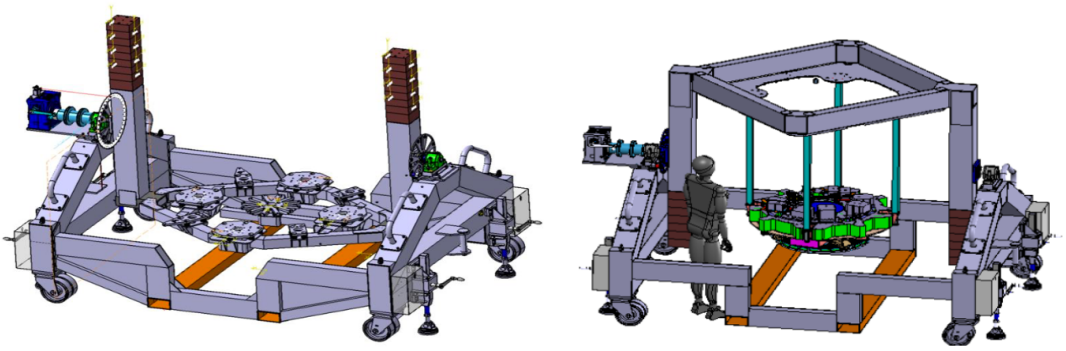

(a) Trolley 2 **(b)** Trolley 2 with bridge blocked at 180°

Figure 1.2: Trolley 2 by HFT

1.2 Present work

The purpose of this work is to develop a modular design of a mechanical trolley sub-assembly of a Mechanical Ground Support Equipment for space application. This system must comply with MGSE requirements of Airbus and Thales Alenia Space. The trolley shall allow the rotation of the instrument around two axes and the support of spatial payloads for on-ground activities. The peculiarity of the structure is that it is modular, so there will be trolleys with different dimensions that will hold payloads of different masses and sizes. The one that will be sized is the larger trolley with the heavier payload.
The aim of this thesis is to have a starting point for future MGSEs of different sizes, not to have a new complete trolley.

1.3 Thesis outline

This thesis is based on an internship carried out in the company Highftech Engineering Srl in Modena.
The work is divided into 6 chapters organized as follow:

- In Chapter 2, beam theory is briefly discussed and then different configurations of the main frame are analyzed in order to choose the proper one. Finally, the section of the beams of the selected configuration is sized;
- Chapter 3 is devoted to flanges and screws. A large part of this chapter is dedicated to the study of their verifications. Subsequently, multiple flanges are sized and it is verified if the checks are overcome;
- In Chapter 4 three kinds of rotating frames are designed and the relative beams and flanges are sized. In the last part also the shaft, which connects the two frames and allows the rotation of the bridge, is sized;
- Chapter 5 is focused on the structural analysis of a part of the trolley. Firstly, the Finite Element Method is presented and all the different topics of the analysis, like mesh, loads and boundary conditions, are explained. Then checks and verifications on FEM, weldings and screws are reported. In the end, the final version is studied and some improvements are discussed;
- In Chapter 6 the conclusions are presented and some proposals for future work are given.

Chapter 2

Beam model of the trolley

This chapter is aimed at recalling the theoretical subject of the beam theory used in this thesis. Different configurations of the main frame of the trolley are studied. Finally, its design is chosen and its beams are defined.

2.1 Beams and De Saint-Venant's solution

In 1855 the french elasticity theorist Adhéman Jean Claude Barré de Saint-Venant published the following statement: "The difference between the effects of two different but statically equivalent loads becomes very small at sufficiently large distances from load" [4]. This expression is known as Saint-Venant's principle. His solid is a 3D body characterized by the following aspects:

- The body is slender, this means that one dimension is much greater than the other two;
- The body is obtained by translating a plane figure along one axis, the z-axis. This plane figure is the section of the body and remains constant along the beam axis;
- The material of the body is isotropic, elastic and homogeneous;
- Loads and constraints are applied at the outer sections.

The goal is to determine the state of stress for a generic section, far enough from constraints and loads.
The 3D body considered is the beam represented in Fig. 2.1; the beam axis is the z-axis and xy is the plane of the section. The origin O of this reference frame is the center of gravity of the section and x and y-axes are principal centroidal axis, so that:

$$\int_A x dA = 0 \qquad \int_A y dA = 0 \qquad \int_A xy dA = 0 \tag{2.1}$$

where A is the area of the section.

Figure 2.1: Beam

Taking into account Fig. 2.2, the applied loads are denoted with the ˆ symbol, are considered in terms of resultants and are taken such that internal shear and axial forces and internal bending and twisting moments are positive according to the right-hand rule convention [19]. The internal actions in terms of the stress components σ_z, τ_{xz} and τ_{yz} are expressed as:

$$N = \int_A \sigma_z dA \qquad T_x = \int_A \tau_{xz} dA \qquad T_y = \int_A \tau_{yz} dA \tag{2.2}$$

$$M_t = \int_A (\tau_{yz} x - \tau_{xz} y) dA \qquad M_x = \int_A \sigma_z y \, dA \qquad M_y = \int_A \sigma_z x \, dA \tag{2.3}$$

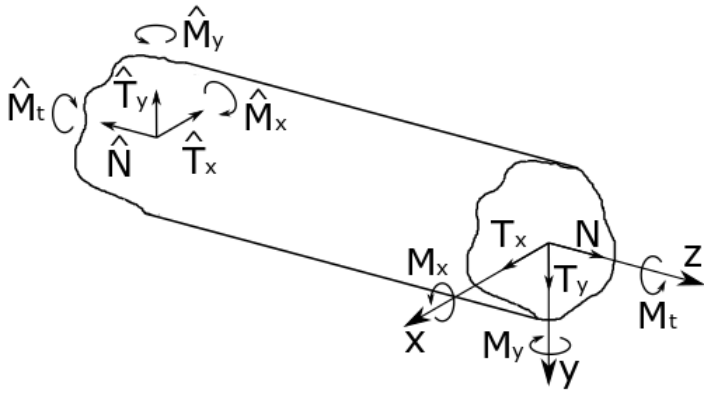

Figure 2.2: Applied loads and internal actions

The De Saint-Venant problem is solved via a semi-inverse approach. It consists of proposing an initial guess solution that will be checked ex-post and if the solution satisfies the relevant equations this means that the guess solution is the exact one. The initial guess is:

$$\sigma_x = \sigma_y = \tau_{xy} = 0 \tag{2.4}$$

This is true for an isotropic material and for a homogeneous section. In the case of composite materials, these stresses are in general non-zero.
Equilibrium equations, constitutive law, compatibility equations and boundary conditions must be verified. Combining these relations with the hypothesis and the expression of internal actions, the equation of the stress σ_z is:

$$\sigma_z = \frac{N}{A} - \frac{M_y(z)}{I_y} x + \frac{M_x(z)}{I_x} y \qquad [6] \tag{2.5}$$

where I_x and I_y are principal moments of inertia evaluated as:

$$I_x = \int_A y^2 dA \qquad and \qquad I_y = \int_A x^2 dA \tag{2.6}$$

This equation holds for principal centroidal axes. σ_z is just a function of internal actions, so for a given set of N, M_x and M_y the state of stress σ_z is identical for two beams made of different materials, in this case, the deformation is different. If the loads applied on the beam are only axial forces and bending moments, Eq. (2.5) can be used to evaluate the stress, but what happens in the presence of torsional loads and shear forces?
In this thesis, the solution of the torsional problem is covered only for beams with closed thin-walled sections and , because beams in trolleys of MGSEs have a rectangular section with a small thickness. In this case, the Bredt's formula can be used. He introduces the hypothesis that the shear stress τ_{zs} is uniform along the thickness t. This hypothesis is adequate for thin-walled beams. Consider the thin-walled profile illustrated in Fig. 2.3, characterized by the presence of a single closed circuit. The hydrodynamic analogy suggests the presence of a flow of shear stresses everywhere directed according to the middle line, therefore:

$$\begin{cases} \tau_{zs} = \tau_{zs}(s, n) \\ \tau_{zn} = 0 \end{cases} \tag{2.7}$$

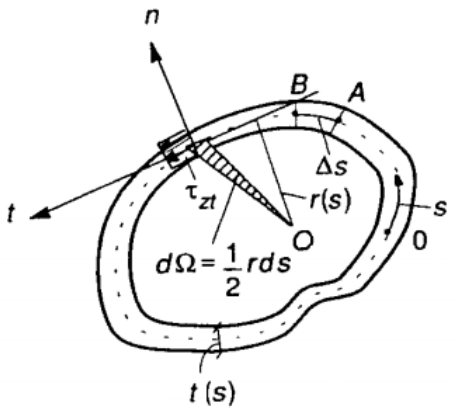

Figure 2.3: Thin-walled closed profile [6]

For the equilibrium condition, the net flow of shear stresses outflowing from the closed region Γ of the beam section is null, so the shear flow q is constant along the section. The total moment can be expressed as:

$$M_t = \oint_\Gamma qr(s)ds = 2q\Omega \tag{2.8}$$

where:

- s is the curvilinear abscissa;
- $r(s)$ is the arm with respect to O;
- Ω is the enclosed area of the median line:

$$\Omega = \frac{1}{2}\oint_\Gamma r(s)ds \tag{2.9}$$

The Bredt's formula is:

$$\tau_{zs} = \frac{M_t}{2\Omega t} \tag{2.10}$$

If the thickness is not constant, shear stress is maximum where t is minimum.
A beam can be stressed with the shear force T_y, represented in Fig. 2.4, passing through a point called the shear center. The shear center is the point of the section plane through which if the external load passes, then there will not be any twisting of the section. If the section has two axes of symmetry, then the shear center coincides with the center of gravity. If T_y is not applied to the shear center, in addition to the beam inflection, it will produce a torsion around the beam axis. This effect can be avoided by moving T_y parallel to itself, until the line of action passes through the shear center, and adding a torque equal to the product between the force and the distance of which it was translated. In this way, it is possible to study a shear problem with T applied in a generic point as the overlap of two problems: a pure shear with the force applied in the shear center and a pure torsion. However, the balance requires the presence of a bending moment M_x equal to the product between the shear force and the length of the beam. In this case, the normal stress is:

$$\sigma_z = \frac{T_y}{I_x} zy = -\frac{M_x(z)}{I_x} y \tag{2.11}$$

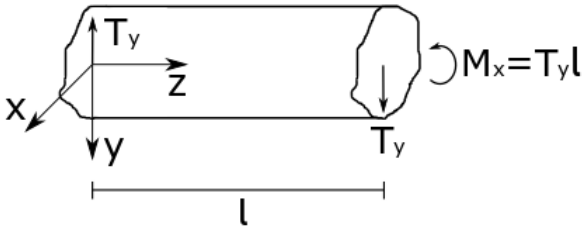

Figure 2.4: Beam subjected to shear force

The problem of torsion has just been addressed, so it only remains to solve that of the shear passing through the shear center. The analytical treatment of this particular case of De Saint-Venant's problem is quite complex, so an approximate theory has been developed by Jourawsky, which leads to sufficiently accurate results for the applications. It is assumed that the transverse section has an axis of vertical symmetry and that along each chord normal to it: $\tau_{zy} = const$ [2] (Fig. 2.5). Jourawsky's formula allows calculating these stresses as:

$$\tau_{zy} = \frac{TS_x^*}{I_x b} \tag{2.12}$$

where S_x^* is the first moment of area A^* about the x-axis.
Consider the case of symmetrical section, which presents a single closed circuit, such as the one illustrated in Fig. 2.6. If the section is divided according to symmetrically positioned chords, the stresses on them are equal. Eq. (2.12) becomes:

$$\tau_{zs} = \frac{TS^*}{I2t} \tag{2.13}$$

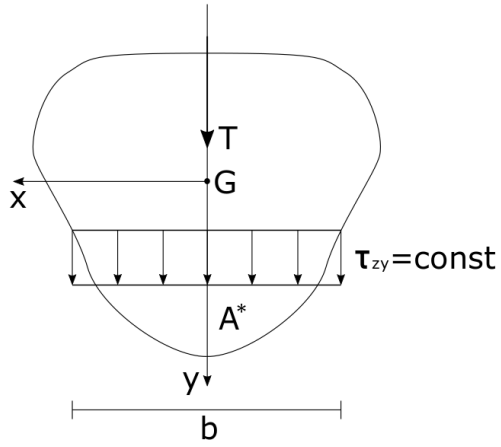

Figure 2.5: Symmetric section subjected to shear force

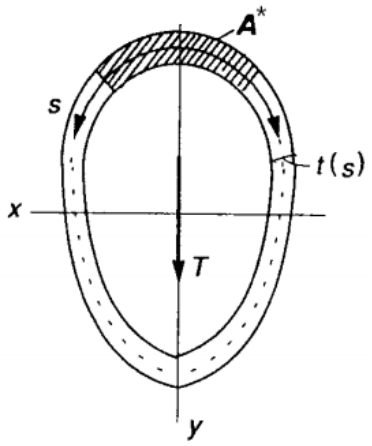

Figure 2.6: Symmetrical thin-walled section [6]

2.2 Von Mises criterion

An experimental approach to studying the strength of materials subjected to static stresses is very challenging. This is because to obtain information on the strength of materials subjected to compound stress, the effects of all possible combinations of the three principal stresses σ_1, σ_2 and σ_3 should be considered, experimentally assessing whether the material, when subjected to a specific tensile state defined by the three principal stresses, resists or fails. There are, therefore, theories whose purpose is to confront a permissible stress. In Fig. 2.7, is represented a cube subject to a triaxial complete tensile state and another subject to the equivalent stress σ_{eq}.

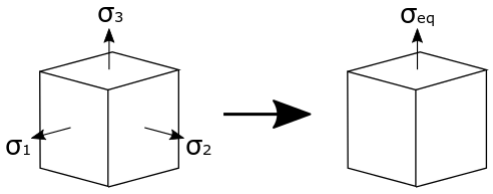

Figure 2.7: Triaxial complete tensile state and the equivalent stress

Some criteria are suitable for fragile materials, while others are applicable to ductile materials. The materials used for MGSEs are mainly metals and therefore ductile materials. In this thesis, the von Mises criterion, suitable for this type of material, will be used. This criterion is also known as the criterion of maximum distortion energy because according to this theory, a complete triaxial state is equivalent to a one-dimensional stress when the distortion energy of the three-dimensional case equals the distortion energy of the one-dimensional stress case.
The distortion energy is obtained by subtracting from the strain energy, which takes into account the entire elastic energy, the hydrostatic energy carried out by the hydrostatic part of the stresses following the volume variation of the cube:

$$U_{dist} = U_{strain} - U_{idr} \tag{2.14}$$

Distortion energy is used because it is believed that the hydrostatic part of the stresses does not lead the material to yielding [17].
Equalizing the distortion energy referred to a generic stress state and expressed in terms of stresses, to the distortion energy of the equivalent one-dimensional state formulated in terms of stresses, it is possible to establish the link between the stresses defining the general stress state, and the equivalent monoaxial stress case.
The distortion energy for a one-dimensional stress state is:

$$U_{dist_{1D}} = \frac{1+\nu}{3E}\sigma_{eq}^2 \tag{2.15}$$

where E is Young's modulus and ν is Poisson's ratio.
The hydrostatic energy can be expressed as a function of the hydrostatic component of stresses σ_{hyd} and of the bulk modulus K:

$$U_{hyd} = \frac{\sigma_{hyd}^2}{2K} \tag{2.16}$$

where:

$$\begin{cases} \sigma_{hyd} = \frac{\sigma_1+\sigma_2+\sigma_3}{3} \\ K = \frac{E}{3(1-2\nu)} \end{cases} \tag{2.17}$$

The strain energy expressed by the three principal stresses is:

$$U_{strain} = \frac{\sigma_1^2 + \sigma_2^2 + \sigma_3^2 - 2\nu(\sigma_1\sigma_2 + \sigma_2\sigma_3 + \sigma_3\sigma_1)}{2E} \tag{2.18}$$

At this point, it is possible to calculate the distortion energy for a complete three-dimensional stress state related to the principal directions:

$$U_{dist_{3D}} = U_{strain} - U_{hyd} = \frac{1+\nu}{3E}(\sigma_1^2 + \sigma_2^2 + \sigma_3^2 - \sigma_1\sigma_2 - \sigma_2\sigma_3 - \sigma_3\sigma_1) \tag{2.19}$$

Imposing the equality between the distortion energy for the complete stress state, expressed in Eq. (2.18), to the distortion energy for the monoaxial state that is wanted equivalent to the three-dimensional one, expressed in Eq. (2.15), the equivalent stress expression for the complete three-dimensional stress state is obtained:

$$\sigma_{eq} = \sqrt{\sigma_1^2 + \sigma_2^2 + \sigma_3^2 - \sigma_1\sigma_2 - \sigma_2\sigma_3 - \sigma_3\sigma_1} \tag{2.20}$$

For a complete three-dimensional state not related to the principal directions, the expression of the equivalent stress becomes:

$$\sigma_{eq} = \sqrt{\sigma_x^2 + \sigma_y^2 + \sigma_z^2 - \sigma_x\sigma_y - \sigma_y\sigma_z - \sigma_z\sigma_x + 3\tau_{xy}^2 + 3\tau_{yz}^2 + 3\tau_{zx}^2} \tag{2.21}$$

Comparisons with experimental data for more general stress states show that the maximum distortion energy criterion is well suited for steels [17]. For this reason, it will be used in this thesis.

2.3 Main frame

The main frame supports the bridge and allows its rotation, so the selection of the structure and the analysis on the beams depends on the masses of rotating frame and payload. The trolley is modular, so there will be structures of different sizes, but the analysis is done on the larger one. The main frame has a base composed of four beams, the axes of two beams are oriented as the Y-axis of the coordinate system that will be used from now on, while the other two are oriented as the X-axis. The Z-axis is perpendicular to the XY plane.
The following calculations provide a starting point for the design, all the results must be verified later using software for structural analysis.

2.3.1 First configuration

The first proposed configuration is the one reported in Fig. 2.8. It has a rectangular base composed of four beams, then there are two beams inclined by 45°, on the girder directed as the Y-axis, surmounted by another horizontal beam.

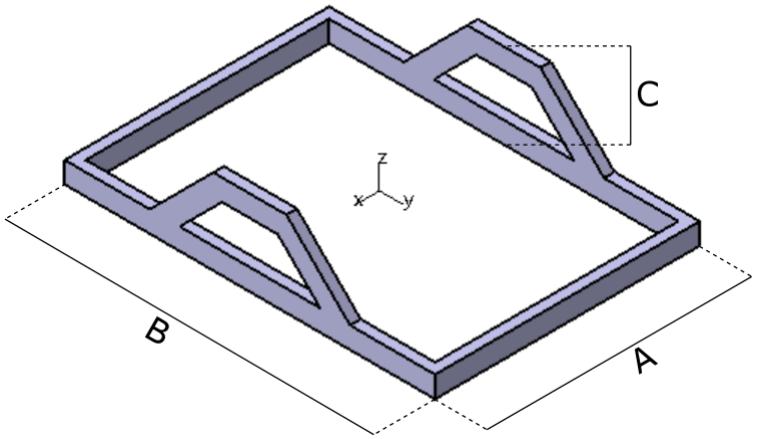

Figure 2.8: First configuration of the main frame

The goal of this thesis is to realize a parameterized trolley of an MGSE, so the ranges of trolley dimensions are reported in Table 2.1. Along the Z-axis $250mm$ represents the encumbrance of the wheels h_{wh}. The maximum payload mass allowed is $600kg$ while the maximum sizes are stated in Table 2.2.

Table 2.1: Ranges of trolley overall dimensions

Name	Axis	Minimum value $[mm]$	Maximum value $[mm]$	Step $[mm]$
A	X	1500	2500	500
B	Y	1000	3500	500
C	Z	$700 - 250$	$1500 - 250$	200

Table 2.2: Maximum sizes of the payload

Name	Maximum value [mm]
x_payload	2000
y_payload	2500
z_payload	1000

The oblique beams are attached to the girder at a distance from its ends equal to a quarter of its length, as can be seen in the scheme of Fig. 2.9. Even if these proportions and the inclination angle are changed, there are only a few configurations realizable combining different values of A, B and C, because increasing the value of C, the inclined beams intersect each other. Since the goal of this work is to obtain trolleys of different dimensions, this configuration cannot be adopted.

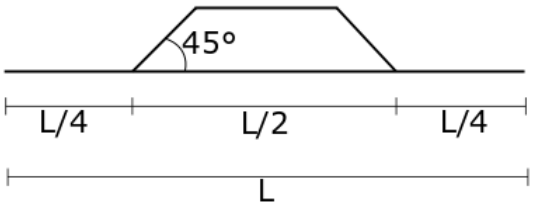

Figure 2.9: Scheme of the first configuration

2.3.2 Second configuration

The second configuration of the trolley, that can be seen in Fig. 2.10, has only a vertical beam placed in the midpoint of the horizontal girder. In this case, of course, all the combinations produce realizable structures. Also the presence of an interface between payload and trolley must be taken into account, which is placed on the payload's face with sides x_payload and z_payload, and that has a thickness t_{int} of $100mm$, and also of an encumbrance under the rectangular base of the trolley, that starting from the floor has height h_{enc} of $200mm$. In Fig. 2.10, the interface is in blue, the encumbrance in green and the floor is red.
The material used for the beams of the trolley is structural steel, it has good ductility, high strength, stiffness, and it is the most common material used for MGSEs. In particular, the chosen one is Fe510, whose properties, that are taken from [26], are reported in Table 2.3. Yield strength indicates the maximum stress that a material can withstand when it is deformed within its elastic limit. Ultimate strength indicates the maximum stress withstanding capability of a material when it is plastically deformed, in fact, it is the maximum stress that a material can withstand.
The trolley is sized as an assembly of beam elements. The problem is approximated as a simply-supported beam with a vertical force applied at the midpoint, due to the masses of payload and bridge. At this point, the margins of safety have to be calculated, using the maximum dimensions of the trolley, to see if the beams are enough robust. In Fig. 2.11, the representation of this configuration and the diagrams of shear and bending moment are shown.

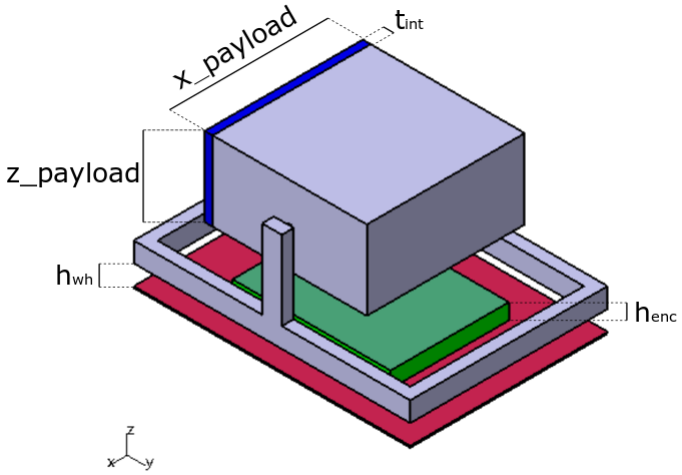

Figure 2.10: Second configuration of the main frame

Table 2.3: Fe510 properties if thickness $< 16mm$

Elastic modulus	E	$[MPa]$	$2.00 \cdot 10^5$
Poisson's ratio	ν	$[-]$	0.29
Yield strength	Ry	$[GPa]$	$3.55 \cdot 10^{-1}$
Ultimate strength	Ru	$[GPa]$	$5.10 \cdot 10^{-1}$
Density	ρ	$\left[\frac{kg}{m^3}\right]$	$7.80 \cdot 10^3$

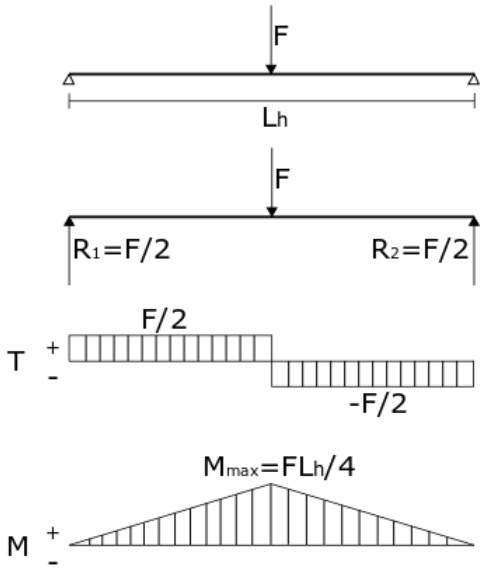

Figure 2.11: Simply supported beam

The beams have a hollow structural section, reported in Fig. 2.12, and their sizes together with masses of payload and bridge are listed in Table 2.4.

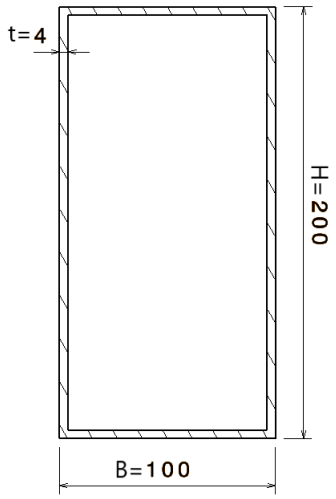

Figure 2.12: Section of the beam, the lengths are in millimeters

Table 2.4: Data

Payload mass	m_p	$[kg]$	600
Bridge mass	m_b	$[kg]$	1500
Height	H	$[mm]$	200
Base	B	$[mm]$	100
Beam thickness	t	$[mm]$	4
Beam length	L_h	$[mm]$	3500

In this first calculation, only the stress due to bending moment is taken into account.
The structure is symmetric, so half of the weight of the masses is carried by the other girder. The force applied to the beam is:

$$F = g \cdot \left(\frac{m_p + m_b}{2}\right) \tag{2.22}$$

where g is the acceleration of gravity.
The distance from the neutral axis and the moment of inertia around the neutral axis are:

$$d_H = \frac{H}{2} \tag{2.23}$$

$$I_B = \frac{1}{12}((B \cdot H^3) - ((B - 2t) \cdot (H - 2t)^3)) \tag{2.24}$$

The bending moment is maximum at the middle of the beam and it is evaluated as:

$$M_{b\_max} = \frac{F \cdot L_h}{4} \tag{2.25}$$

The maximum stress on the section can be found using the equation Eq. (2.5):

$$\sigma_{max} = \frac{M_{b\_max} \cdot d_H}{I_B} \tag{2.26}$$

There would be another component of stress due to the shear force, but in this case, it is not taken into account.
An important value is the margin of safety (MoS), that indicates if a structure can support certain loads, taking into account all the possible uncertainties in the definition of design and verification parameters. The safety factors represent these uncertainty parameters. MGSE shall be designed with the safety factors against the maximum operating, transport S/C handling load, so the yield and ultimate safety factors are [7]:

$$\begin{cases} SF_y = 3 \\ SF_u = 4 \end{cases} \tag{2.27}$$

Yield and ultimate margins of safety are evaluated as [18]:

$$\begin{cases} MoS_y = \frac{R_y}{\sigma_{max} \cdot SF_y} - 1 \\ MoS_u = \frac{R_u}{\sigma_{max} \cdot SF_u} - 1 \end{cases} \tag{2.28}$$

Both margins of safety shall be positive, otherwise, the beam will fail before reaching its design load in service. In Table 2.5, the values of the quantities mentioned above are reported.

Table 2.5: Results

F $[N]$	d_H $[m]$	I_B $[m^4]$	M_{b_max} $[Nm]$	σ_{max} $[Pa]$	MoS_y $[-]$	MoS_u $[-]$
$1.03 \cdot 10^4$	0.100	$1.24 \cdot 10^{-5}$	$9.01 \cdot 10^3$	$7.27 \cdot 10^7$	$6.28 \cdot 10^{-1}$	$7.55 \cdot 10^{-1}$

For the MGSE used for handling, the maximum stress induced in the structure shall be the result of the stress due to static gravity load multiplied by the vertical and lateral dynamic factors:

$$\begin{cases} fd_v = 2g \\ fd_l = 1.5g \end{cases} \tag{2.29}$$

In this thesis, fd_v has the same direction but the opposite orientation of the Z-axis and fd_l same direction and opposite orientation of X-axis.
Taking into account only the vertical dynamic factor, the force becomes:

$$F = fd_v \cdot \left(\frac{m_p + m_b}{2}\right) = 2.06 \cdot 10^4 N \tag{2.30}$$

In this case the margins of safety are negative:

$$\begin{cases} MoS_y = -1.86 \cdot 10^{-1} \\ MoS_u = -1.23 \cdot 10^{-1} \end{cases} \tag{2.31}$$

This structure is not able to support this load, so, of course, it will not be able to resist the additional load due to the lateral dynamic factor. It is possible to increase the thickness of the beam or change the configuration. Keeping this configuration and increasing t will result in a too heavy trolley, so the configuration must be changed.

2.3.3 Third configuration

In this configuration, two supports are added. They start at half of the vertical beam and reach the girder with an inclination of 45°, as can be seen in Fig. 2.13. At this point, consider all the mass of the bridge applied at only one point is too conservative and far from reality. So the mass of the rotation frame is split into four different points: two points are on the top and at the middle of the vertical beam, the other two are on the horizontal beam and they are distant $\frac{L_h}{10}$ from the center of the beam, as can be seen in Fig. 2.14. In Table 2.6, the values of the new masses are reported.

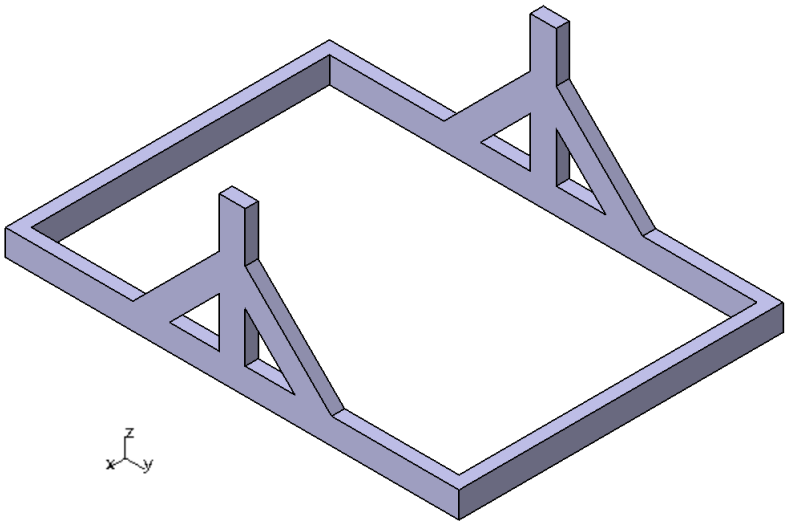

Figure 2.13: Third configuration of the main frame

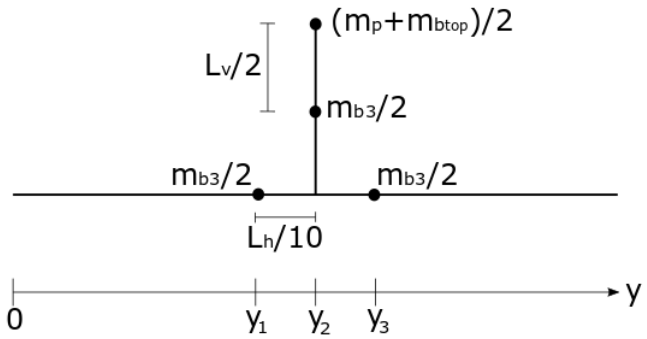

Figure 2.14: Mass division in the third configuration

Table 2.6: New masses

Payload mass		m_p	$[kg]$	600.0
Bridge mass	at the top	$m_{b_{top}}$	$[kg]$	500.0
	in 3 points	m_{b_3}	$[kg]$	333.3

At this point, the same procedure described before to analyze the robustness of the structure is followed. Taking into consideration both the dynamic factors, there are vertical and lateral loads. Each mass is subjected to the vertical acceleration, while only the two masses applied on the vertical beam are affected also by lateral acceleration. These forces generate bending and torsional moments on the girder, so the degree of freedom of torsional rotation has to be constrained. For example, a cantilever beam can be studied. In the real configuration, the horizontal beam is a fixed-end beam, because it is connected to the two horizontal beams with axis aligned to the X-axis through the use of two flanges, which will be analyzed in Ch. 3, so this choice is too conservative. The girder can be approximated as a simply-supported beam, both in the vertical and lateral directions, with a prismatic constraint that prevents the rotation around Y-axis.
There are three vertical loads applied on three different points of the girder. Forces and their distance of application from the left end of the beam are:

$$\begin{cases} F_{v_1} = fd_v \cdot \frac{m_{b3}}{2} \\ F_{v_2} = fd_v \cdot \left(\frac{m_{b3}+m_{b_{top}}+m_p}{2}\right) \\ F_{v_3} = F_{v_1} \end{cases} \qquad \begin{cases} y_1 = \frac{L_h - \frac{L_h}{5}}{2} \\ y_2 = \frac{L_h}{2} \\ y_3 = \frac{L_h + \frac{L_h}{5}}{2} \end{cases} \tag{2.32}$$

In Fig. 2.15, the scheme of the problem and the diagrams of shear and momentum related to the vertical forces are reported.

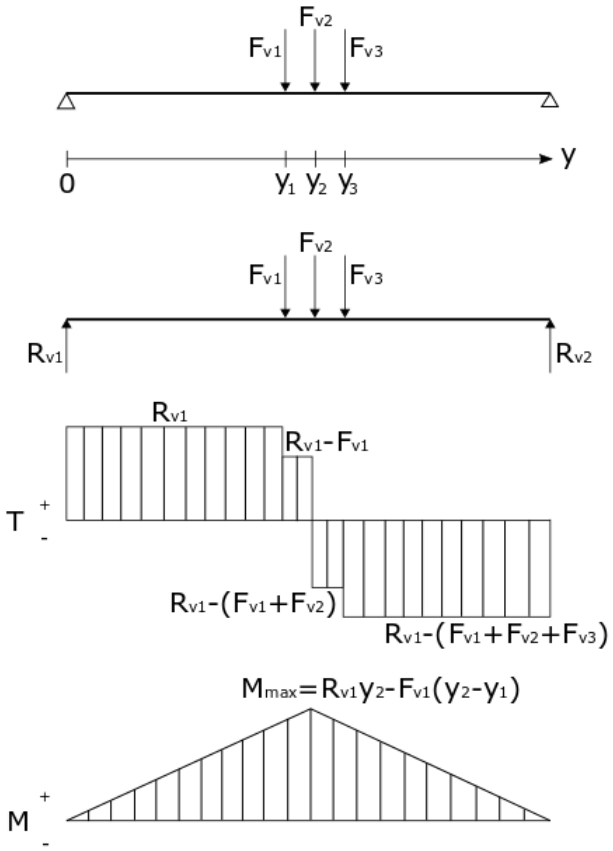

Figure 2.15: Scheme of the third configuration and diagrams of shear and momentum

The two vertical reaction forces are equal and can be evaluated as:

$$R_{v_1} = R_{v_2} = \frac{F_{v_1} + F_{v_2} + F_{v_3}}{2} \tag{2.33}$$

The bending moment is maximum at the center of the girder:

$$M_{b\_max} = R_{v_1} \cdot y_2 - F_{v_1} \cdot (y_2 - y_1) \tag{2.34}$$

The maximum bending stress is find using again Eq. (2.5).
The lateral loads are only two, their expressions and distances of application with respect to the girder are:

$$\begin{cases} F_{l_1} = fd_l \cdot \left(\frac{m_{b_{top}} + m_p}{2}\right) \\ F_{l_2} = fd_l \cdot \frac{m_{b3}}{2} \end{cases} \qquad \begin{cases} z_1 = L_v \\ z_2 = \frac{L_v}{2} \end{cases} \tag{2.35}$$

where L_v is the length of the vertical beam, that is $1m$.
Also the lateral reaction forces are equal to each other:

$$R_{l_1} = R_{l_2} = \frac{F_{l_1} + F_{l_2}}{2} \tag{2.36}$$

The bending moment induced by these forces is maximum in the middle point of the beam and it is calculated as:

$$M_{b\_Fl_{max}} = \frac{(F_{l_1} + F_{l_2}) \cdot L_h}{4} \tag{2.37}$$

From Eq. (2.5), the stress is:

$$\sigma_{Fl} = \frac{M_{b\_Fl_{max}} \cdot d_B}{I_H} \tag{2.38}$$

where the distance from the neutral axis and the moment of inertia around the neutral axis are:

$$\begin{cases} d_B = \frac{B}{2} \\ I_H = \frac{1}{12}((H \cdot B^3) - ((H - 2t) \cdot (B - 2t)^3)) \end{cases} \tag{2.39}$$

The torques of torsion due to lateral loads are:

$$\begin{cases} M_{t1} = F_{l_1} \cdot z_1 \\ M_{t2} = F_{l_2} \cdot z_2 \end{cases} \tag{2.40}$$

The stress induced by torsion can be evaluated through the Bredt's formula reported in Eq. (2.10) and discussed in Sec. 2.1, because the beam has a thin cross section:

$$\tau_{M_t} = \frac{M_t}{2\Omega \cdot t} \tag{2.41}$$

where Ω is the enclosed area of the median line computed as:

$$\Omega = (H - t) \cdot (B - t) \tag{2.42}$$

This time also the stress due to shear induced by vertical and lateral loads is considered. The shear stress can be evaluated using Jourawsky's formula (Eq. (2.12)), previously analyzed in Sec. 2.1:

$$\tau_T = \frac{T \cdot S}{2tI} \tag{2.43}$$

where the values of the shear forces are:

$$\begin{cases} T_V = R_{v_1} \\ T_L = R_{l_1} \end{cases} \tag{2.44}$$

and S is the first moment of area about an axis. Their values in points 1, 2 and 3 of the beam section, reported in Fig. 2.16, are:

$$\begin{cases} S_{b_{in2}} = \frac{B \cdot H^2}{8} - \frac{(B-2t)\cdot(H-2t)^2}{8} \\ S_{h_{in3}} = \frac{B^2 \cdot H}{8} - \frac{(H-2t)\cdot(B-2t)^2}{8} \\ S_{b_{in1}} = S_{h_{in1}} = \frac{t(B-t)(H-t)}{2} \end{cases} \tag{2.45}$$

As can be seen in Fig. 2.16, the stress produced by the vertical shear is maximum in point 2, where the one of the lateral shear is zero, instead it is maximum in point 3, where $\tau_{T_L} = 0Pa$, so the most stressed point of the beam is 1, as can be seen in Table 2.7 where the values of shear stresses in these relevant points are reported.

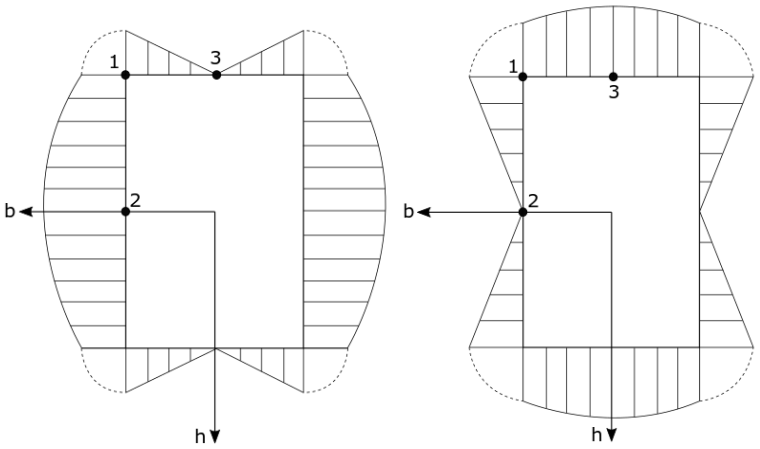

(a) Stress due to T_v **(b)** Stress due to T_l

Figure 2.16: Stress due to shear force

Table 2.7: Shear stresses in different points of beam section

τ_{T_V} in 2	τ_{T_L} in 3	τ_{T_V} in 1	τ_{T_L} in 1
$7.9 \cdot 10^6 Pa$	$7.34 \cdot 10^6 Pa$	$3.91 \cdot 10^6 Pa$	$5.89 \cdot 10^6 Pa$

The equivalent stress can be evaluated using von Mises criterion (Eq. (2.21)):

$$\sigma_{eq} = \sqrt{\sigma_{F_v}^2 + \sigma_{F_l}^2 - \sigma_{F_v}\sigma_{F_l} + 3(\tau_{T_v} + \tau_{T_l} + \tau_{M_t1} + \tau_{M_t2})^2} \tag{2.46}$$

Finally, also the margins of safety can be calculated using Eq. (2.28). In Table 2.8, are reported the results obtained using the data already given.
In this case, the margins of safety are negative, so the thickness of the beam must increase to withstand the loads. The minimum value of t is $7mm$. Also base B and height H can change to find the lighter beam for which $MoS_y > 0.1$. The mass of the horizontal beam is:

$$m_{beam} = \rho((L_h \cdot H \cdot B) - (L_h(H-2t)\cdot(B-2t))) \tag{2.47}$$

In Table 2.9, the outcomes of different combinations that comply with the requirements are shown.

Table 2.8: Results of calculations of the third configuration of the main frame

$F_{v_1} = 3.27 \cdot 10^3 N$ $F_{v_2} = 1.41 \cdot 10^4 N$ $F_{v_3} = 3.27 \cdot 10^3 N$ $R_{v_1} = R_{v_2} = 1.03 \cdot 10^4 N$	$y_1 = 1.40m$ $y_2 = 1.75m$ $y_3 = 2.10m$	$M_{b\_Fv_{max}} = 1.69 \cdot 10^4 Nm$ $\sigma_{Fv} = 1.36 \cdot 10^8 Pa$ $T_{V_1} = T_{V_2} = 1.03 \cdot 10^4 N$ $\tau_{T_V} = 3.91 \cdot 10^6 Pa$	
$F_{l_1} = 8.09 \cdot 10^3 N$ $F_{l_2} = 2.45 \cdot 10^3 N$ $R_{l_1} = R_{l_2} = 5.27 \cdot 10^3 N$	$z_1 = 1.00m$ $z_2 = 0.50m$	$M_{b\_Fl_{max}} = 9.22 \cdot 10^3 Nm$ $\sigma_{Fl} = 1.10 \cdot 10^8 Pa$ $T_{L_1} = T_{L_2} = 5.27 \cdot 10^3 N$ $\tau_{T_L} = 5.38 \cdot 10^6 Pa$	$M_{t1} = 8.09 \cdot 10^3 Nm$ $M_{t2} = 1.23 \cdot 10^3 Nm$ $\tau_{M_{t1}} = 5.38 \cdot 10^7 Pa$ $\tau_{M_{t2}} = 8.15 \cdot 10^6 Pa$
$\sigma_{eq} = 1.76 \cdot 10^8 Pa$		$MoS_y = -3.28 \cdot 10^{-1}$	$MoS_u = -2.76 \cdot 10^{-1}$

Table 2.9: Choice of the beam section

$B \times H \times t$ $[mm]$	MoS_y $[-]$	MoS_u $[-]$	m_{beam} $[kg]$
$100 \times 200 \times 7$	$1.15 \cdot 10^{-1}$	$2.01 \cdot 10^{-1}$	$1.09 \cdot 10^2$
$100 \times 250 \times 6$	$2.45 \cdot 10^{-1}$	$3.41 \cdot 10^{-1}$	$1.11 \cdot 10^2$
$150 \times 200 \times 5$	$1.73 \cdot 10^{-1}$	$2.64 \cdot 10^{-1}$	$9.28 \cdot 10^1$
$150 \times 250 \times 4$	$2.23 \cdot 10^{-1}$	$3.18 \cdot 10^{-1}$	$\boxed{8.56 \cdot 10^1}$

Parts in weldable structural steels must have a thickness of $4mm$ and over [3]. The section of the lighter beam meets this requisite, so the chosen characteristics of the beams are:

$$\begin{cases} B = 150mm \\ H = 250mm \\ t = 4mm \end{cases} \tag{2.48}$$

This configuration of the main frame is reported in Fig. 2.17, together with a box in purple, representing the space allowable for rotating frame and payload, which is connected to the main frame through two shafts, that will be sized in Sec. 4.4. Here also flanges are reported to have a more complete idea of the structure, but they will be studied in Ch. 3.
The goal of the thesis is to size a modular trolley, so three structures with different dimensions are illustrated in Fig. 2.17. It is possible to switch from one trolley to another changing only three independent values: the total encumbrance along X and Y-axes (Lim_x and Lim_y, respectively) and the height of the vertical beam L_v. In addition, the oblique supports can be smaller than other beams, in particular for smaller trolleys, so also the section height H_v of these supports is a parameter that varies from trolley to trolley. The characteristic values of each trolley are written in Table 2.10.
In Fig. 2.17a, the large trolley is reported, all sizing are done based on it, because it is the most critical and stressed case and, in this way, smaller trolleys will definitely support the same loads. In Fig. 2.17b, is illustrated the trolley with the smallest possible dimensions, instead in Fig. 2.17c, a medium case is reported.

Table 2.10: Values of the variables of the trolleys expressed in millimeters

Variable	UM	Large trolley	Medium trolley	Small trolley
Lim_x	$[mm]$	2500	2000	1500
Lim_y	$[mm]$	3500	2500	1500
L_v	$[mm]$	1000	800	400
H_v	$[mm]$	200	150	100

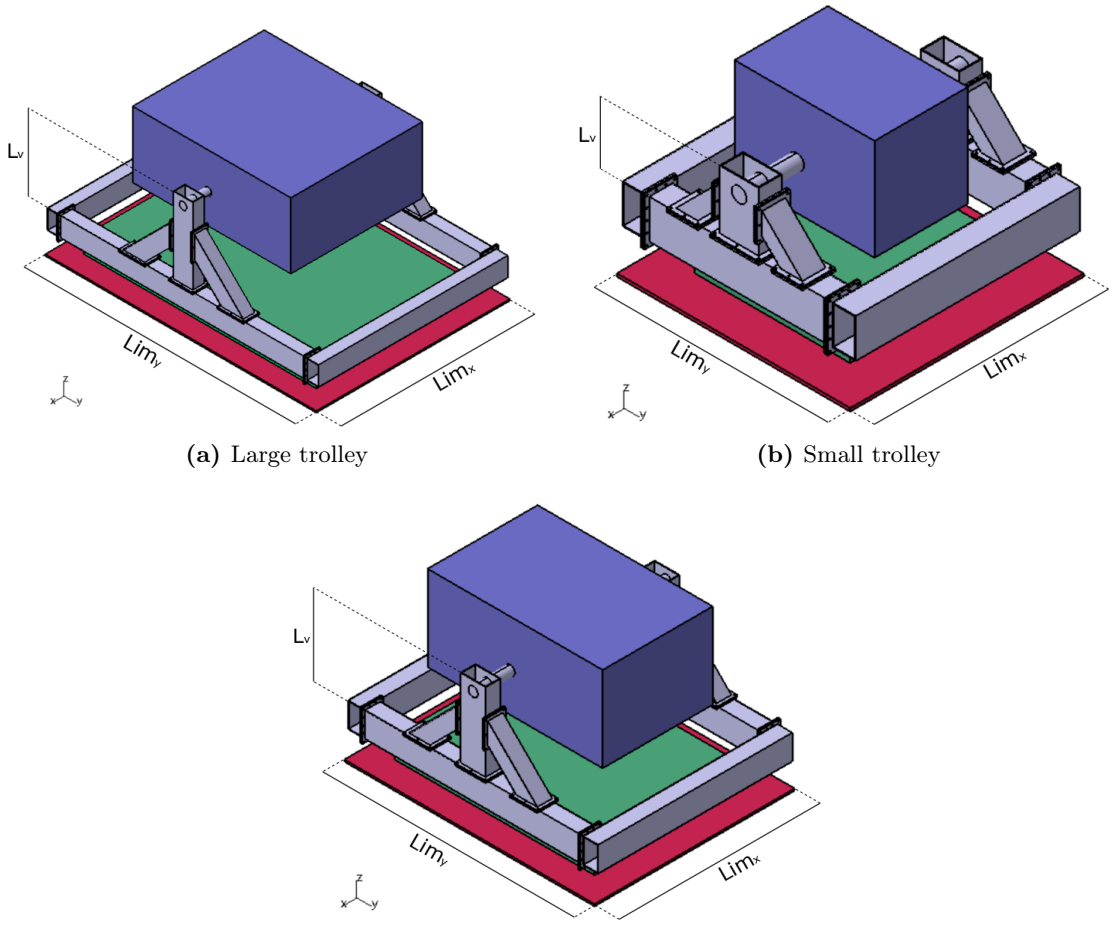

(a) Large trolley

(b) Small trolley

(c) Medium trolley

Figure 2.17: Third configuration of the main frame

Chapter 3

Flanges and screws

In this chapter, the flanges of the main frame are sized choosing the parameters and the screws needed to overcome the checks on screws and flanges integrity. The verifications used, based on *Criteria for preloaded bolts* (NASA), are discussed. Finally, the results of the preliminary version of the flanges are reported.

3.1 Flanges

A flange is a perforated plate which is connected to a beam by a welded joint and which, by the use of bolts, allows the connection to another flange of equal size. The main frame needs a flange between the vertical and the horizontal beams (Flange A) and another between horizontal beams along Y and X-axes (Flange B). The material of the flanges is Fe510, the same as the beams.
Initially, the sizes of the flanges are considered $30mm$ larger, for each side, than the ones of the beam. This is done in order to have enough space for screws and washers. Their relevant dimensions are:

$$\begin{cases} B_{flange} = 210mm \\ H_{flange} = 310mm \\ t_{flange} = 16mm \end{cases} \tag{3.1}$$

3.1.1 Flange A

In Fig. 3.1a, the vertical beam, flange, masses and dynamic factors are reported. It is a cantilever beam, so first of all moments and loads at the fixed-end must be calculated. In this case, there are the bending moments and shear loads generated by the lateral forces and an axial load due to the vertical force. The values can be seen in Table 3.1, while the vectors are reported in Fig. 3.1b. This flange is also used to connect the two oblique supports to vertical and horizontal beams, but the height of the flange is different depending on the section height of the supports. Concerning the three trolleys reported in Fig. 2.17, the flange of the large one has a height higher than $310mm$, while for the other two trolleys it is lower.

Table 3.1: Loads at Flange A

Bending moment	$M_{b\_Fl} = F_{l_1} \cdot z_1 + F_{l_2} \cdot z_2 = 9319.5Nm$
Lateral Shear load	$T_b = F_{l_1} + F_{l_2} = 10545.75N$
Axial load	$N = F_{v_2} = 14061N$

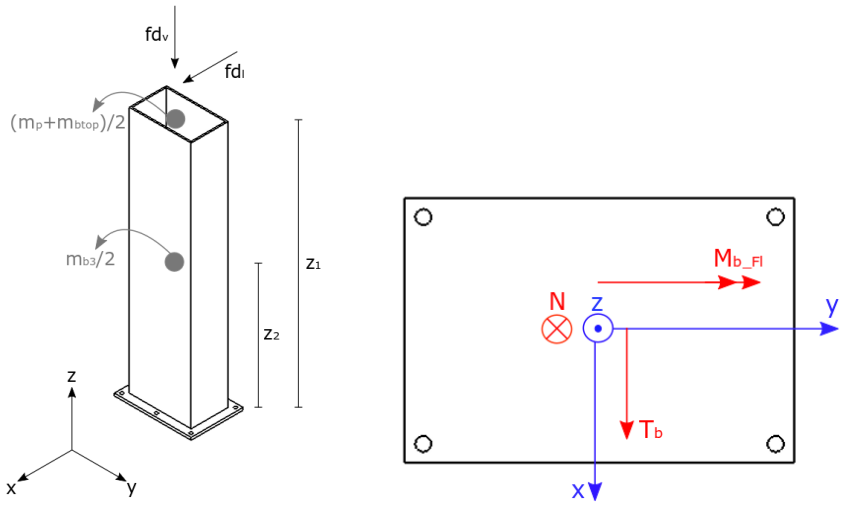

(a) Draw of vertical beam and flange A

(b) Loads on Flange A

Figure 3.1: Vertical beam and Flange A

3.1.2 Flange B

Now turning to Flange B, the loads and moments on the horizontal beam have been already analyzed while it has been sized in Sec. 2.3.3. The beam is welded at both ends with a flange, as can be seen in Fig. 3.2a, so the shear loads are the same, but the moments are half of the values previously calculated. In Table 3.2, the absolute value of the loads that will be used to size the Flange B are reported and in Fig. 3.2b, their vectors are displayed. In particular, there are the shear loads in lateral and vertical directions, the maximum bending moments due to vertical and lateral forces and the torsional moment due to lateral forces.

Table 3.2: Loads at Flange B

Lateral shear load	$T_b = T_{L_1} = 5272.88N$
Vertical shear load	$T_h = T_{V_1} = 10300.5N$
Bending moment 1	$M_{b\_Fv} = 8440.7Nm$
Bending moment 2	$M_{b\_Fl} = 4613.77Nm$
Torsional moment	$M_t = 4659.75Nm$

The values in Table 3.1 and Table 3.2 are the same find in Table 2.8 because loads and moments do not depend on the sectional properties of the beam, so they are identical even if the values of B, H, and t are changed.

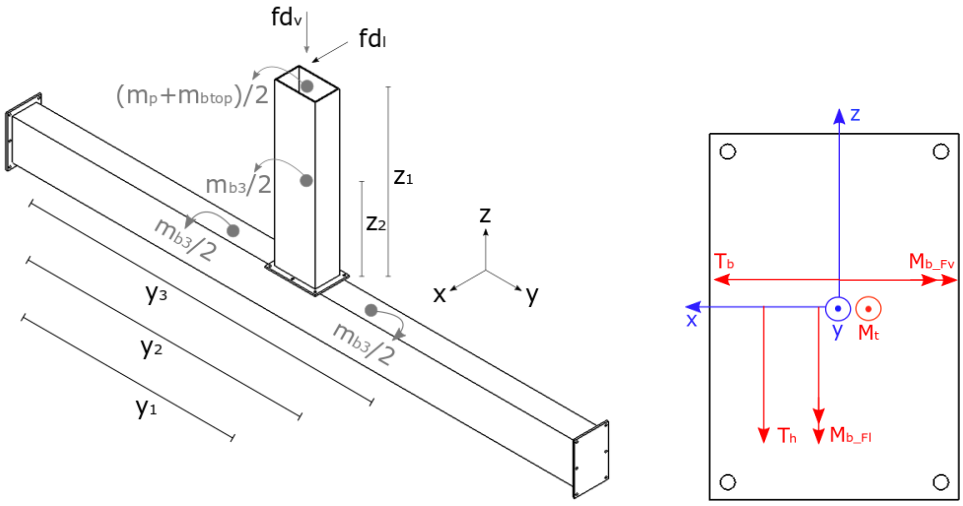

(a) Draw of beams and flanges **(b)** Loads on Flange B

Figure 3.2: Beams and Flange B

3.2 Screws

Flanges are connected between each other through discontinuous junctions, in particular through screws. A screw is a mechanical element composed of a cylindrical part, that can be fully or just in part threaded, which has an enlargement at the end, called the head, that enables the application of a tool by which it is possible to turn the screw (Fig. 3.3a). The pitch of a thread P is the distance from a point on the thread to the corresponding point on the next form, measured parallel to the axis of the screw.
The screw is engaged on a nut screw that can be obtained in the part to be connected or in a nut, which is a hexagonal or square prism with a central threaded hole. In the case reported in Fig. 3.3c, the connection is obtained through the force exerted by the screw head and by the surface of the last element in which is obtained the nut screw.
Often, a washer is placed under the screw head. It is a thin perforated disk (Fig. 3.3b) that is commonly added to screw systems to keep them tight and to distribute the load over a greater area.
As a first approximation, the flanges are sized calculating manually the loads, axial and shear, on each screw, dividing appropriately the loads acting on the flanges, reported in Table 3.1 and Table 3.2.

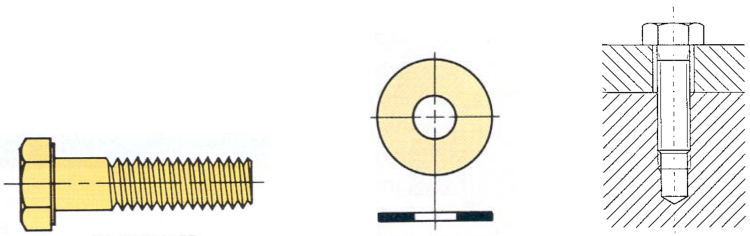

(a) Screw and thread representation [22] **(b)** Flat washer [22] **(c)** Draw of a screw [5]

Figure 3.3: Screw

It can be assumed that in the case of axial and shear forces, the load is equally splitted between the screws. Screws react to torsion with a shear load proportional to the distance of the screw with respect to the center of gravity of the flange, and the direction of the reaction is perpendicular to the line joining the CoG and the screw. The bending moment induces a compression on the screws on a certain side of the neutral axis, and a tension on the other. The magnitude of the load increases linearly with the distance from this axis. It is important to highlight that this is an ideal way to partition the loads. In reality, there will be concentrations of loads in some screws, so at this point, just a preliminary design of the flange is needed. This initial flange will be studied through a structural analysis in order to have a simulation of a behavior nearer to the real one, which will be studied in Ch. 5.
In Fig. 3.4 the divisions of the loads are reported and the equations used to evaluate the axial and shear loads on each screw, respectively defined P and V, are:

- From axial force: $P_i = \frac{N}{\#screws}$;
- From bending moment: $P_i = \frac{M_b}{\sum_i d_i^2} d_i$;
- From shear force: $V_i = \frac{T}{\#screws}$;
- From torsional moment: $V_i = \frac{M_t}{\sum_i r_i^2} r_i$.

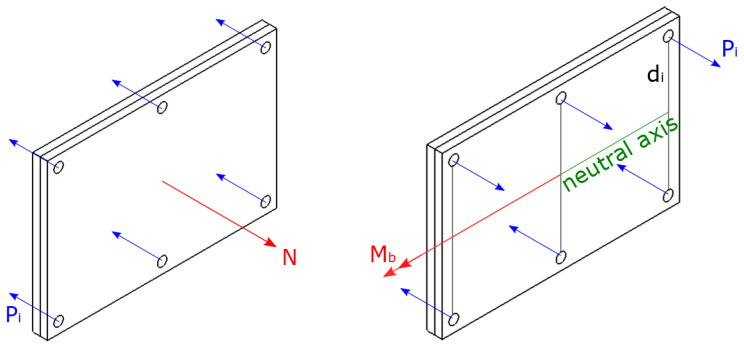

(a) Splitting of axial force **(b)** Splitting of bending moment

(c) Splitting of shear force **(d)** Splitting of torsional moment

Figure 3.4: Splitting of loads between screws

3.3 Factors affecting verifications

Before calculating axial and shear loads on each screws, it is important to see what are the main parameters that influence loads and checks.
First of all, the number of screws influences the split of the loads on each screw, but also the stiffness of the flange. An overestimated number of screws could grant a tight connection between the flanges, but weakens the flanges themselves; this due to the notch effect introduced by the holes on the plates. In some cases it is hard to access the screw because of the encumbrance of the structure, making the integration difficult or even impossible. It is important to guarantee the space needed to tighten the screws.
A critical role is played by material and metric size of the screws. Stainless steel is chemical and corrosion resistant, it contains a great number of variants, depending on their metallurgical structure this field has been divided into three groups: austenitic (A), ferritic (F) and martensitic (C) [30]. The austenitic group is the most used for fasteners and is further subdivided into five steel grades, each with a different chemical composition and so a different resistance to corrosion. The most common steel grade is A2. Austenitic stainless steel can be strengthened by cold-working, increasing the mechanical properties. The austenitic grades are divided into three property classes 50, 70 and 80, depending on the method of manufacturing. The minimum tensile strength, that denotes the load at which the material breaks, with measure of unit $\left[\frac{N}{mm^2}\right]$, is obtained multiplying the property class by 10. 70 is the most universal and applied property class, while 80 is the highest one. Another important mechanical property is the 0.2% yield strength, that denotes the load that will lead to 0.2 plastic deformation, for A2-70 is $450\left[\frac{N}{mm^2}\right]$ [25].
There are classes of screws with an higher tensile strength but a lower corrosion resistance, that had been heat treated. Class 8.8 is made of medium carbon steel, quenched and tempered, or classes 10.9 and 12.9 are made of medium carbon alloy steel, quenched and tempered. The number before the decimal point, when multiplied by a hundred, gives the nominal tensile strength in $[MPa]$. The digit following the decimal point, multiplied by ten and by the previous digit, gives the yield stress in $[MPa]$ [23]. For example, class 12.9 has a tensile strength of $1200MPa$ and a yield stress of $1080MPa$.
Screw metric size is defined by the letter M followed by a number that is the major nominal diameter of the screw in millimeters. For example, a screw with metric size M12 has the widest diameter of the threaded section that is $12mm$. This number is related to the pitch. There are two kind of pitch, coarse and fine, the coarse pitch is the commonly used default pitch and, if the nominal diameter of the screw is $12mm$, it will be $1.75mm$. This value is linked to the length of threads used, L_{TU}, which is equal to the pitch per the number of threads used, that must be at least four. This number influences the thread pull-out that will be described in Sec. 3.4.2.
The other main characters are the flanges. Sizes and material are of great importance to pass the checks. In particular, material and thickness of the flange influence all the verification explained in Sec. 3.5. A material with higher ultimate and yield strength and a flange thicker lead to a stronger flange. The last parameter is the distance between center hole and plate edge, c, that impacts on failure in tension (Sec. 3.5.1) and on shear tear out (Sec. 3.5.2).
In the following are reported the values chosen for preliminary calculations. The selected screw metric size is M12 and the material is an alloy steel, quenched and tempered, class 12.9. This means that the thread diameter of the screw is $12mm$ and the pitch is $1.75mm$ [27]. The material class 12.9 has a nominal tensile strength of $1200MPa$, that denotes the load at which the material breaks, while the 0.2% yield strength is $1080MPa$.

The washer has been selected following the International standard DIN 433. The relevant dimensions, represented in Fig. 3.5, are:

$$\begin{cases} d_1 = 13mm \\ d_2 = 20mm \\ h = 2mm \end{cases} \tag{3.2}$$

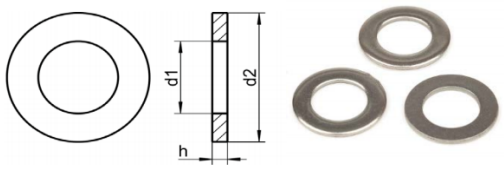

Figure 3.5: Washer [24]

In Fig. 3.6 and Table 3.3, relevant lengths and their values are reported.

Table 3.3: Sizes for verifications

Plate thickness	t_{flange}	$[mm]$	16.00
Flexible screw length	L_f	$[mm]$	18.00
Distance between center hole and plate edge	c	$[mm]$	15.00
Length of threads used	L_{TU}	$[mm]$	12.00
Plate hole diameter	d_f	$[mm]$	12.50
Thread mean diameter	d_{pitch}	$[mm]$	10.86
Washer mean diameter	d_w	$[mm]$	18.00
Nominal diameter of screw	d_n	$[mm]$	12.00
Minimum stem diameter	d_{Cyl}	$[mm]$	12.00

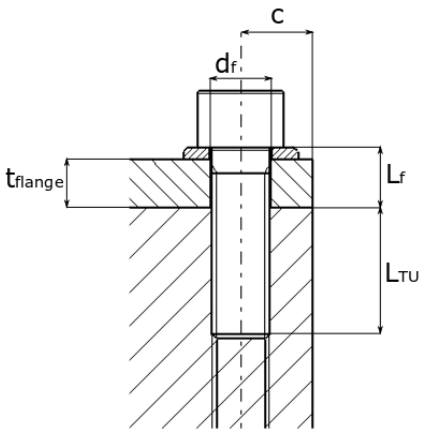

Figure 3.6: Relevant lengths in screw verification

3.4 Screws verifications

In this section, it will be discussed how the screws can be verified, in order to dimension the flanges. Structural screws have been verified against ultimate, yield, pull out of threads, joint separation and sliding, according to [13].
First of all, the maximum and minimum preloads are introduced. They are a reasonable estimate of the maximum and minimum expected preloads in a bolted joint at operating conditions, respectively. They are calculated in the following way:

$$\begin{cases} PLD_{max} = (1+\Gamma)PLD + P_{t_{pos}} \\ PLD_{min} = (1-\Gamma)PLD - P_{t_{neg}} - P_{loss} \end{cases} \tag{3.3}$$

where:

- Γ is a uncertainty, that for torque-measurement of lubricated bolts is $\Gamma = \pm 35\%$;
- PLD is the nominal preload;
- $P_{t_{pos}}$ is the positive thermal load, the thermally induced load that increases the preload;
- $P_{t_{neg}}$ is the negative thermal load, the thermally induced load that decreases the preload;
- P_{loss} is the expected preload loss, a method of calculating this loss in joints, that have metal-to-metal contact throughout their thickness, is $P_{loss} = 5\% \, of \, PLD_{max}$, Paragraph 3.6 of [13].

The nominal preload can be calculated in this way:

$$PLD = \frac{T_{eff}}{\frac{d_{pitch}}{2} \cdot \tan(\alpha + \varphi) + \mu_1 \cdot \frac{d_w}{2}} \tag{3.4}$$

where:

- T_{eff} is the effective torque: the applied torque T_{app} minus the torque absorbed by self-locking helicoil T_h;
- d_{pitch} is the medium diameter of thread;
- $\alpha = \arctan\left(\frac{p}{d_{pitch}\pi}\right)$, where p is the thread pitch;
- $\varphi = \arctan\left(\frac{\mu_2}{\cos(30°)}\right)$, where μ_2 is the friction coefficient on screw thread;
- μ_1 is the friction coefficient between bolt and plate;
- d_w is the medium diameter of screw head.

The effective torque is:

$$T_{eff} = T_{app} - T_h = \left[v \cdot \left(\frac{\mu_1 d_w}{2} + \frac{d_{pitch}}{2} \cdot \tan\left(\alpha + \varphi\right)\right) + T_h\right] \cdot F_{TT} - T_h \tag{3.5}$$

where:

- $v = f(\sigma_{ys}, \alpha, \varphi, d_{pitch}, d_{core})$, where $d_{core} = d_n - 1.2269 \cdot p$, is the thread working section diameter and d_n is the nominal screw diameter;
- F_{TT} is the ration between applied torque and yield torque.

The axial bolt load is calculating using the following equation:

$$Pb_i = PLD_{max} + n\phi(FF \cdot SF_i \cdot P) \tag{3.6}$$

where:

- n is the loading plane factor;
- ϕ is the stiffness parameter;
- FF is the fitting factor to be applied to axial and shear loads;
- SF_i is the safety factor;
- P is the external axial load;
- $i = u$, y, po stays for: ultimate, yield and thread pull-out.

The stiffness parameter can be calculated in this way:

$$\phi = \frac{k_s}{k_s + k_g} \tag{3.7}$$

where:

- $k_s = \frac{E_s A_{pitch}}{L_f}$ is the screw's stiffness, the screw mean section is $A_{pitch} = \frac{d_{pitch}^2 \pi}{4}$;
- $k_g = \frac{E_g A_g}{L_f}$ is the washer's stiffness, the equivalent section clamped flange is $A_g = \frac{d_n^2 \pi}{4}$.

3.4.1 Screw integrity

Screws must maintain their form in order to properly work. Their integrity is based on yield and ultimate strength, screws must not break but also must not deform plastically. Bolt strength is checked at maximum external load and maximum preload.
Screw verification in case of axial and shear loads combined is controlled in the following way:

$$SV_i = 1 - [R_{a_i}^2 + R_{s_i}^3] \tag{3.8}$$

where:

- $R_{a_i} = max\left(\frac{Pb_i}{PA_t}; \frac{SF_i \cdot P}{PA_t}; \frac{PLD_{max}}{PA_t}\right)$, where PA_t is the axial load allowable of bolt due to tension, SF_i is the screw safety factor;
- $R_{s_i} = \frac{V \cdot SF_i}{VA}$, where V is the external shear load and VA is the shear load allowable of bolt;
- $i = u$, y stays for: ultimate and yield.

The axial loads allowable of bolt due to tension for yield and ultimate strength are:

$$\begin{cases} PA_{tys} = \sigma_{ys} A_{min} \\ PA_{tus} = \sigma_{us} A_{min} \end{cases} \tag{3.9}$$

where A_{min} is the smallest area between the working stem section and the working thread section:

$$A_{min} = min\Big(A_{Cyl} = \frac{d_{Cyl}^2 \pi}{4}; A_{core} = \frac{d_{core}^2 \pi}{4}\Big) \tag{3.10}$$

d_{Cyl} is the minimum stem diameter.
The shear loads allowable of bolt are:

$$\begin{cases} VA_{ys} = \sigma_{\nu ys} A_{min} \\ VA_{us} = \sigma_{\nu us} A_{min} \end{cases} \tag{3.11}$$

where:

$$\begin{cases} \sigma_{\nu ys} = 0.62 \cdot \sigma_{ys} \\ \sigma_{\nu us} = 0.62 \cdot \sigma_{us} \end{cases} \tag{3.12}$$

Conditions that shall be verified are:

$$\begin{cases} SV_y > 0 \\ SV_u > 0 \end{cases} \tag{3.13}$$

It can be interesting to discuss how a screw behaves if it meets a plastic deformation. In a flange, there is a certain number of screws that partition the loads. Depending on the position of a screw, it will receive a certain load, that can be lower or greater than the one on another screw in a different position. So there will be a screw reaching the plastic field firstly. The load inducing a plastic deformation depends on the material of the screw, when the specific yield strength is reached that screw cannot overcome this stress, so the remaining load will be divided only between the screws that are still in the elastic field. This attitude, described in [17], allows having an additional safety in case of an unforeseen event bringing to plastic deformation, that wards off the risk of screw break.

3.4.2 Thread pull-out

For thread pull-out (Fig. 3.7), margins of safety are:

$$MS_{po} = \frac{PA_{po_i}}{Pb_{po}} - 1 \tag{3.14}$$

where:

- PA_{po_i} is the allowable load of screw thread or female thread, that is linearly dependent on the number of threats used;
- $i = s,\ f$ stays for: screw and female;

The allowable loads of screw thread and female thread are:

$$\begin{cases} PA_{pouts} = \frac{\pi L_{TU} d_{core} \cdot 0.75 \cdot \sigma_{us}}{\sqrt{3}} \\ PA_{poutf} = \frac{\pi L_{TU} d_n \cdot 0.875 \cdot \sigma_{uf}}{\sqrt{3}} \end{cases} \tag{3.15}$$

The condition that shall be verified is:

$$MS_{po} > 0 \tag{3.16}$$

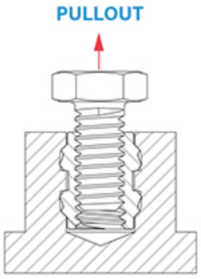

Figure 3.7: Thread pull-out [29]

3.4.3 Joint separation and sliding

Joint separation is checked at maximum external load and minimum preload.
Safety margins for joint separation and sliding are:

$$MS_{js} = \frac{PLD_{min}}{[(1 - n \cdot \phi)P_{js}]} - 1 \tag{3.17}$$

$$MS_{sl} = \frac{[PLD_{min} - (1 - n \cdot \phi)P_{sl}]\mu_{sl}}{V \cdot FF} - 1 \tag{3.18}$$

where:

- $P_{js} = P \cdot FF \cdot SF_{js}$, where SF_{js} is the screw safety factor against joint separation;
- $P_{sl} = P \cdot FF \cdot SF_{sl}$, where SF_{sl} is the screw safety factor against sliding;
- μ_{sl} is the friction coefficient between screwed flanges.

Conditions that shall be verified are:

$$\begin{cases} MS_{js} > 0 \\ MS_{sl} > 0 \end{cases} \tag{3.19}$$

When the local sliding is not verified, the global sliding has to be checked, because it is not considered critical if the structural integrity of all screws and flanges is verified and because it does not affect the functionality. The global sliding is calculated as:

$$MoS_{sl} = \frac{PLD_{min} \cdot \mu_{sl} \cdot n_s}{P_{shear} \cdot FOS} - 1 \tag{3.20}$$

where:

- n_s is the number of screws of the junction;
- $P_{shear} = m_{sist} \cdot a_i \cdot g$, where m_{sist} is the mass of the sistem and a_i is the number of g;
- FOS is the factor of safety for global sliding.

3.5 Flanges verifications

Not only screws need to be verified, but also flanges must be checked. Flange of structural screws is verified against plate failure by tension, shear tear out and bearing, according to [1]. The verification is performed with the assumption that shear load is fully supported by screw and not by friction. All the margins of safety must be positive to avoid any flange failure.

3.5.1 Tension

Fig. 3.8 indicates how a flange can pull apart due to tension stress on a section through the centerline of the bolt hole. In this case, the safety margins are:

$$MS_{i_{pt}} = \frac{PA_{i_{pt}}}{V \cdot FF \cdot SF_{ip}} - 1 - 0.25 \tag{3.21}$$

where:

- $PA_{i_{pt}} = \sigma_{i_p} A_{pt}$ is the axial load allowable to tension of plate material, where $A_{pt} = (L_{pt} - D)t$ is the cross section area;
- 0.25 is a coefficient that takes into account that tensile stress on cross section is not uniform, because there is a stress concentration around the hole [1];
- $i = u$, y stays for ultimate and yield.

Failure by tension must be considered only for plates where the joint geometric condition is tension critical, so in cases with $\frac{L_{pt}}{2} > 5D$ this verification is not considered.

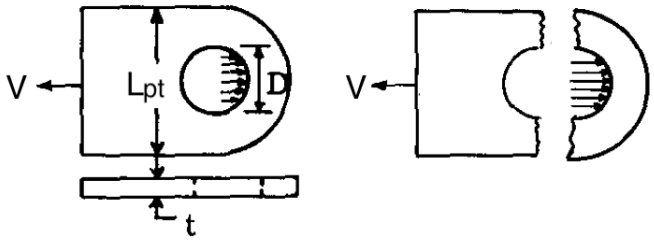

Figure 3.8: Flange failure by tension [1]

3.5.2 Shear tear out

In Fig. 3.9 is reported the flange failure by shear tear out of a plate sector in front of the bolt. The load V causes the bolt to press on the plate around the bolt hole edge and the stresses produced tend to tear out the portion. The safety margins are calculated in the following way:

$$MS_{i_{sto}} = \frac{VA_{i_p}}{V \cdot FF \cdot SF_{i_p}} - 1 \tag{3.22}$$

where:

- $VA_{i_p} = \sigma_{\nu_{i_p}} A_{sto}$, where $\sigma_{\nu_{i_p}} = \frac{\sigma_{ip}}{\sqrt{3}}$ is the shear strength of plate material and $A_{sto} = 2\left(c - \frac{d_p}{2}\right) \cdot t_{flange}$ is the shear out area and t_{flange} is the plate thickness. This is slightly conservative since the actual shear area is larger;
- $i = u$, y stays for ultimate and yield.

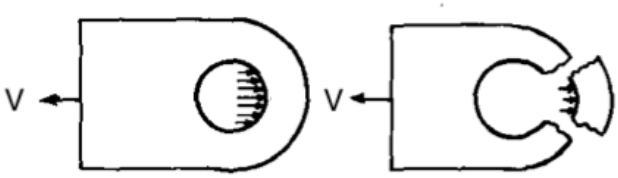

Figure 3.9: Flange failure by shear tear out [1]

3.5.3 Bearing

The pull V causes the bolt to press against the bushing wall which in turn presses against the plate wall, if the pressure is high enough the plate portion adjacent to the wall will crush, which results in the elongated hole reported in Fig. 3.10. The safety margin is:

$$MS_b = \frac{PA_{bup}}{V \cdot FF \cdot SF_{up} \cdot SF_b} - 1 \tag{3.23}$$

where:

- PA_{bup} is the bearing load allowable for plate material;
- SF_{up} is the plate safety factor against ultimate;
- SF_b is the bearing safety factor.

The bearing load allowable for plate material is:

$$PA_{bup} = \sigma_{cup} A_b \tag{3.24}$$

where:

- $\sigma_{cup} = \sigma_{up} \cdot 1.55$ is the ultimate compression strength of plate material;
- $A_b = D_b t$ is the bearing area, D_b is the bolt diameter.

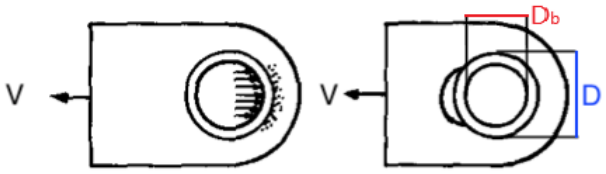

Figure 3.10: Flange failure by bearing [1]

In Table 3.4, are reported stresses and young modules of different parts, needed for calculations, while coefficients and values of terms described before can be found in Table 3.5.

Table 3.4: Material properties used for verifications

Young module of screws	E_s	$[MPa]$	$2.10 \cdot 10^5$
Yield stress of screws	σ_{ys}	$[GPa]$	$1.08 \cdot 10^0$
Ultimate stress of screws	σ_{us}	$[GPa]$	$1.20 \cdot 10^0$
Ultimate stress of female screw	σ_{uf}	$[GPa]$	$5.10 \cdot 10^{-1}$
Young module of clamped flange	E_g	$[MPa]$	$2.10 \cdot 10^5$

Table 3.5: Values used for verifications

Positive thermal load	$P_{t_{pos}}$	$[N]$	0
Negative thermal load	$P_{t_{neg}}$	$[N]$	0
Self-locking helicoil friction torque	T_h	$[N \cdot mm]$	0
Friction coefficient between screw head and washer	μ_1	$[-]$	0.15
Ration between applied torque and yield torque	F_{TT}	$[-]$	0.80
Friction coefficient between screw head and insert threads	μ_2	$[-]$	0.10
Loading plane factor	n	$[-]$	0.50
Fitting factor	FF	$[-]$	1.15
Yield safety factor	SF_y	$[-]$	3
Ultimate safety factor	SF_u	$[-]$	4
Safety factor against thread pull-out	SF_{po}	$[-]$	2
Screw safety factor against joint separation	SF_{js}	$[-]$	1.20
Screw safety factor against sliding	SF_{sl}	$[-]$	1.20
Sliding friction coefficient	μ_2	$[-]$	0.20
Factor of safety for global sliding	FOS	$[-]$	1.15
Plate safety factor against yield	SF_{yp}	$[-]$	3
Plate safety factor against ultimate	SF_{up}	$[-]$	4
Bearing safety factor	SF_b	$[-]$	3

3.6 Results of verifications

In this section are exposed flanges A and B with their screws and the results of verifications. The first step is to calculate manually shear and axial loads on each screw dividing the total loads as discussed in Sec. 3.2. V and P on each screw depend only on the number of screws and their positions. Once the loads have been calculated, an approximated idea of the screw's metric and material needed is obtained and also if the values, reported in Table 3.3, can be suitable for the specific flange. To improve the situation the margins of safety must be evaluated.
Starting with Flange B, the quantities proposed in Table 3.3 are good and using ten screws M12 and material class 12.9 the verifications are reported in Table 3.6, while the scheme of Flange B with relevant dimensions and ID number of each screw is in Fig. 3.11b.
Flange A is subjected to lower loads then Flange B, so the number of screws can be reduced to eight. Keeping the other quantities unchanged, all the checks are overcome easily, in particular, margins of safety for shear tear out and bearing are high, so flange's thickness can be reduced from $16mm$ to $12mm$. The results are showed in Table 3.6 and Flange A is reported in Fig. 3.11a.
Negative values in the verifications are written in red. Even if some safety margins for sliding are negative, the check is passed because, as discussed in Sec. 3.4.3, the global slidings are:

$$\begin{cases} MoS_{sl\_A} = 2.46 \\ MoS_{sl\_B} = 2.94 \end{cases} \tag{3.25}$$

In the column "Joint separation", is written "FALSE" when this condition is impossible to be reached since P is negative so there is a compression and the flanges cannot separate.

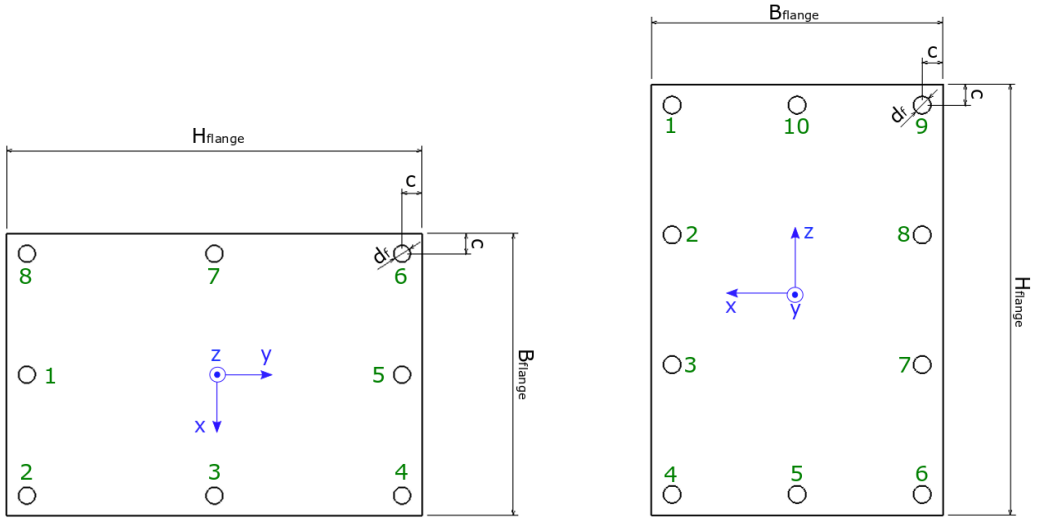

(a) Flange A **(b)** Flange B

Figure 3.11: Flanges A and B with relevant lengths

The flanges A that are welded to oblique supports have a different H_{flange}, but equal number of screws, so their relative distance will be smaller or higher depending on the trolley sizes.

Table 3.6: Results of verifications on Flange A and B

Flange A												
			Tension	SV Screw		Pull Out		Joint sep.	Sliding	Shear tear out		Bearing
# Screw	V [N]	P [N]	$\sigma_{id}\,[MPa]$	SV_u	SV_y	MS_{po_s}	MS_{po_f}	MS_{js}	MS_{sl}	MS_{u_sto}	MS_{y_sto}	MS_b
1	1318	-14701	857	0.91	0.89	1.73	0.65	FALSE	5.00	9.20	8.46	5.26
2	1318	-14701	857	0.91	0.89	1.73	0.65	FALSE	5.00	9.20	8.46	5.26
3	1318	-14701	857	0.91	0.89	1.73	0.65	FALSE	5.00	9.20	8.46	5.26
4	1318	-14701	857	0.91	0.89	1.73	0.65	FALSE	5.00	9.20	8.46	5.26
5	1318	11186	852	0.43	0.33	1.80	0.69	0.99	0.79	9.20	8.46	5.26
6	1318	11186	852	0.43	0.33	1.80	0.69	0.99	0.79	9.20	8.46	5.26
7	1318	11186	852	0.43	0.33	1.80	0.69	0.99	0.79	9.20	8.46	5.26
8	1318	11186	852	0.43	0.33	1.80	0.69	0.99	0.79	9.20	8.46	5.26
Flange B												
			Tension	SV Screw		Pull Out		Joint sep.	Sliding	Shear tear out		Bearing
# Screw	V [N]	P [N]	$\sigma_{id}\,[MPa]$	SV_u	SV_y	MS_{po_s}	MS_{po_f}	MS_{js}	MS_{sl}	MS_{u_sto}	MS_{y_sto}	MS_b
1	5092	2947	856	0.43	0.34	1.97	0.80	6.54	-0.19	2.52	2.27	1.16
2	3629	-3290	847	0.88	0.87	1.97	0.79	FALSE	0.51	3.94	3.58	2.03
3	3282	-9526	855	0.89	0.88	1.83	0.71	FALSE	1.07	4.46	4.07	2.35
4	4328	-15763	871	0.87	0.86	1.71	0.64	FALSE	0.88	3.14	2.84	1.54
5	3065	-9355	854	0.90	0.88	1.84	0.71	FALSE	1.21	4.85	4.43	2.59
6	3112	-2947	844	0.89	0.88	1.97	0.80	FALSE	0.73	4.76	4.34	2.53
7	1315	3290	839	0.49	0.38	1.97	0.79	5.76	2.09	12.63	11.65	7.37
8	2032	9526	851	0.44	0.34	1.83	0.71	1.33	0.34	7.82	7.19	4.41
9	4109	15763	870	0.36	0.27	1.71	0.64	0.41	-0.66	3.36	3.05	1.68
10	4073	9355	859	0.41	0.32	1.84	0.71	1.38	-0.32	3.40	3.08	1.70

Chapter 4

Rotating frame

This chapter is focused on the rotating frame of the trolley. In the first part, different kinds of bridges are presented and their beams are sized. Later, flanges and screws of the rotating frames are designed and verified, like in Ch. 3. Finally, the shafts, that connect the two frames and allow the rotation of the bridge, are studied.

4.1 Bridges

The other frame of the trolley is the rotating frame or bridge. The bridge is the rotating deck and it has a main structure composed of beams, that can be welded or connected through flanges, sustaining a dedicated plate on which the instrument interfaces in its different configurations. The interface is the part of the trolley that connects the rotating frame to the payload. It must allow access to the bottom of the instrument or, at least, foreseen the ability to remove part of itself to obtain it. In fact, the interface can be composed of different plates regulated to be one single plane, so it is possible to vary the interface changing the plates according to the configuration of the payload.
On the bridge are screwed shafts that connect it to the main frame and enable the rotation. Acting on the rotation mechanism it is possible to vary the orientation of the Z-axis of the payload with respect to the gravity.
Balancing masses are foreseen on the bridge to allow rotation for all the different configurations of the instrument because each configuration can have different mass and different CoG position. The goal is to have the center of gravity position of rotating mass as close as possible to the rotation axis. These masses can be on different locations to enable adjustments of CoG position along different axes.

Since the trolley is modular and it is not designed for a specific payload, different kinds of bridges will be studied to allow its use to different instruments or parts of them. In this chapter, the main structure of the bridges is sized and its beams are connected through flanges. The choice of the flanges is preferred to weldings because of the main goal of this thesis, i.e. the aim of design a modular trolley. Screws can be removed do disassemble flanges, while weldings are permanent connections, so different trolleys can be build starting from a common beam.
The three types of projected rotating frames are:

- Bridge 1: its main structure is U-shaped, composed of three beams, as can be seen in Fig. 4.1a;
- Bridge 2: it is made up of only one beam placed on the rotational axis (Fig. 4.1b).

This kind of rotating frame is used for instruments with a dimension much smaller than the other two;

- Bridge 3: this configuration has a rectangular base that allows access to the instrument from below and it is reported in Fig. 4.1c.

The sizing is performed for the large trolley, so these bridges have the largest possible sizes. The maximum available encumbrance has the following values along the three principal directions X, Y, Z:

$$\begin{cases} L_x = 2000mm \\ L_y = 2100mm \\ L_z = 1000mm \end{cases} \tag{4.1}$$

The beams are sized using these values even if, as can be seen in Fig. 4.1, usually, they are shorter. This is done to consider the worst possible condition to be sure that the beams will withstand the loads in each configuration.

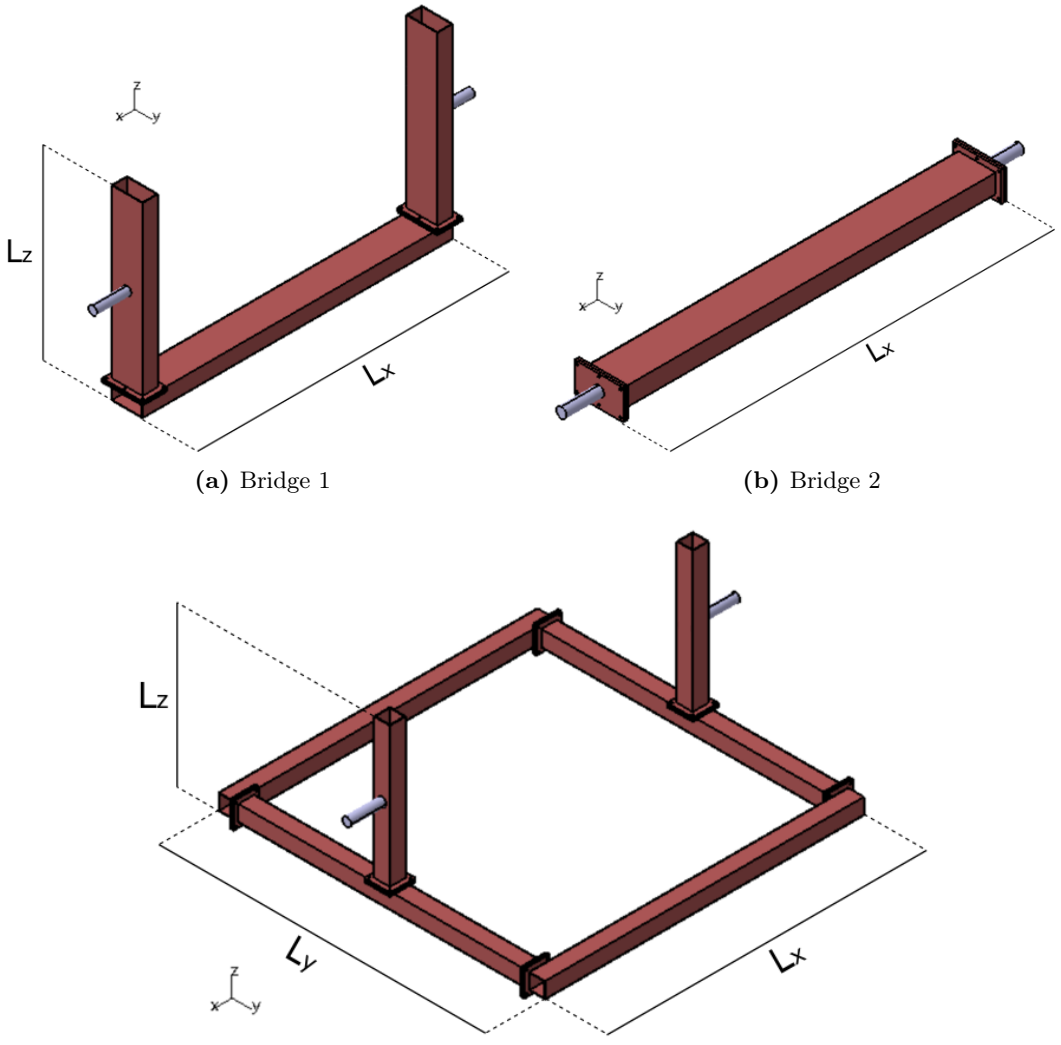

(a) Bridge 1

(b) Bridge 2

(c) Bridge 3

Figure 4.1: Three rotating frames

4.2 Sizing beams

In this section, beams of the different rotating frames are sized. This is done in the same way as the sizing of beams of the main frame in Sec. 2.3.3. Both lateral and vertical accelerations must be considered, but this time there is only the mass of the payload, not the one of the bridge, and it is concentrated in the center of gravity of the payload, taking into account maximum dimensions and homogeneous distribution of the mass. Bridge 2 can be seen as Bridge 1 with vertical beams with zero length, so the sizing for these two rotating frames is the same. Concerning Bridge 3, the payload is supported by two beams, so its mass is split between them. In Fig. 4.2, are reported the drawing of the main beams of the three bridges together with the position of flanges, characteristic lengths and mass. The values are:

$$\begin{cases} x_2 = \frac{L_x}{2} = 1000mm \\ z_2 = \frac{L_z}{2} = 500mm \\ m_p = 600kg \end{cases} \tag{4.2}$$

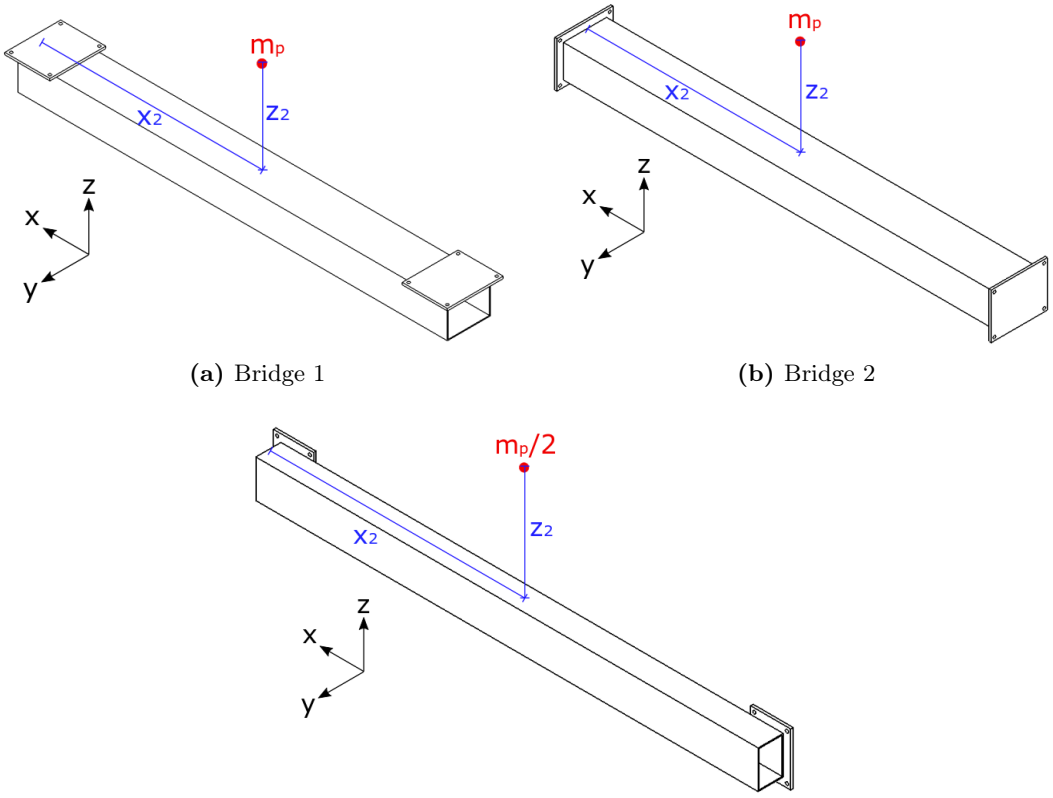

(a) Bridge 1

(b) Bridge 2

(c) Bridge 3

Figure 4.2: Schemes of rotating frames

The beams have the same constraints of the beam in Sec. 2.3.3, so they are simply-supported both in vertical and lateral directions, and they have a constraint that avoids the rotation around the axis of the beam.

After some comparisons of masses and margins of safety changing the section of the beam, the characteristic dimensions of beams of Bridges 1 and 2, that are associated with the lower mass, are:

$$\begin{cases} B_{B12} = 100mm \\ H_{B12} = 200mm \\ t_{B12} = 4mm \end{cases} \tag{4.3}$$

These beams, like the ones of the main frame, are made of Fe510, whose properties are shown in Table 2.3. The masses of the bridges are:

$$\begin{cases} m_{B1} = 70.88kg \\ m_{B2} = 34.44kg \end{cases} \tag{4.4}$$

In the following, the calculations to obtain the margins of safety are reported. The shear forces and their stresses are:

$$\begin{cases} T_v = \frac{F_v}{2} = \frac{f_v m_p}{2} = 5.89 \cdot 10^3 N \\ T_l = \frac{F_l}{2} = \frac{f_l m_p}{2} = 4.41 \cdot 10^3 N \\ \tau_{F_v} = \frac{T_v S}{2 t_{B12} I_H} = 6.58 \cdot 10^{-3} GPa \\ \tau_{F_l} = \frac{T_l S}{2 t_{B12} I_B} = 1.67 \cdot 10^{-3} GPa \end{cases} \tag{4.5}$$

where:

$$\begin{cases} S = t_{B12} \frac{(B_{B12} - t_{B12}) \cdot (H_{B12} - t_{B12})}{2} \\ I_B = \frac{1}{12} \Big((B_{B12} H_{B12}^3) - (B_{B12} - 2t_{B12})(H_{B12} - 2t_{B12})^3 \Big) \\ I_H = \frac{1}{12} \Big((H_{B12} B_{B12}^3) - (H_{B12} - 2t_{B12})(B_{B12} - 2t_{B12})^3 \Big) \end{cases} \tag{4.6}$$

Bending and torsional moments and the stresses induces by them are:

$$\begin{cases} M_{b\_F_v\_max} = \frac{F_v L_{hB}}{4} = 5.89 \cdot 10^3 Nm \\ M_{b\_F_l\_max} = \frac{F_l L_{hB}}{4} = 4.41 \cdot 10^3 Nm \\ M_{t\_F_l} = \frac{F_l L_{vB}}{2} = 4.41 \cdot 10^3 Nm \\ \sigma_{F_v} = \frac{M_{b\_F_v\_max} B_{B12}}{2 I_H} = 6.99 \cdot 10^{-2} GPa \\ \sigma_{F_l} = \frac{M_{b\_F_l\_max} H_{B12}}{2 I_B} = 3.56 \cdot 10^{-2} GPa \\ \tau_{M_t} = \frac{M_{t\_Fl}}{2 \Omega t_{B12}} = 2.93 \cdot 10^{-2} GPa \end{cases} \tag{4.7}$$

where:

$$\Omega = (B_{B12} - t_{B12}) \cdot (H_{B12} - t_{B12}) \tag{4.8}$$

The equivalent stress is:

$$\sigma_{eq} = \sqrt{\sigma_{F_v}^2 + \sigma_{F_l}^2 - \sigma_{F_v} \sigma_{F_l} + 3(\tau_{F_v} + \tau_{F_l} + \tau_{M_t})^2} = 8.89 \cdot 10^{-2} GPa \tag{4.9}$$

Finally, the margins of safety are:

$$\begin{cases} MoS_y = \frac{R_y}{\sigma_{eq} \cdot SF_y} - 1 = 3.31 \cdot 10^{-1} \\ MoS_u = \frac{R_u}{\sigma_{eq} \cdot SF_u} - 1 = 4.34 \cdot 10^{-1} \end{cases} \tag{4.10}$$

where the safety factors are again 3 for yield stress and 4 for ultimate stress.

The same procedure is used to size the beams of Bridge 3. This time the mass of the payload to be considered is just half of the total mass because the instrument leans on two beams. The material is always Fe510. The characteristics of section and mass of this bridge are:

$$\begin{cases} B_{B3} = 100mm \\ H_{B3} = 100mm \\ t_{B3} = 4mm \\ m_{B3} = 122.2kg \end{cases} \tag{4.11}$$

Hereafter the values of shear forces and their tensions are reported:

$$\begin{cases} T_v = \frac{F_v}{2} = \frac{f_v m_p}{4} = 2.94 \cdot 10^3 N \\ T_l = \frac{F_l}{2} = \frac{f_l m_p}{4} = 2.21 \cdot 10^3 N \\ \tau_{F_v} = \frac{T_v S}{2 t_{B3} I_B} = 2.87 \cdot 10^{-3} GPa \\ \tau_{F_l} = \frac{T_l S}{2 t_{B3} I_H} = 2.15 \cdot 10^{-3} GPa \end{cases} \tag{4.12}$$

where:

$$\begin{cases} S = t_{B3} \frac{(B_{B3} - t_{B3}) \cdot (H_{B3} - t_{B3})}{2} \\ I_B = \frac{1}{12} \Big((B_{B3} H_{B3}^3) - (B_{B3} - 2t_{B3})(H_{B3} - 2t_{B3})^3 \Big) \\ I_H = \frac{1}{12} \Big((H_{B3} B_{B3}^3) - (H_{B3} - 2t_{B3})(B_{B3} - 2t_{B3})^3 \Big) \end{cases} \tag{4.13}$$

Bending and torsional moments and the stresses induces by them are set out below:

$$\begin{cases} M_{b\_F_v\_max} = \frac{F_v L_{hB}}{4} = 2.94 \cdot 10^3 Nm \\ M_{b\_F_l\_max} = \frac{F_l L_{hB}}{4} = 2.21 \cdot 10^3 Nm \\ M_{t\_F_l} = \frac{F_l L_{vB}}{2} = 2.21 \cdot 10^3 Nm \\ \sigma_{F_v} = \frac{M_{b\_F_v\_max} B_{B3}}{2 I_B} = 6.23 \cdot 10^{-2} GPa \\ \sigma_{F_l} = \frac{M_{b\_F_l\_max} H_{B3}}{2 I_H} = 4.67 \cdot 10^{-2} GPa \\ \tau_{M_t} = \frac{M_{t\_Fl}}{2 \Omega t_{B3}} = 2.99 \cdot 10^{-2} GPa \end{cases} \tag{4.14}$$

where:

$$\Omega = (B_{B3} - t_{B3}) \cdot (H_{B3} - t_{B3}) \tag{4.15}$$

The equivalent stress is:

$$\sigma_{eq} = \sqrt{\sigma_{F_v}^2 + \sigma_{F_l}^2 - \sigma_{F_v} \sigma_{F_l} + 3(\tau_{F_v} + \tau_{F_l} + \tau_{M_t})^2} = 8.26 \cdot 10^{-2} GPa \tag{4.16}$$

The margins of safety are:

$$\begin{cases} MoS_y = \frac{R_y}{\sigma_{eq} \cdot SF_y} - 1 = 4.33 \cdot 10^{-1} \\ MoS_u = \frac{R_u}{\sigma_{eq} \cdot SF_u} - 1 = 5.44 \cdot 10^{-1} \end{cases} \tag{4.17}$$

4.3 Sizing flanges

In this section, the flanges of the bridges are sized. Beams of Bridge 3 have a section different from the one of the other rotation frames, so also its flanges will be different. Bridges 1 and 2 have the same beams, but the flanges are welded in different points, so they will transmit the loads not in the same way. Therefore, each rotation frame has its flange: Flange C is the flange of Bridge 1, Flange C1 is the one of Bridge 2, while Flange D is associated with Bridge 3.
In Fig. 4.3, are reported the flanges with their characteristic sizes, the usual reference frame in blue, loads vectors in red and numbers of screws in green. Loads had been evaluated in Sec. 4.2 and, since on each beam there are two flanges, the values on each flange are:

- Flange C:

$$\begin{cases} N = 2.94 \cdot 10^3 N \\ T = 2.21 \cdot 10^3 N \\ Mb_{F_v} = 2.94 \cdot 10^3 Nm \\ Mb_{F_l} = 2.21 \cdot 10^3 Nm \\ Mt_{F_l} = 2.21 \cdot 10^3 Nm \end{cases} \tag{4.18}$$

- Flange C1:

$$\begin{cases} T_z = 2.94 \cdot 10^3 N \\ T_x = 2.21 \cdot 10^3 N \\ Mb_{F_v} = 2.94 \cdot 10^3 m \\ Mb_{F_l} = 2.21 \cdot 10^3 Nm \\ Mt_{F_l} = 2.21 \cdot 10^3 Nm \end{cases} \tag{4.19}$$

- Flange D:

$$\begin{cases} N = 1.10 \cdot 10^3 N \\ T = 1.47 \cdot 10^3 N \\ Mb_{F_v} = 1.47 \cdot 10^3 Nm \\ Mb_{F_l} = 1.10 \cdot 10^3 Nm \\ Mt_{F_l} = 1.10 \cdot 10^3 Nm \end{cases} \tag{4.20}$$

Dimensions of the flanges are:

$$\begin{cases} B_{flange\_C} = B_{flange\_C1} = 160mm \\ H_{flange\_C} = H_{flange\_C1} = 260mm \\ t_{flange\_C} = t_{flange\_C1} = 12mm \end{cases} \tag{4.21}$$

$$\begin{cases} B_{flange\_D} = 160mm \\ H_{flange\_D} = 160mm \\ t_{flange\_D} = 12mm \end{cases} \tag{4.22}$$

Verification on screws and flanges is performed referring to the approach outlined in Sec. 3.2. All the flanges have screws with metric size M12 and material class 12.9. The relevant lengths used in the verifications are reported in Table 4.1.
Since the loads on each flange are lower than the ones on Flange A and B, the expected number of screws is lower. The results are reported in Table 4.2.

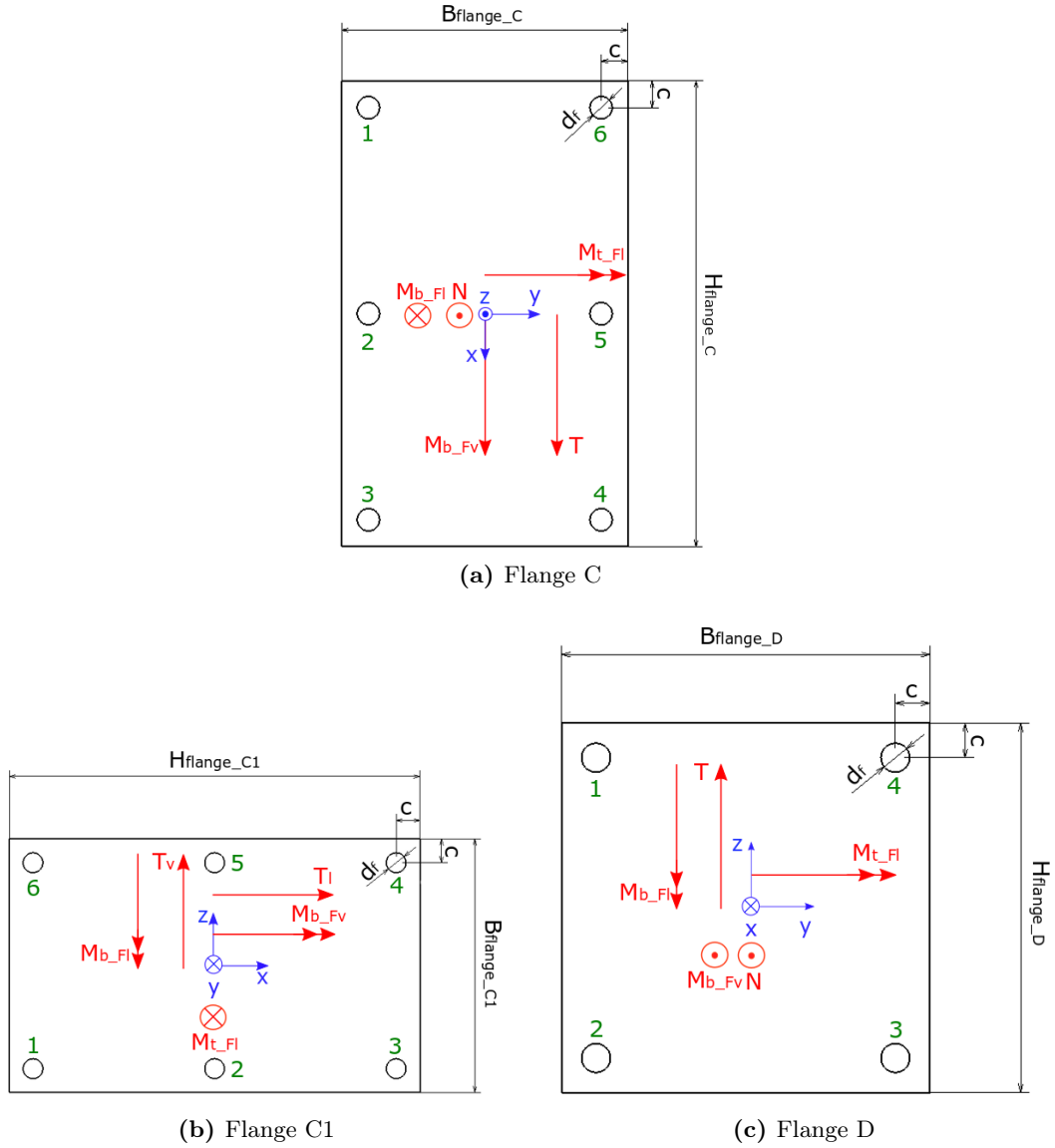

(a) Flange C

(b) Flange C1

(c) Flange D

Figure 4.3: Flanges of rotating frames

In Flange C, the highest loads are the ones on screws number 1 and 4, but the screw integrity of screw 4 is much lower than the one of screw 1. This is because the axial load on screw 1 is negative, so is a compression load that shall be added to the pre-load, that on the contrary is a tension load.
Regarding the pull out, the one of the flanges is always lower than MoS_{po} of the screw. This is due to the material: screws material is stronger than Fe510, so threads of flanges will always break before threads of screws. Anyway, this will not happen since the checks are verified. The global slidings are positive, so it is not important if some values of local sliding are negative:

$$\begin{cases} MoS_{sl\_C} = 5.20 \\ MoS_{sl\_C1} = 2.27 \\ MoS_{sl\_D} = 5.20 \end{cases} \tag{4.23}$$

Table 4.1: Lengths for verifications

Plate thickness	t_{flange}	$[mm]$	12.00
Flexible screw length	L_f	$[mm]$	14.00
Distance between center hole and plate edge	c	$[mm]$	15.00
Length of threads used	L_{TU}	$[mm]$	12.00
Plate hole diameter	d_f	$[mm]$	12.50
Thread mean diameter	d_{pitch}	$[mm]$	10.86
Washer mean diameter	d_w	$[mm]$	18.00
Nominal diameter of screw	d_n	$[mm]$	12.00
Minimum stem diameter	d_{Cyl}	$[mm]$	12.00

Table 4.2: Results of verifications on flanges of rotating frames

Flange C												
			Tension	SV Screw		Pull Out		Joint sep.	Sliding	Shear tear out		Bearing
# Screw	V [N]	P [N]	$\sigma_{id}\,[MPa]$	SV_u	SV_y	MS_{po_s}	MS_{po_f}	MS_{js}	MS_{sl}	MS_{u_sto}	MS_{y_sto}	MS_b
1	3425	-13326	862	0.89	0.88	1.76	0.66	FALSE	1.22	2.93	2.64	1.41
2	1098	-8527	847	0.91	0.89	1.85	0.72	FALSE	5.00	11.25	10.36	6.51
3	3425	-3729	847	0.89	0.88	1.96	0.78	FALSE	0.62	2.93	2.64	1.41
4	4138	11364	863	0.39	0.30	1.79	0.69	0.96	-0.44	2.25	2.01	0.99
5	2569	6565	848	0.46	0.35	1.89	0.75	2.39	0.31	4.23	3.86	2.21
6	4138	1767	847	0.47	0.37	2.00	0.81	11.58	0.06	2.25	2.01	0.99
Flange C1												
			Tension	SV Screw		Pull Out		Joint sep.	Sliding	Shear tear out		Bearing
# Screw	V [N]	P [N]	$\sigma_{id}\,[MPa]$	SV_u	SV_y	MS_{po_s}	MS_{po_f}	MS_{js}	MS_{sl}	MS_{upt}	MS_{ypt}	MS_b
1	3424	2748	845	0.48	0.37	1.98	0.80	7.09	0.22	2.93	2.64	1.41
2	2750	7546	850	0.45	0.35	1.87	0.73	1.95	0.14	3.89	3.54	2.00
3	4945	12345	869	0.36	0.28	1.78	0.68	0.80	-0.57	1.72	1.52	0.67
4	4365	-2748	850	0.87	0.86	1.98	0.80	FALSE	0.23	2.08	1.86	0.89
5	1472	-7546	846	0.91	0.89	1.87	0.73	FALSE	3.33	8.13	7.47	4.60
6	2515	-12345	857	0.90	0.88	1.78	0.68	FALSE	1.94	4.34	3.96	2.28
Flange D												
			Tension	SV Screw		Pull Out		Joint sep.	Sliding	Shear tear out		Bearing
# Screw	V [N]	P [N]	$\sigma_{id}\,[MPa]$	SV_u	SV_y	MS_{po_s}	MS_{po_f}	MS_{js}	MS_{sl}	MS_{upt}	MS_{ypt}	MS_b
1	3520	-552	842	0.89	0.88	2.03	0.83	FALSE	0.39	2.82	2.54	1.34
2	3520	7938	854	0.43	0.34	1.86	0.73	1.80	-0.13	2.82	2.54	1.34
3	4552	-552	848	0.86	0.86	2.03	0.83	FALSE	0.07	1.95	1.74	0.81
4	4552	-9041	862	0.86	0.86	1.84	0.72	FALSE	0.47	1.95	1.74	0.81

"FALSE" in the column "Joint separation" means that this condition is impossible to be reached since P is negative so there is compression and flanges cannot separate.

4.4 Shafts

Shafts are solid cylinders that connect the main frame and the rotating part, as can be seen in Fig. 4.4.

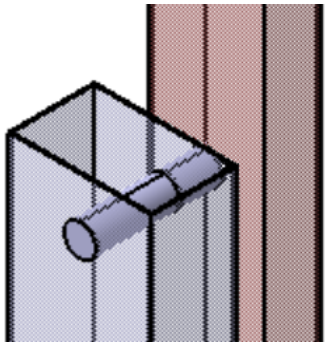

Figure 4.4: Shaft and beams

They are made of Fe510 and are verified referring to a beam model. Their length is the sum between the base B of the vertical beam of the main frame and the gap between it and the bridge equal to $70mm$. In the case of Bridge 2, this gap is $50mm$, but the shaft is the same sized for the other rotation frames.
This sizing is done via an iterative procedure, where the unknown is the diameter of the shaft. Introducing at the beginning an initial guess it is possible to dimension the shaft, finding the lower diameter guaranteeing positive margins of safety.
The relevant characteristics of the shafts are:

$$\begin{cases} D_{shaft} = 55mm \\ L_{shaft} = 220mm \\ m_{shaft} = 4.08kg \end{cases} \tag{4.24}$$

In this case, both the mass of payload and bridge are considered, but they are divided by two since there are two shafts. The shaft is approximated as a simply supported beam both in vertical and lateral directions because of the two dynamic accelerations. First of all, the stresses induced by the vertical load are evaluated. The vertical force is:

$$F_v = fd_v \frac{m_p + m_b}{2} \tag{4.25}$$

The situation is reported in Fig. 4.5.

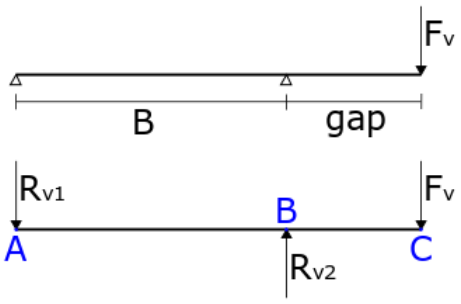

Figure 4.5: Scheme of the shaft

The sums of forces and moments about point A give the reaction forces, so shear forces and bending moments can be calculated.

$$\begin{cases} \sum F = 0 \\ \sum M_A = 0 \end{cases} \quad \begin{cases} R_{v2} = R_{v1} + F_v \\ R_{v1} \cdot 0 + R_{v2} \cdot B - F_v \cdot L_{shaft} = 0 \end{cases} \quad \begin{cases} R_{v2} = \frac{F_v \cdot L_{shaft}}{B} \\ R_{v1} = R_{v2} - F_v \end{cases} \tag{4.26}$$

$$\begin{cases} T_A = R_{v1} = 9.61 \cdot 10^3 N \\ T_B = R_{v2} - T_A = 2.06 \cdot 10^4 N \end{cases} \quad \begin{cases} M_{b(A)} = 0Nm \\ M_{b(B)} = R_{v1} \cdot B = 1.44 \cdot 10^3 Nm \\ M_{b(C)} = 0Nm \end{cases} \tag{4.27}$$

The stresses induced by maximum shear force and maximum bending moment are:

$$\begin{cases} \tau_{F_v} = \frac{4}{3\pi} \frac{T_B}{\left(\frac{D_{shaft}}{2}\right)^2} = 1.16 \cdot 10^{-2} GPa \\ \sigma_{F_v} = \frac{32 M_{b(B)}}{\pi D_{shaft}^3} = 8.83 \cdot 10^{-2} GPa \end{cases} \quad [17] \tag{4.28}$$

The same procedure is done to evaluate the stresses induced by lateral loads. Results are reported in Table 4.3.

Table 4.3: Stresses induced by lateral force F_l

$T_A = 7.21 \cdot 10^3 N$ $T_B = 1.55 \cdot 10^4 N$	$M_{b(A)} = 0Nm$ $M_{b(B)} = 1.08 \cdot 10^3 Nm$ $M_{b(C)} = 0Nm$	$\tau_{F_l} = \frac{4}{3\pi} \frac{T_B}{(\frac{D_{shaft}}{2})^2} = 8.67 \cdot 10^{-3} GPa$ $\sigma_{F_l} = \frac{32 M_{b(B)}}{\pi D_{shaft}^3} = 6.62 \cdot 10^{-2} GPa$

Lastly, the maximum stress on the shaft is obtained using Eq. (2.21) and then the margins of safety are evaluated. They are positive and guarantee the robustness of the shafts.

$$\sigma_{eq} = \sqrt{\sigma_{F_v}^2 + \sigma_{F_l}^2 - \sigma_{F_v} \sigma_{F_l} + 3(\tau_{F_v} + \tau_{F_l})^2} \tag{4.29}$$

$$\begin{cases} MoS_y = \frac{R_y}{\sigma_{eq} FS_y} - 1 = 3.61 \cdot 10^{-1} \\ MoS_u = \frac{R_u}{\sigma_{eq} FS_u} - 1 = 4.66 \cdot 10^{-1} \end{cases} \tag{4.30}$$

The most important structural elements of the trolley have been sized. The maximum allowable space for the payload, in the different cases associated with the three bridges, has been found and its dimensions are reported in Table 4.4.

Table 4.4: Maximum dimensions of the payload in trolleys with different rotation frames

Edge	UM	Bridge 1	Bridge 2	Bridge 3
$x\_payload$	$[mm]$	1700	1800	1700
$y\_payload$	$[mm]$	2100	2100	2000
$z\_payload$	$[mm]$	1000	250	900

In Fig. 4.6, the large trolley is illustrated together with each rotation frame and the maximum allowable encumbrance of the payload in orange.
Up to this point, everything has been designed referring to a beam model of the structure and an ideal distribution of loads on the screws of a flange. This is done to achieve a preliminary design, which is now verified and improved using finite element calculations.

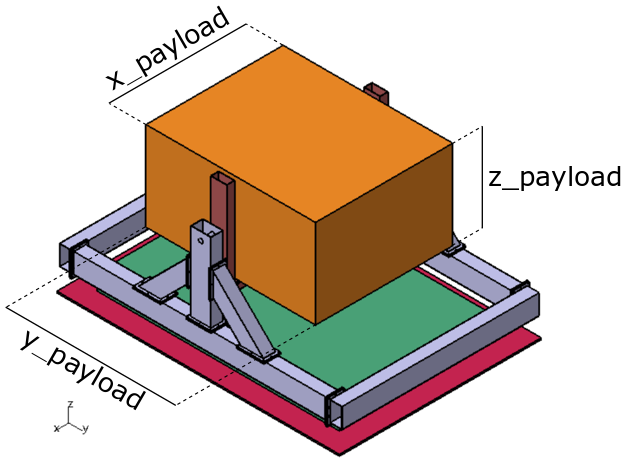

(a) Trolley with Bridge 1

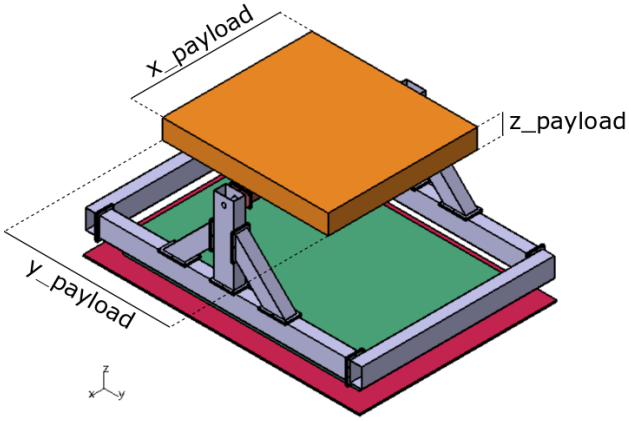

(b) Trolley with Bridge 2

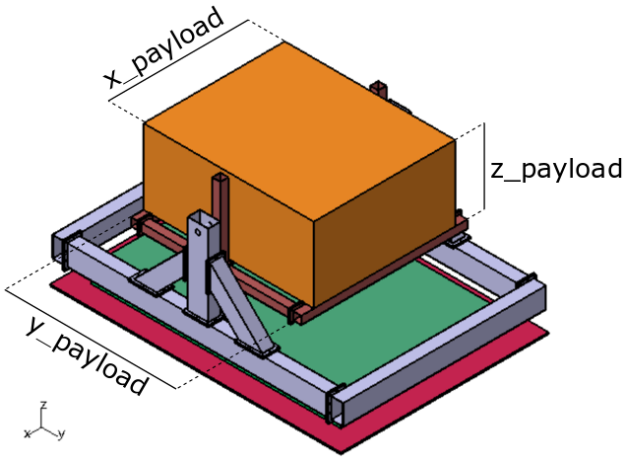

(c) Trolley with Bridge 3

Figure 4.6: Trolleys with the three rotating frames

Chapter 5

Structural analysis

In this chapter, one of the most critical parts of the trolley is analyzed. This is the corner of the main frame, that is the connection, through Flange B, between the beams of the main frame, and it is reported in Fig. 5.1. Half-length of the beams is considered, beam with axis along the X-axis is fixed-end, while on the other beam appropriate loads and boundary conditions are applied. Through the use of the software Catia V5, the design of the structure, which will be analyzed using MSC Nastran, is obtained. The structural analysis is based on the Finite Element Method. Through the use of Patran, the finite element model is built and the results of the analysis are displayed. Moreover, some critical parts are deeply analyzed and solutions to solve eventual problems are developed.

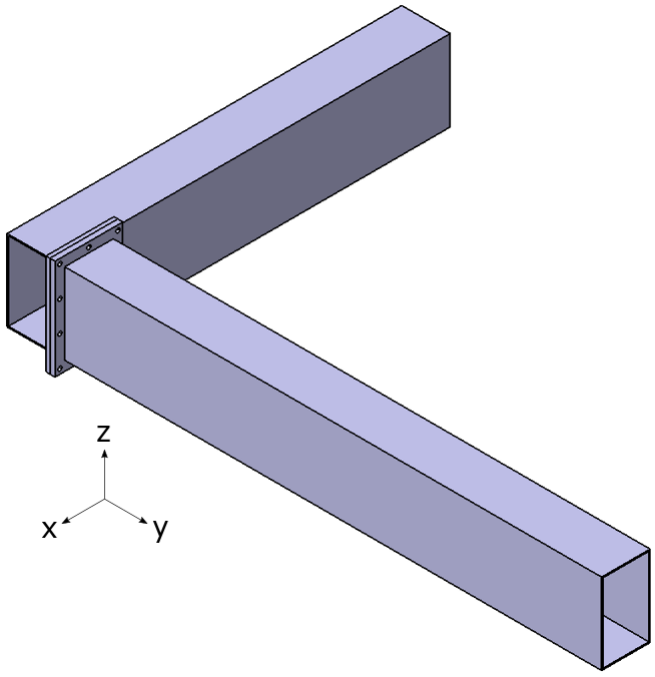

Figure 5.1: Part of the structure to analyze

5.1 Finite Element Method (FEM)

The finite element method is used to solve physical problems in engineering analysis and design. The physical problem is represented by the structure and the applied loads. Idealizing it through the use of assumptions leads to the governing differential equations of the mathematical model. Finally, the Finite Element Analysis (FEA) solves it.
A general FEA can be divided into three phases:

- Pre-process;
- Process;
- Post-process.

The pre-processing phase includes building the geometry and the finite element model, giving them the right properties, setting the boundary conditions and loads and setting up the analysis.
The process stage gives the numerical solution. In all applications the analyst seeks to calculate a field quantity: in structural analysis, it is the displacement field or the stress field.
In the post-processing phase, the results are plotted and studied to evaluate their accuracy. Using an FEA, an approximated solution can be obtained, not the exact one unless the problem is so simple that the exact formula is already available.
The pre and post-processing phases are performed by the software Patran, instead, MSC/-Nastran is used for the analysis.
The FE method consists in dividing a structure into several elements and reconnecting them through nodes. Over an element, a field quantity is interpolated from values of the field quantity at nodes [14]. The values of the field quantity at nodes are those that minimize some function such as total energy. In this way, a set of equations is obtained and it can be expressed in a matrix form as:

$$Ku = f \tag{5.1}$$

where u is the vector of unknowns, that is the values of the field quantity at nodes, f is the vector of loads and K is the global stiffness matrix composed of known constants.
Calculation algorithms allow to solve the system of equations by reversing the matrix K, so the vector of the nodal displacements u is obtained, and from that, the field quantity of the elements can be evaluated.
Elements can be 1D, 2D or 3D, depending on what is the structure that must be represented. A three-dimensional element can be composed of 3D elements, instead, a thin plate can be approximated using 2D elements, or a slender beam using 1D elements. The different kinds of elements will be discussed in Sec. 5.4.
The validity of the results obtained by FEM depends on many variables, like the correct idealization of the problem, the applied loads and BCs, so it is necessary to have an approximated idea of the results that will be obtained and to do all possible checks to avoid errors. These checks will be explained in Sec. 5.5.
The FE modeling allows to study the behavior of a complex system, to predict its structural response and to carry out structural optimizations before it is made. All the defects that it would have in operating conditions can be seen and corrected before the production, reducing time and costs, in general very high in the aerospace industry.

5.2 Generative Shape Design

The Generative Shape Design workbench of Catia is used in Highftech to create the geometry of the structure to be imported in Patran. It allows to quickly model both simple and complex shapes using wireframe and surface features. In this way, a representation of the structure to analyze is obtained and, in this case, it is composed only of 2D surfaces or 1D elements.
Using this workbench, median planes of each part are created and a rectangle is sketched on these planes, whose dimensions are the same as the initial structure.
Beams are very long and thin, so they are represented as a set of four rectangles with zero thickness. The thickness of the beams has an important rule in the response of the application of a load, and it will be included in the analysis in the properties applied to each element in the pre-processing phase of the FEA. The same applies for flanges, but in this case, the area of the holes for screws must be removed.
On the other end, screws are represented as a 1D element with length equal to the sum of washer and flange thicknesses.
The final design can be found in Fig. 5.2.

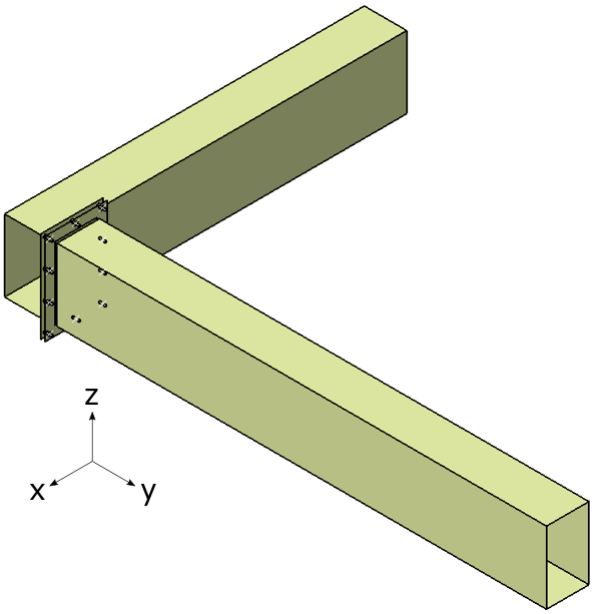

Figure 5.2: Outline of the structure

The obtained surfaces are saved as .stp file and then they are imported into Patran. The use of a global reference system reported in black in Fig. 5.2, in Catia, allows to report the surfaces in Patran in the same position of the CAD.
It is the praxis in HFT to create two groups for each geometric component imported into Patran: one named with the prefix GEO (e.g. GEO_Beam_y) and the other with the prefix FEM (e.g. FEM_M16). All groups with the prefix GEO contain only geometric entities, while groups with the prefix FEM include only elements or nodes.

5.3 Overview of the analysis

It may be useful to have an overview of the analysis, before describing the various aspects of the FEA in detail. Main points of the analysis are listed below:

- the type of analysis that will be done is a structural analysis;
- the goals of the analysis are to study the behavior of the structure, to discover and solve eventual problems and to improve the initial structure;
- the quantities that will be investigated are displacements and von Mises stresses;
- the types of elements used in the analysis will be: beam elements, which are two nodes members, in particular CBAR elements, and shell elements, which are 4 to 8 node isoparametric quadrilaterals or 3 to 6 node triangular elements [20], in particular, CQUAD4 and CTRIA3 elements;
- the mesh density is controlled by mesh seed and the global edge length parameter, which will be described in Sec. 5.4 and in Sec. 5.6, where is explained the procedure used to select elements size, i.e. the convergence study.

5.4 Mesh, loads and BCs

The finite element modeling starts with the import of CAD geometry in the FEM preprocessor Patran. Next, the mesh must be done. Different element types can be used: line, surface and solid elements.
Linear elements are one-dimensional elements used to represent rod and beam behavior: the first supports tension, compression and axial torsion, while the second supports also bending. CBAR element is used for beam whose properties do not vary with cross section, while CBEAM elements can represent more complex beams, but in this analysis, only CBAR elements will be used, as said in Sec. 5.3. Beam elements have six degrees of freedom, three translations and three rotations.
Shell elements are two-dimensional elements used to represent a structure whose thickness is small compared to its other dimensions and whose deflection of the plate midsurface is small compared with its thickness. They have five DOFs because there is no stiffness associated with the rotation about the normal to the plate. The surface element that will be used, as already mentioned in Sec. 5.3, is the quadrilateral plate element (CQUAD4), which is an element connecting four nodes that can represent in-plate, bending and transverse shear behavior, and the triangular plate element (CTRIA3), that is a triangular plate connecting three nodes commonly used for mesh transitions and filling in irregular boundaries.
Finally, solid elements, that will not be used in this thesis, are three-dimensional elements used to represent the behavior of thick plates and solids. They have only translational degrees of freedom.

If the structure is regular and does not have geometric singularities, like a beam, the mesh density will be uniform, otherwise, a concentration of elements is needed in appropriate regions, remembering that a finer mesh is more accurate, but also more computationally expensive. This can be controlled through the mesh seeding. The mesh seeding is defined on a curve or an edge and it allows to control the number and size of elements to be generated in the model. The mesh seed is fundamental for modeling screws and weldings.

The mesh seed on the curve of a hole has a number of elements almost equal to twice the metric of the screw, so for a screw with metric M12, the number of elements is 24, as can be seen in Fig. 5.3c. Where there are two parts linked by welding, the connected edges must have the same number of nodes, and this is imposed using an appropriate mesh seed. There are two different meshers in Patran: IsoMesh, which is used for simple parametric geometry, and Paver, which can be used for all kinds of surface both simple or complex and it meshes first along the contour of the surface then it moves spirally towards the interior. Different parts of the structure have meshes done with different meshers. For example, for beams (Fig. 5.3a) IsoMesh has been used, instead, for flange (Fig. 5.3b) Paver has been used.

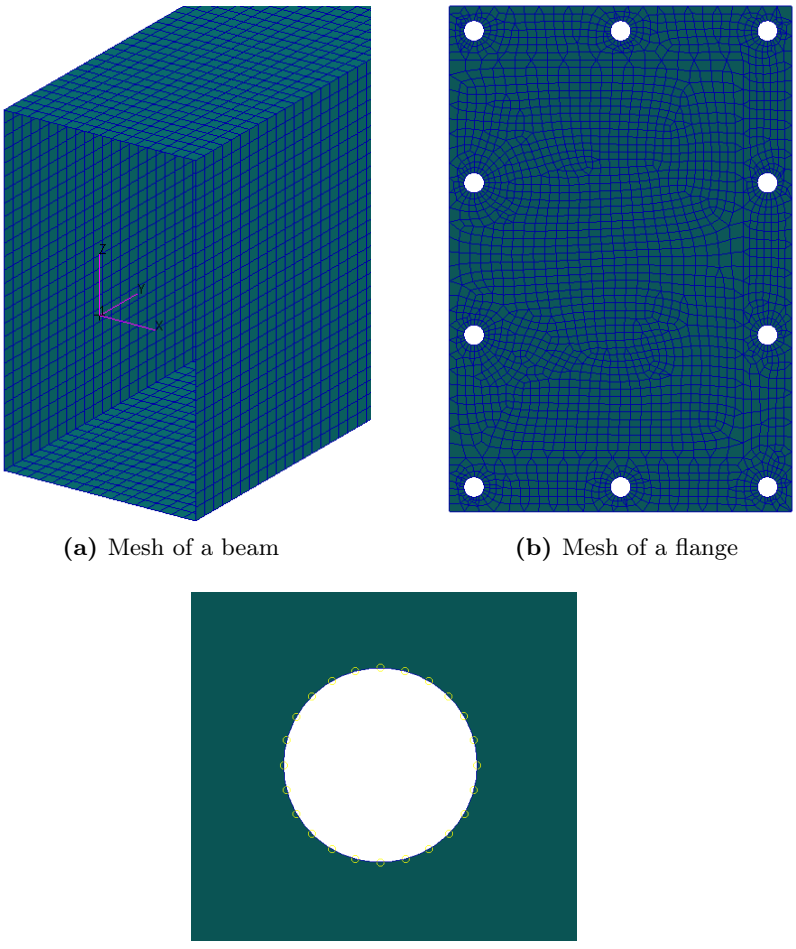

(a) Mesh of a beam

(b) Mesh of a flange

(c) Mesh seed of a hole

Figure 5.3: Different kinds of mesh and mesh seed

Before generating the mesh, the properties of the parts must be created. Depending on the object, different types of properties can be produced, like beam, rod, shell, etc... Each property is characterized by material and attributes on the section, like area for a beam and thickness for a shell. Different kinds of material properties can be modeled on Patran, like isotropic, anisotropic, orthotropic, non-linear, fluid and temperature-dependent. The material modeled in this analysis is linear, elastic, homogeneous, isotropic and temperature independent. The values needed depends on the kind of element to which they are

to be applied. For CQUAD4 and CTRIA3 they are Young's modulus E, Poisson's ratio ν and density ρ, these can be found in Table 2.3, while for CBAR ν is not used. The shear modulus G is a function E and ν, in particular, $G = \frac{E}{2(1+\nu)}$, so it is not important to write it manually.

Before describing screws and weldings modeling, the multi-point constraint (MPC) must be introduced. A MPC is a mathematical constraint relationship between one grid point and another grid point or set of grid points [10]. These relationships are defined between degrees of freedom of independent and dependent nodes. MPCs can be used to model certain physical phenomena that cannot be easily modeled using finite elements, such as rigid links and joints, and they can also be used to allow load transfer between incompatible meshes. When a multi-point constraint creates a rigid mechanism between the independent and dependent nodes it is called RBE2. This mechanism is defined via a linear relationship among selected nodal DOFs. The RBE2 element adds infinite stiffness to the structure [8].

Different components of a structure are assembled by jointing methods like weldings and bolted joints. The way of modeling these joints influence the overall behavior of the structure. Weldings characteristics and verifications will be presented in Sec. 5.7, here only the way of modeling them is reported. Weld joints are used to connect beams and flange and they are modeled with RBE2, with all degrees of freedom transferred node to node. Each independent node of the beam is linked with only one dependent node of the flange, as can be seen in Fig. 5.4a. This point to point connection needs meshes of different parts to match at the welding connection points. As said before, in this case, an important rule is played by the mesh seed, the number of nodes of one edge must be equal to the number of nodes on the welded edge.
Screw joints, too, are modeled with RBE2. Each screw, represented with a bar element with two nodes, is linked to both plates. Screw nodes are independent nodes, with hole nodes are dependent nodes. An example of screw modeling is given in Fig. 5.4b. This is called spider-type connection: each connection has a single central node with multiple leg nodes that branch out from the central node in a spider-like pattern [31].

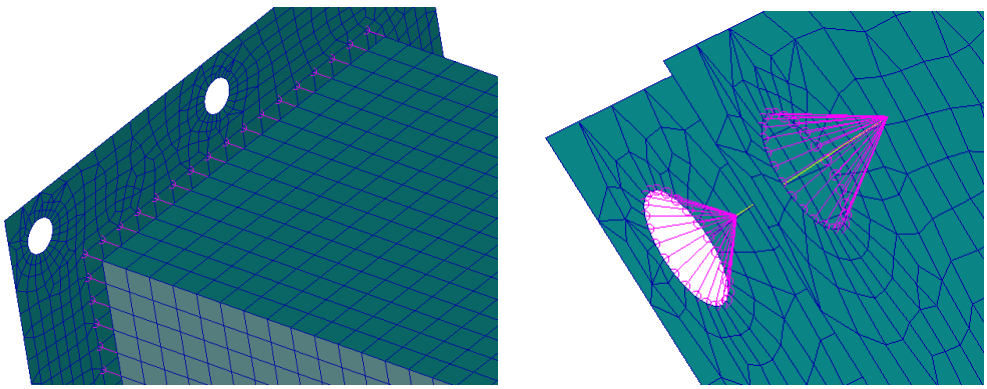

(a) Modeling of a welding **(b)** Modeling of a screw

Figure 5.4: Modelings with RBE2

Many types of loads and boundary conditions can be modeled in Patran. Possible loads are concentrated forces and moments, distributed loads, pressure loads, etc... Boundary conditions, in most cases, are modeled by constraining appropriate degrees of freedom to zero displacement. The choice of constraints influences the structure response to loading, so BCs must resemble as much as possible the real conditions.
The structure analyzed represents a fourth of the main frame. The beam, whose axis is aligned to the X-axis, is a fixed ended beam. This constraint is applied to each node of the end-section and it can be seen Fig. 5.5 in light blue. On the other beam are applied half of the initial loads, because there is only half of the beam and in the complete structure, the loads would be symmetrically distributed. This applies to shear forces and bending moments, but the torsional moment is constant along the section, it is independent on the length of the beam, but it is linearly proportional to the load. In this way, only half of the torsion is considered, so the remaining half will be taken into account adding a moment about the Y-axis on the beam axis.
The slope of the beam oriented on the Y-axis must be null at its free end, which is the middle point of the full beam, in both vertical and horizontal directions. This means that the rotation about X and Z-axis must be zero at the beam free end. Finally, also the axial deformation along the Y-axis must be null in this point, so another constraint is the displacement along Y equal to zero. All loads and constraints, with their nodes of application, are summarized in Table 5.1, and shown in Fig. 5.5, where for each node is reported the resultant of applied loads. RBE2 can be used also to apply loads that are not on the structure. Two RBE2 have been used to connect forces applied on independent nodes C and D to two dependent nodes each, on the beam. A third RBE2 spider-like, connects node A in the center of the beam, to all the dependent nodes of the beam section with the same Y-coordinate of the independent one.

Nodes	Coordinates $[m]$	Loads	Constraints
A	$[0, 1.660, 0]$	$M_y = -4659.75Nm$	$T_y = 0$ $R_x = 0$ $R_z = 0$
B	$[0, 1.500, 0.123]$	$F_z = -1635N$	/
C	$[0, 1.660, 0.573]$	$F_x = -1226.25N$ $F_z = -1635N$	/
D	$[0, 1.660, 1.022]$	$F_x = -4046.625N$ $F_z = -5395.5N$	/

Table 5.1: Loads and constraints applied to nodes

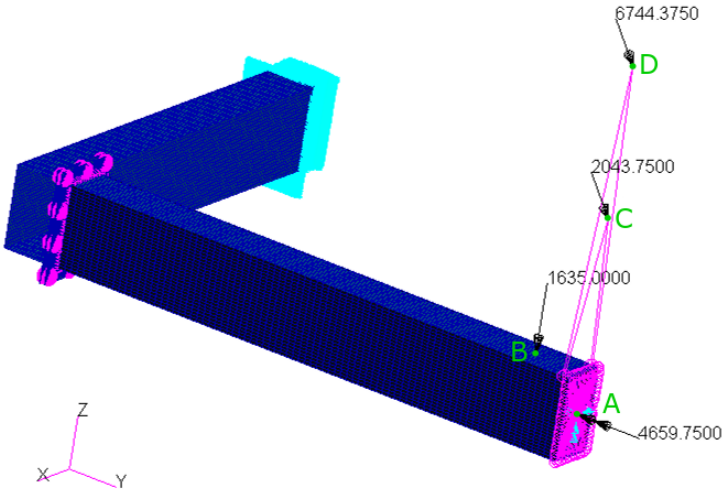

Figure 5.5: Loads and boundary conditions on the structure

5.5 Checks on FEM

To achieve a good analysis and obtain proper results, the FE model is opportunely checked at different stages of the work. Some checks shall be done before ending the meshing phase, others before running the analysis and still others before displaying the results.
When the mesh of a part of the structure is done, the shape of the elements must be checked, because the accuracy of a finite element degrades as its shape is distorted. The 2D elements used in this work, as said in Sec. 5.4, are tria and quad elements. There are two basic types of tria element distortions:

- Tria Aspect ratio: it is calculated as:

$$Aspect\,Ratio = \frac{\sqrt{3}}{2}\frac{h_2}{h_1} \tag{5.2}$$

  where h_1 and h_2 are reported in Fig. 5.6a. The ratio is multiplied by the factor $\frac{\sqrt{3}}{2}$ such that a "perfect" element in the shape of an equilateral triangle will equal one [11]. The largest aspect ratio must be lower than 5;

- Tria Skew: it is the smaller angle of the triangular element, as can be seen in Fig. 5.6b. It shall be larger than 10°.

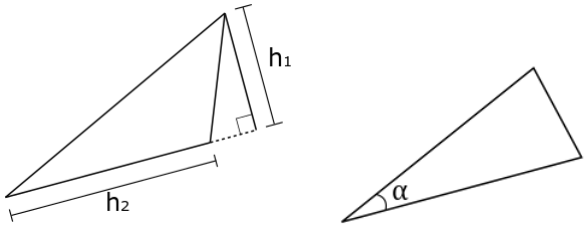

(a) Tria Aspect ratio **(b)** Tria Skew

Figure 5.6: Tria element distortions

There are four basic types of quad element distortions:

- Quad Aspect ratio: it is the ratio of the element longest side to its adjacent side, $\frac{a}{b}$ (Fig. 5.7a). It shall be less than 5;
- Quad Warp: it is the extent to which an element deviates from being planar ($\frac{h}{a}$), which can be seen in Fig. 5.7b. It shall be less than 5%;
- Quad Skew: it is the angle between the lines that join opposite midsides, the sketch is reported in Fig. 5.7c. Quad elements should be as square as possible. The skew angle shall be greater than 30°;
- Quad Taper: it is the ratio of the area of a triangle formed at one corner grid, two of these areas are reported in Fig. 5.7d, to one half the area of the quadrilateral [20]:

$$Taper\ Ratio = \frac{A_{TRI_i}}{\frac{1}{2}A_{QUAD}} \tag{5.3}$$

  The largest of the four ratios shall be lower than 0.5. As the ratio approaches zero, the shape approaches a rectangle.

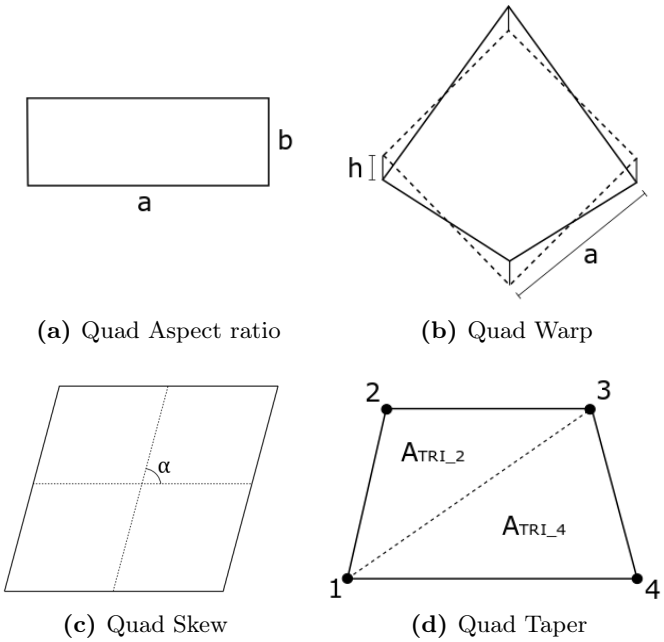

(a) Quad Aspect ratio **(b)** Quad Warp

(c) Quad Skew **(d)** Quad Taper

Figure 5.7: Quad element distortions

If the taper ratio is greater than 0.5, this quad can be corrected manually using the command "Break Elements". In Fig. 5.8, there is a Quad Taper near to a hole of the flange. The taper is found and highlighted by Patran and it can be divided into two tria elements so that the two triangles are as equal as possible to each other.

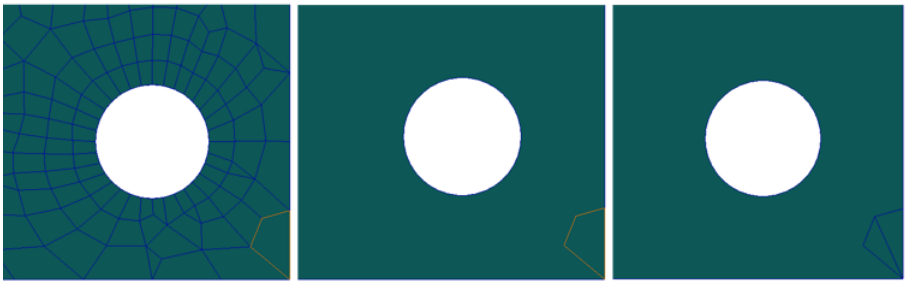

Figure 5.8: Correction of a Quad Taper

An important check on the nodes is the equivalencing. It is the process of reducing all nodes that coexist at a point to a single node [11]. Overlapping nodes can involve problems in the analysis and errors in the Nastran output file. The equivalencing method available in Patran is called Geometric Equivalencing and it is based upon the coordinates of the node points. The distance between nodes is compared with a tolerance parameter, the one used in this work is the Tolerance Cube. In this case, two node points are equivalenced if all of their coordinates in the global Cartesian frame lie within the tolerance of each other.

Other checks that must be done are:

- Boundaries: it plots the boundaries as free edges or free faces, where a boundary is an edge or face of a finite element that is not shared by at least one other element. So, this test will display interior and exterior edges or faces but also interior cracks;
- Duplicates: it checks elements for identical corner (or end) nodes and deletes one of them. This error is often due to unintentionally meshing the same line, surface, or volume more than once;
- Normals: it compares adjacent shell normals. When a model is created, the elements shall always be generated consistently. For example, the grid points for each element are connected in a clockwise direction, so the normals of each element are in the same direction, as can be seen in Fig. 5.9. If the model is not generated consistently, an offset or a load (such as a pressure load) might be inadvertently applied in the wrong direction.

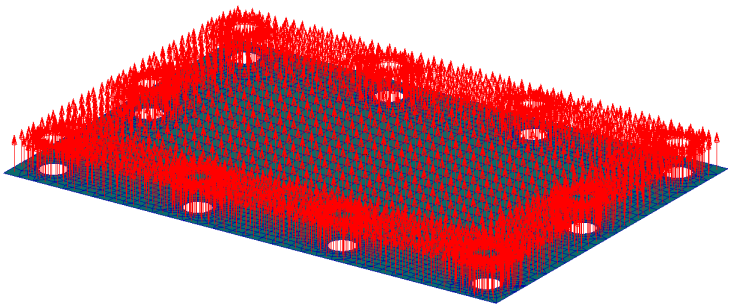

Figure 5.9: Display of the vectors normal to the shell elements of the flange

The checks that are done on the Nastran output file ".f06" are:

- Mass property check: the mass of the model calculated in Patran must be consistent with the one calculated in Catia V5 and mass values shall be the same for axes X, Y, Z;

- OLOAD check: OLOAD resultant represents the resultants of all applied loads referenced to the origin of the basic coordinate system [16]. It shall be equal to applied forces. SPCFORCE resultant is the summation of all forces of single point constraint with respect to the origin of the basic coordinate system [16]. It shall be equal in modulus but opposite to OLOAD resultant;

- Strain energy check: the result of a non free-free model shall be PASS for the first two sets and FAIL for the last two;

- Epsilon: ϵ is based on a strain energy error ration, and provides a measure of round-off error and numerical ill-conditioning [10], in particular, epsilon is the ratio of the work done by the residual forces to the external work (the work done by the applied forces):

$$\epsilon = \frac{u^T \delta P}{u^T P} \tag{5.4}$$

  where u is the calculated displacement vector, P is the applied load, $\delta P = Ku - P$ is the residual load vector and K is the stiffness matrix [28].
  A system of linear equation is said to be ill-conditioned if small perturbations in the system lead to large changes in the solution. A large value of ϵ is evidence of numerical ill-conditioning, while a small value of ϵ indicates a numerically stable problem. Ill-conditioning does not necessarily result in a fatal error but can lead to inaccurate answers. Possible causes of it can be unconnected degrees of freedom, rigid body motion, incorrect multipoint constraints, the presence of mechanisms, the high difference in stiffness between adjacent elements in the model, or DOFs without stiffness because of missing elements. ϵ shall be lower than 10^{-8}, it does not matter if it is positive or negative, as long as it is small.

5.6 Convergence study

The mesh convergence is related to how small elements need to be to ensure that the results of the finite element analysis are not affected by changing the size of the mesh. As the mesh density increases, the quantity of interest starts to converge to a particular value. If two subsequent mesh refinements do not change the result substantially, then it can be assumed that the result has converged [9].
This analysis is done on a quarter of the base of the main frame of the trolley, so the time needed to do the calculations must be reasonable, because the analysis, in the end, should be done on the entire trolley together with the rotation frame.
Mesh dimensions depend on two parameters:

- Mesh seed: it allows to manage the density of the mesh on the edges of the components of the structure;

- Global edge length: it assigns the default element edge length for a mesh, but it will only be applied where mesh seed has not been defined.

Beam elements dimension depends only on mesh seeds; they are chosen in order to have square elements and to have the same number of nodes of the flange on which they are welded. The cause has been explained in Sec. 5.4.
The global edge length is used only for flanges: they are components connected through welds and screws and they have holes, so they need a finer mesh with respect to the one of the beams. For these reasons, the global edge is half of the mesh seed.
Three different models have been done and, for each one, mesh size, CPU time, stress and displacements have been compared.
Model 1 is the case with the higher elements dimensions. The mesh seeds on all edges, except the holes one, have elements with lengths of 20 mm, while the global edge length is equal to 10 mm. The number of elements on the holes is 6; they are too low to capture the boundary exactly, but increasing this number leads to having adjacent elements with too different sizes, so this model is not good.
Model 2 has elements on edges with length halved with respect to the previous model. The global mesh length is 5 mm. The CPU time has increased, but in this model, the number of elements on the holes is 24, the double of the screw metric, which is M12.
The last model, Model 3, has mesh seeds with length equal to 7 mm. The global edge length is 35 mm and the number of elements on the holes of the flanges is 24. For this model, the mesh seed is not half of the previous one because a mesh size of 7 mm on a beam with length equal to 3320 mm is already very small.
The results of these models that are compared are translational displacements, von Mises stresses, CPU time and number of elements.
The displacements are very low for this structure and there are no relevant changes between the models, as can be seen in Fig. 5.10.

A more interesting result can be found in the von Mises stresses. The overall behavior of the three models is the same, as illustrated in Fig. 5.11, but the peak of the stress is different. The results will be analyzed in Sec. 5.9, in this section only the convergence study is done.

The maximum von Mises stresses σ_{beam} on a particularly stressed region of the beam with axis aligned to X-axis, reported in Fig. 5.12, are compared. The exact values are reported in Table 5.2, and, as can be seen in Fig. 5.13, it increases for finer meshes, i.e. augmenting the number of elements.

The time needed to do the computations increases going from Model 1 to Model 3, because the mesh sizes are decreased.
All the results are summarized in Table 5.2 and the plot of von Mises stress and CPU time versus the number of elements of each model is reported in Fig. 5.13.
The CPU time of Model 1 is very low, but its mesh is coarse, so it cannot be used.
Model 2 and Model 3 give similar results in terms of deformations and stresses, but Model 3 has a finer mesh, so the number of elements is higher with respect to Model 2. This implies a relevant increment in the CPU time, but a small change in stress analysis, so this mesh refinement is unnecessary and the selected mesh is the one of Model 2.

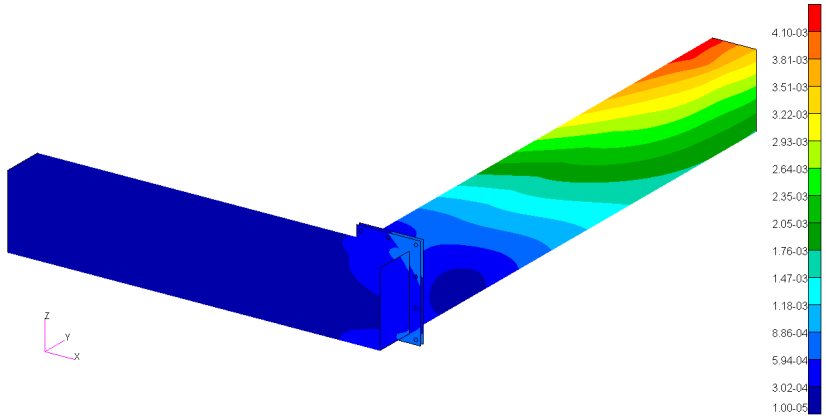

(a) Displacements of Model 1

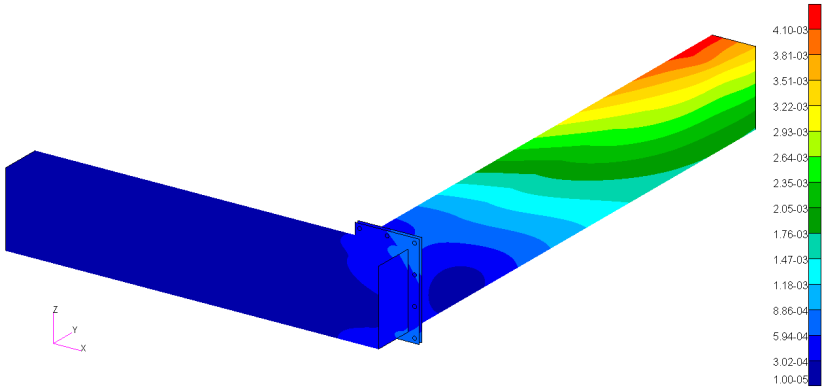

(b) Displacements of Model 2

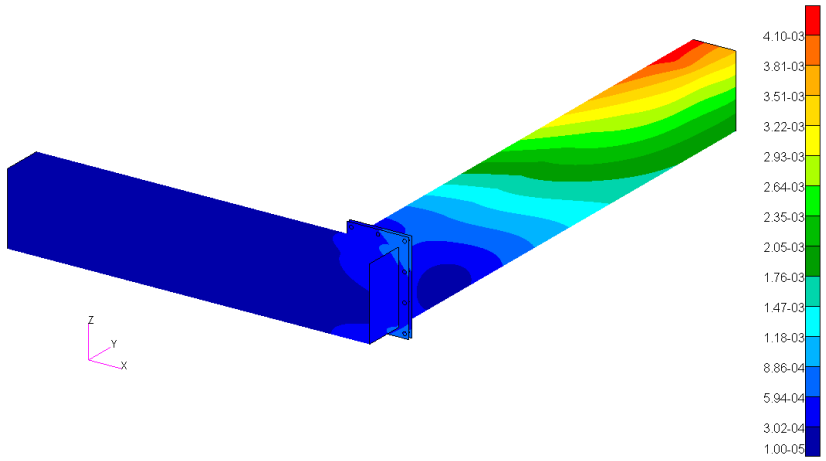

(c) Displacements of Model 3

Figure 5.10: Results of structural analysis on different meshes reporting displacements in meters

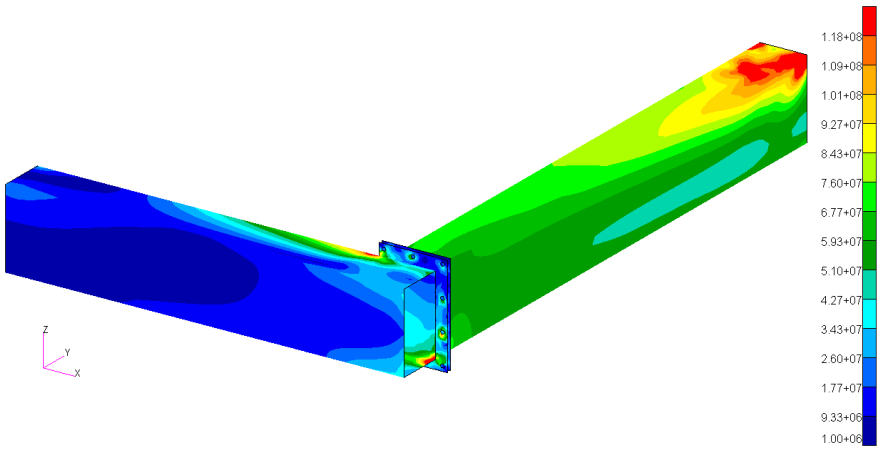

(a) Von Mises stresses of Model 1

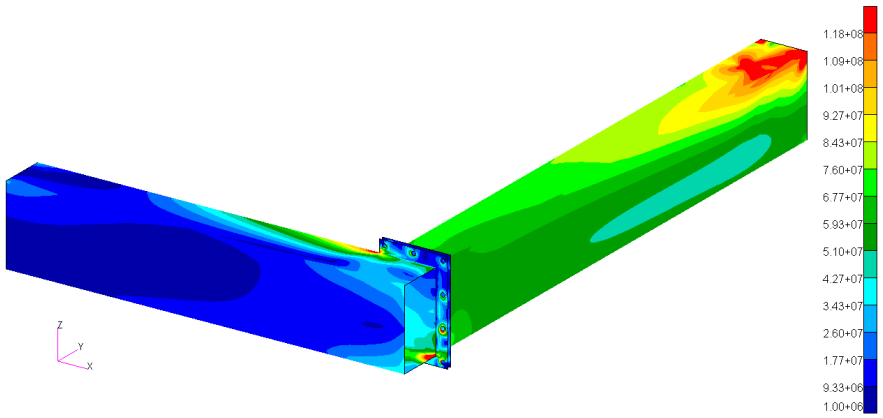

(b) Von Mises stresses of Model 2

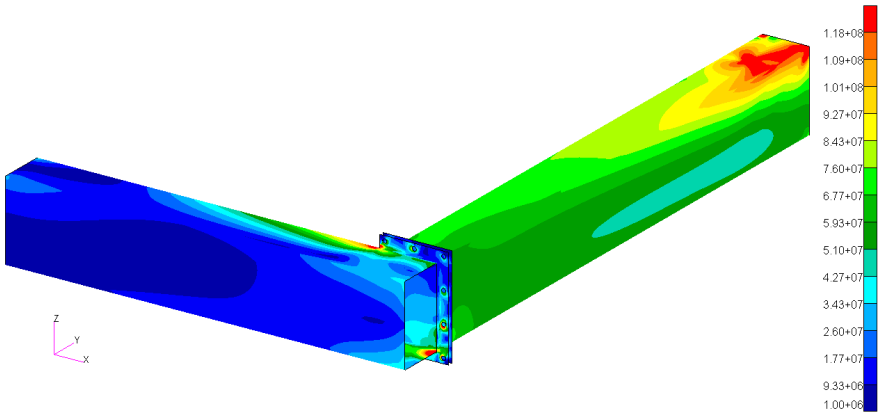

(c) Von Mises stresses of Model 3

Figure 5.11: Results of structural analysis on different meshes reporting von Mises stresses in pascal

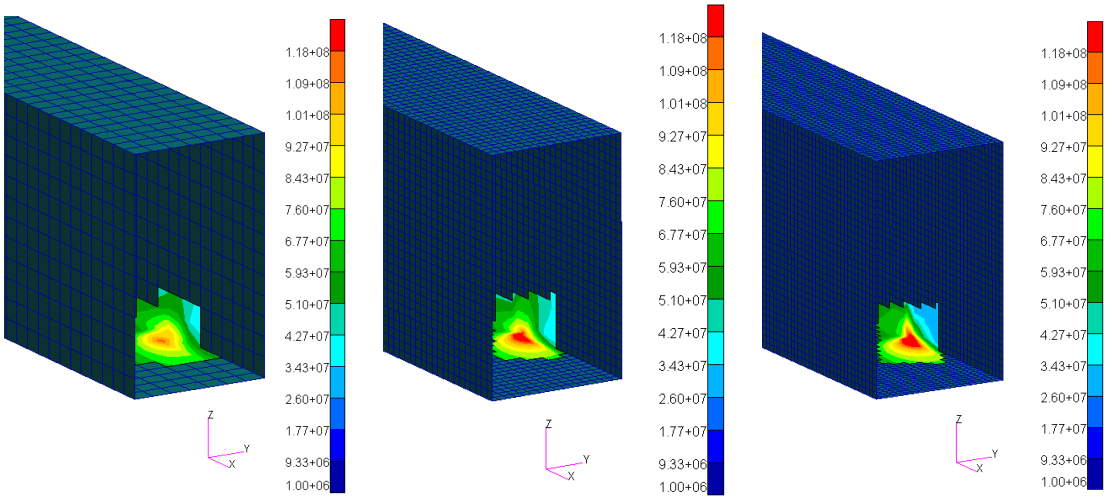

(a) Von Mises stresses of Model 1

(b) Von Mises stresses of Model 2

(c) Von Mises stresses of Model 3

Figure 5.12: Von Mises stresses in pascal on a stressed region of beam with axis aligned to X-axis

Table 5.2: Results of convergence study

Model	Mesh seed $[mm]$	Global edge length $[mm]$	$\sigma_{beam}\,[MPa]$	$t_{CPU}\,[s]$	$\#\ elements\,[-]$
Model 1	20	10.0	117	8	6637
Model 2	10	5.0	142	21	29344
Model 3	7	3.5	147	55	51587

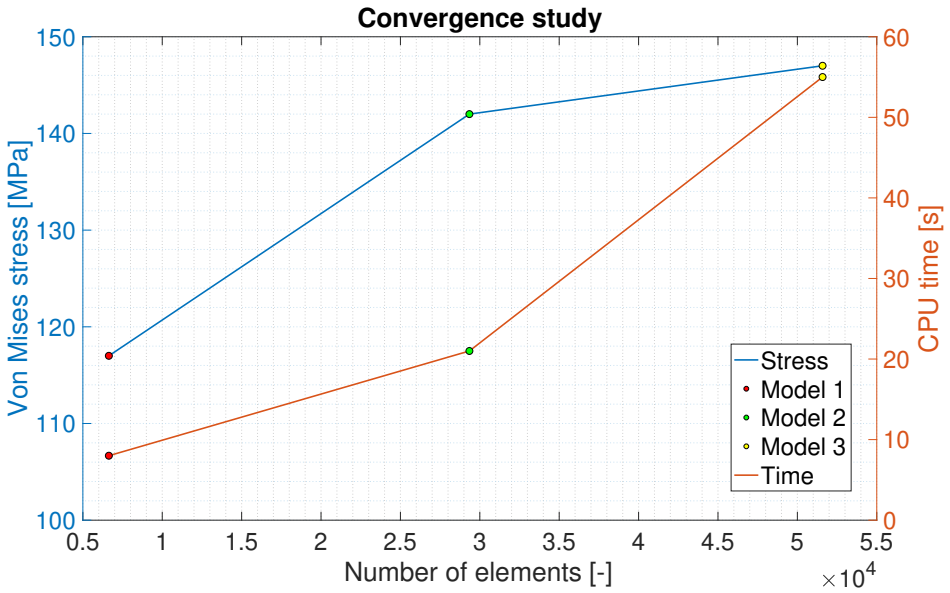

Figure 5.13: Plot of the von Mises stress and CPU time of each model vs. the number of elements

5.7 Design resistance of a fillet weld

Welding is a metal joining process wherein coalescence is produced by heating the metal to suitable temperatures, with or without the application of pressure and with or without the use of filler metals. The types of joint used in this project are the lap welding joint and the tee welding joint. A lap joint, reported in Fig. 5.14a, is formed when two pieces are placed in an overlapping pattern on top of each other. T joints are used to weld two plates or sections with surfaces located approximately 90° to each other at the joint, but the surface of one plate or section is not in the same plane as the end of the other surface, as can be seen in Fig. 5.14b. The weld type is the fillet weld, which is the most common connection in welded fabrication. The basic cross-section of fillet welds includes an isosceles rectangular triangle. In strength checks of fillet welds, the rectangle lying in the center plane dividing the fillet into two identical parts is the dangerous weld section. One of the most important characteristics of the fillet joint is the effective throat thickness a: it is the height of the largest triangle that can be inscribed within fusion faces and the weld surface, measured perpendicular to the outer side of this triangle [3]. a should not be less than $3mm$ [3]. Another important property is the effective length of a fillet weld l_{eff}, which can be calculated as the overall length of the weld l reduced by twice the effective throat thickness a. If l_{eff} is less than $30mm$ or less than 6 times its throat thickness, the fillet weld should not be designed to carry load [3]. The design throat area A_w is equal to the product of throat thickness and effective length.
The resistance of fillet welds is verified respecting "EN 1993-1-8: Eurocode 3" and the directional method is used. A uniform distribution of stresses is assumed on the throat section of the weld, leading to the stresses shown in Fig. 5.15:

- $\sigma_\perp$ is the normal stress perpendicular to the throat;
- $\sigma_\parallel$ is the normal stress parallel to the axis of the weld, but it is not considered when verifying the design resistance of the weld [3];
- $\tau_\perp$ is the shear stress, in the plane of the throat, perpendicular to the axis of the weld;
- $\tau_\parallel$ is the shear stress, in the plane of the throat, parallel to the axis of the weld.

The design resistance of the fillet weld will be sufficient if the following inequalities are both satisfied:

$$\begin{cases} \sqrt{\sigma_\perp^2 + 3 \cdot (\tau_\perp^2 + \tau_\parallel^2)} \leq \frac{f_u}{\beta_w \gamma_{M2}} \\ \sigma_\perp \leq 0.9 \frac{f_u}{\gamma_{M2}} \end{cases} \tag{5.5}$$

where:

- f_u is the nominal ultimate tensile strength of the weaker part joined;
- β_w is the correlation factor, that depends on the material;
- γ_{M2} is the partial safety factor for welds.

The material is $S\,355$, so the values of the previously described factors, taken from [3], are:

$$\begin{cases} f_u = 5.10 \cdot 10^2 MPa \\ \beta_w = 0.90 \\ \gamma_{M2} = 1.25 \end{cases} \tag{5.6}$$

The values of the right parts of Eq. (5.5) are:

$$\begin{cases} \frac{f_u}{\beta_w \gamma_{M2}} = 453.3MPa \\ 0.9\frac{f_u}{\gamma_{M2}} = 367.2MPa \end{cases} \tag{5.7}$$

The stresses reported in Fig. 5.15 are calculated as:

$$\begin{cases} \sigma_\perp = \frac{F_{\sigma_\perp}}{A_w} \\ \tau_\parallel = 1.5\frac{F_{\tau_\parallel}}{A_w} \\ \tau_\perp = 1.5\frac{F_{\tau_\perp}}{A_w} \end{cases} \tag{5.8}$$

where F_i are the maximum forces acting on MPCs of a specific fillet weld along a certain direction. These forces can be found in Patran, after having defined a proper coordinate system aligned with the three stresses. This matter will be further addressed in Sec. 5.11.2.

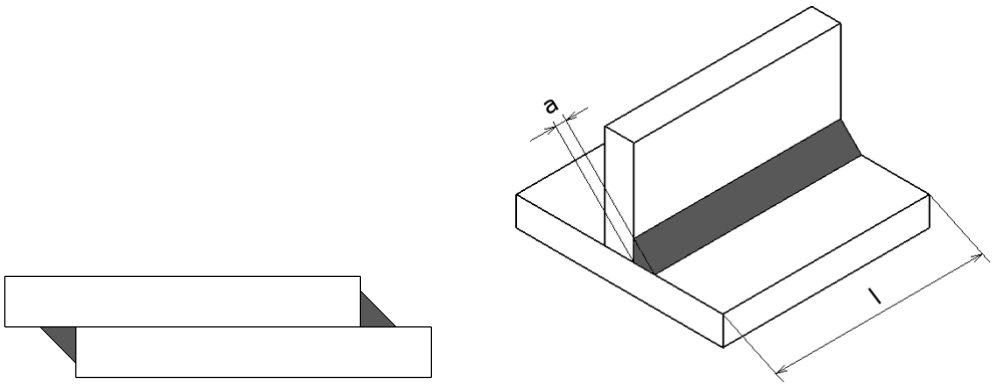

(a) Fillet weld of a lap joint **(b)** Fillet weld of a T joint

Figure 5.14: Joints and fillet weld

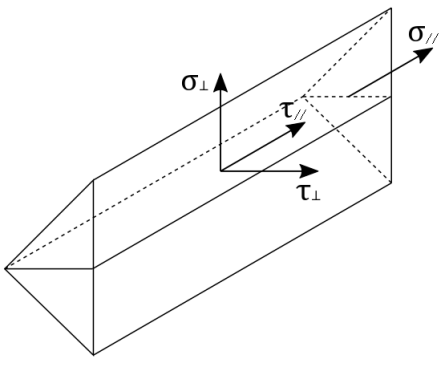

Figure 5.15: Stresses on the throat section of a fillet weld

5.8 Screws and flange verifications

Verifications of screws and flanges have been explained in Sec. 3.4 and Sec. 3.5.
A report with loads carried each screw can be obtained from Patran. The load is decomposed in the three components X, Y, Z of the coordinate system of the screw. In Fig. 5.16, the ID and the reference system of each screw are displayed, together with Flange B and the beam with axis aligned to the Y-axis. X-axis, in red, is in the direction of the screw axis, while Y and Z-axes, in green and blue respectively, are perpendicular to it.
In Table 5.3, the loads along the axes of the screws and the results of the verifications are reported. This time not only margins of safety for sliding are negative, but also few for bearing and shear tear out. Furthermore, the screw integrity of screws 24934 and 24936 is not guaranteed. To improve this factor, there are two possible ways: increase the number of screws or increase the metric of the screws. In this case, it has been chosen to change the metric, so the smallest area between the working stem section and the working thread section A_{min}, described in Eq. (3.10), is increased and as a consequence also SV. In this way, the sliding safety margins raise because increasing the metric means increasing PLD_{min}. Having increased the metric of screws, the distance between the center hole and plate edge c has to be raised. The margin of safety for the bearing is proportional to the nominal diameter of screw d_n and to the thickness of the flange t_{flange}. Also, margins of safety for shear tear out are proportional to t_{flange}, so it is a good choice to increase it.

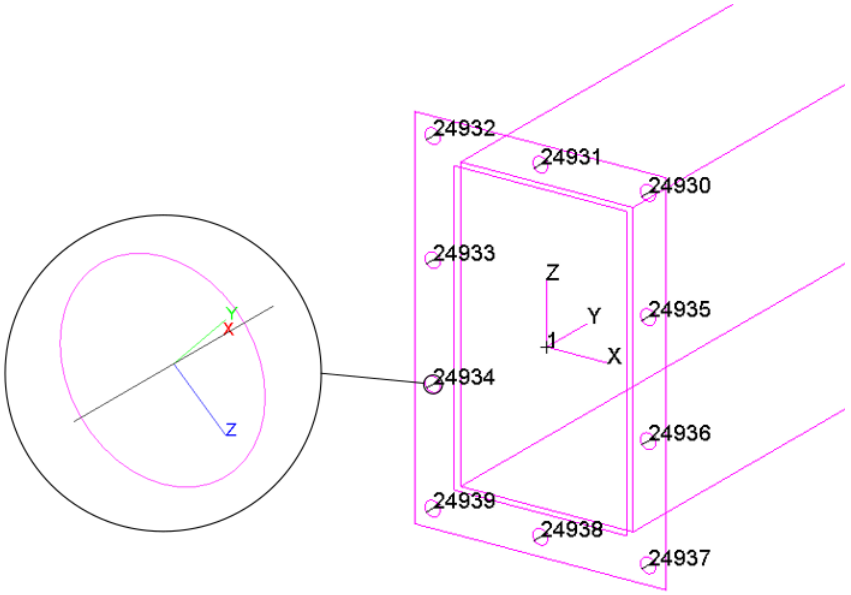

Figure 5.16: ID and coordinate system of screws

Table 5.3: Results of verifications on screws of Flange B with loads calculated from Patran

	Loads			Tension	SV Screw		Pull Out		Joint sep.	Sliding	Shear tear out		Bearing
# Screw ID	P [N]	V_y [N]	V_z [N]	$\sigma_{id}\,[MPa]$	SV_u	SV_y	MS_{po_s}	MS_{po_f}	MS_{js}	MS_{sl}	MS_{u_sto}	MS_{y_sto}	MS_b
24930	1212	579	-3748	845	0.48	0.38	2.01	0.82	17.34	0.19	3.73	3.39	1.90
24931	19	-5145	-4418	865	0.35	0.31	2.04	0.84	1168.76	-0.30	1.64	1.45	0.62
24932	-2613	-7387	-1842	878	0.68	0.75	1.98	0.80	FALSE	-0.30	1.35	1.18	0.44
24933	-821	-8157	6477	909	0.31	0.54	2.02	0.83	FALSE	-0.53	0.72	0.60	0.06
24934	-3879	-11420	12289	1022	-1.61	-0.57	1.95	0.78	FALSE	-0.67	0.07	-0.01	-0.34
24935	619	5502	-6403	884	0.19	0.22	2.03	0.83	34.91	-0.45	1.12	0.97	0.30
24936	3225	11186	-6793	954	-0.70	-0.31	1.97	0.79	5.89	-0.69	0.37	0.27	-0.16
24937	8002	6418	184	874	0.32	0.27	1.86	0.73	1.78	-0.53	1.79	1.59	0.71
24938	1443	2253	2543	843	0.49	0.38	2.01	0.82	14.40	0.31	4.28	3.90	2.24
24939	-11200	-3685	4111	872	0.82	0.84	1.80	0.69	FALSE	0.30	2.25	2.01	0.99

5.9 Stress analysis

Before introducing the corrections on flanges and screws, the stresses on the beams must be analyzed. When the process stage is concluded and the checks are done, the results can be displayed. The equivalent stress is calculated, using the von Mises criterion explained in Sec. 2.2, at each node of each element. In particular, stresses are calculated at distances Z1 and Z2 from the element reference plane. The default for Z1 is $-\frac{t}{2}$, and for Z2 is $+\frac{t}{2}$, where t is the local plate thickness [10]. An example is reported in Fig. 5.17. It is an extract of the Nastran file ".f06" where can be seen the values of Z1 and Z2 (fiber distance), of stresses in the element coordinate system, of principal stresses and von Mises stresses, all evaluated at nodes and at the centroid of the element.

```
                S T R E S S E S   I N   Q U A D R I L A T E R A L   E L E M E N T S   ( Q U A D 4 )       OPTION = BILIN

ELEMENT            FIBER            STRESSES IN ELEMENT COORD SYSTEM        PRINCIPAL STRESSES (ZERO SHEAR)
  ID      GRID-ID  DISTANCE        NORMAL-X      NORMAL-Y      SHEAR-XY     ANGLE       MAJOR         MINOR         VON MISES
  4096    CEN/4  -2.000000E-03  -2.187446E+06  1.067133E+06 -1.216672E+07   -48.8090  1.171490E+07 -1.283522E+07  2.126840E+07
                  2.000000E-03  -2.930811E+06 -1.177627E+06 -1.117383E+07   -47.2428  9.153940E+06 -1.326238E+07  1.952148E+07

            4418  -2.000000E-03  -4.910778E+05  1.070991E+06 -1.216672E+07   -46.8365  1.248172E+07 -1.190180E+07  2.111874E+07
                  2.000000E-03  -1.297472E+06 -1.200542E+06 -1.117383E+07   -45.1243  9.924925E+06 -1.242294E+07  1.939408E+07

            4390  -2.000000E-03  -4.910754E+05  1.063274E+06 -1.216672E+07   -46.8275  1.247761E+07 -1.190541E+07  2.111826E+07
                  2.000000E-03  -1.297469E+06 -1.154712E+06 -1.117383E+07   -45.1830  9.947964E+06 -1.240015E+07  1.939283E+07

            4391  -2.000000E-03  -3.883817E+06  1.063274E+06 -1.216672E+07   -50.7459  1.100534E+07 -1.382588E+07  2.155067E+07
                  2.000000E-03  -4.564153E+06 -1.154712E+06 -1.117383E+07   -49.3372  8.443687E+06 -1.416255E+07  1.978529E+07

            4419  -2.000000E-03  -3.883815E+06  1.070991E+06 -1.216672E+07   -50.7546  1.100997E+07 -1.382279E+07  2.155174E+07
                  2.000000E-03  -4.564151E+06 -1.200542E+06 -1.117383E+07   -49.2797  8.417339E+06 -1.418203E+07  1.978273E+07
```

Figure 5.17: Part of Nastran output file .f06 where are reported Z1, Z2 and stresses at each node

The von Mises stress plotted in Patran is the maximum stress between the one at Z1 and the one at Z2. The results are illustrated in Fig. 5.18, together with the translational displacement of each node. In the fringe are reported the values of stress in $[Pa]$ from $10^6 Pa$ to $\frac{R_y}{SF_y} = 1.18 \cdot 10^8 Pa$ and the range from blue to red, where R_y is the yield strength and the value for Fe510 is $3.55 \cdot 10^8 Pa$, and SF_y is the yield safety factor equal to 3. When the stress calculated by MSC Nastran is lower than $1.18 \cdot 10^8 Pa$ the margin of safety MoS_y is positive. In this way, parts in blue are not stressed, while parts in red are too stressed and they do not respect the safety factor of 3 on yield.

In Fig. 5.18a, the deformed pattern is amplified because the true deformations are too small (the maximum default deformation is located at the beam end section where loads are applied and its value is $4.36 \cdot 10^{-3} m$), as can be seen in Fig. 5.18b.

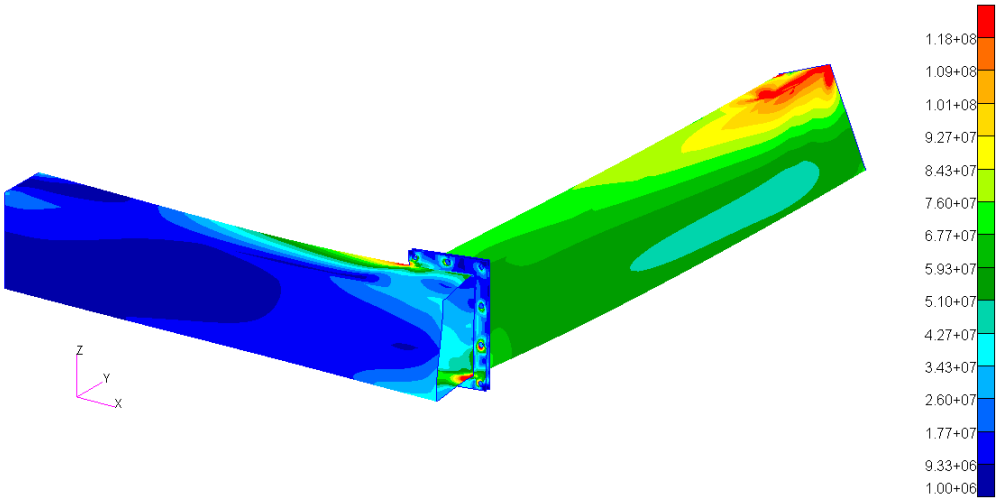

(a) Scale factor= 0.1 for deformations

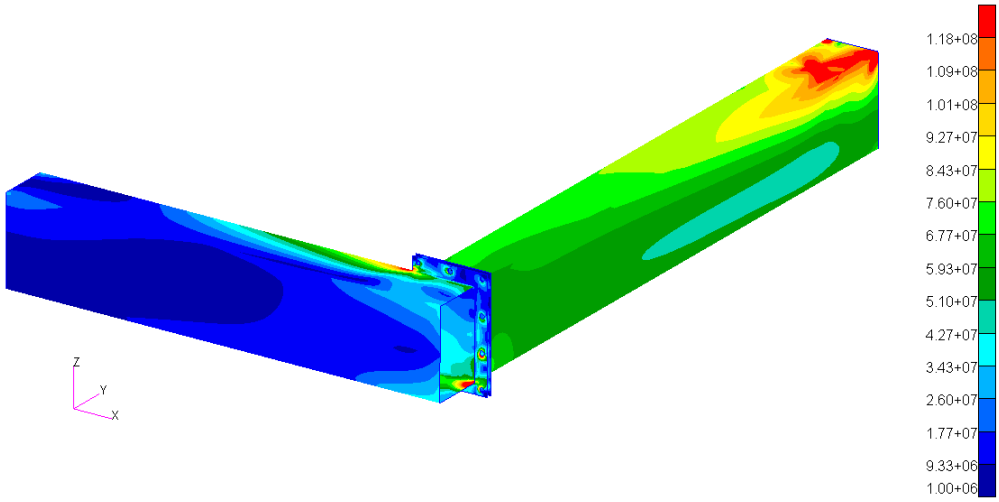

(b) True scale for deformations

Figure 5.18: Results of structural analysis reporting deformation and von Mises stress in pascal

This analysis aims to study and improve the current situation of the corner of the main frame. If the analysis was done on the complete trolley, the boundaries of the corner would have had different behavior. The reasons are that the beam on the left-hand side of Fig. 5.18a, in reality, is not a fixed ended beam, and the loads on the beam on the right-hand side in practice are not applied in this way. The loads are applied to a larger area with respect to the infinitesimal one of the nodes, because they are distributed on Flange A, as shown in Fig. 2.17. This flange increments the thickness of the beam locally, increasing its stiffness. In addition, loads are applied using MPCs, which are infinitely rigid elements, as said in Sec. 5.4, while beams are not. Because of that, this analysis is meaningful only far from boundaries.

Analyzing the results, some small regions with high stress concentration, highlighted in red, can be seen. A detail of the beam is reported in Fig. 5.19. The three highly stressed areas are on edges connected to the flange. First of all, the welded connections in these regions must be verified. Secondly, a solution must be found to counteract the torsion of the beam, in order to avoid these stresses concentrations. Possible solutions are presented in Sec. 5.10.

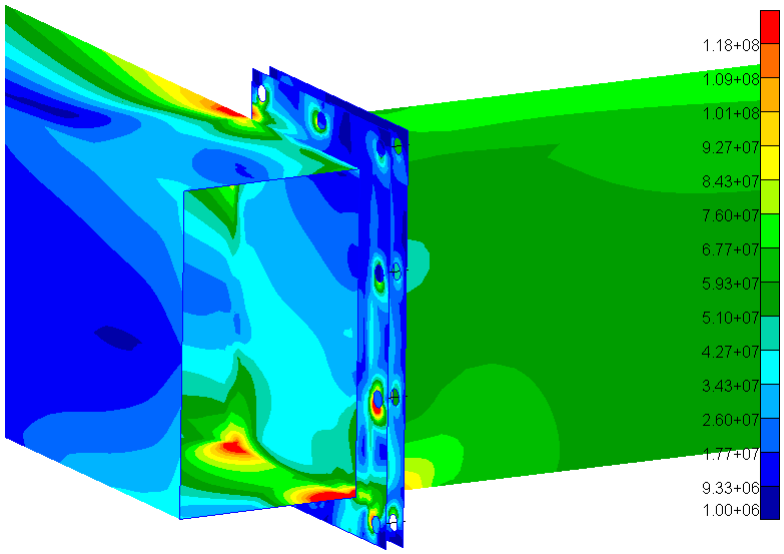

Figure 5.19: Detail of the analysis reporting von Mises stress in pascal

In Fig. 5.20, the von Mises stresses on flanges can be seen. Near some holes and welded connections there are highly stressed regions, the red ones. These parts shall be verified through screws and flange verifications and design resistance of a fillet weld, respectively. In addition, changes anticipated in Sec. 5.8, which will be presented in detail in Sec. 5.10, lead to improvements in the behaviour of the flanges.

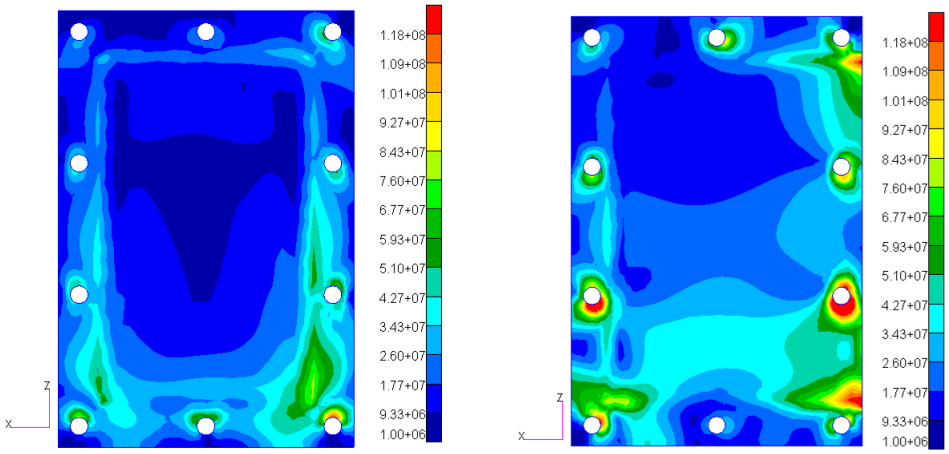

(a) Flange with thickness $t = 16mm$ **(b)** Flange with thickness $t = 12mm$

Figure 5.20: Von Mises stresses expressed in pascal on flanges

5.10 Design changes

After having seen the critical points of the structure, in this section, some solutions are proposed and studied, and the updated structure is presented.
Firstly, the problem of the highly stressed regions on the beam reported in Fig. 5.19 is analyzed. In order to counteract the torsion of this beam, a plate can be welded to both beams, as illustrated in Fig. 5.21. The plate middle plane forms an angle of 45° with both beams and it transfers part of the stress from the beam with axis align to the Y-axis to the other one, unloading the flange. This is not an applicable solution because in this way beams are permanently connected and the advantage of having a modular trolley is lost.

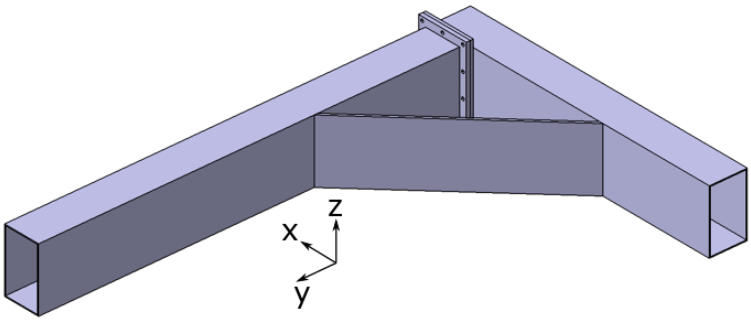

Figure 5.21: Plate welded to both beams

The second studied solution, reported in Fig. 5.22, consists of prolonging, in X negative direction, the flange plate welded to the beam with axis aligned to the X-axis of the global reference frame. The positions of the holes have not changed. Thanks to this method, two of the three red regions are less stressed, but the area at the end section is still critical.

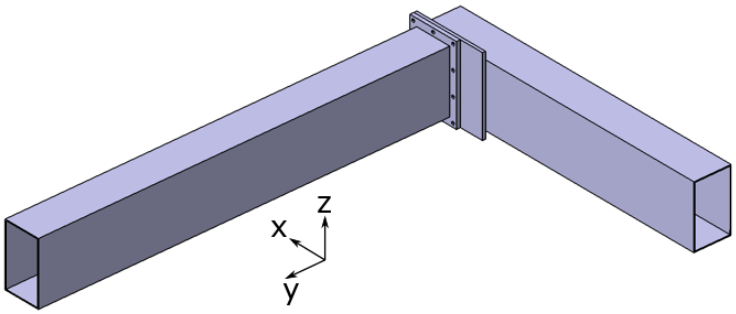

Figure 5.22: Prolonged flange

Finally, the adopted solution consists of two plates that can be welded inside this beam. They have the same section of the beam and are placed perpendicularly to the beam axis. One plate is placed near the end section of the beam and the other is near to the edge of the flange, where the most stressed regions are. This is done in order to reduce the deformations of the section induced by torsional moment and to distribute the stress on larger regions.
These two strengthening plates have dimensions slightly lower than the beam inner section to avoid interference, in particular, they are 142 x 242 mm. The plate close to the edge of the flange cannot be too far away from the end section of the beam, because it must be

reached to be welded. In addition, a circular hole of diameter $D_{hole} = 100mm$ is done in the center of both plates. This hole allows the welder to put an object that keeps the plate in place before the welding and to clean the beam from weld waste. Different combinations of thicknesses and positions of these plates had been tried. A plate is placed at $10mm$ from the end section, while the other is welded at $10mm$ from the flange edge, so at $200mm$ from the end section of the beam, as can be seen in Fig. 5.23. The selected thickness is $8mm$. The final design of the plates is illustrated in Fig. 5.23.

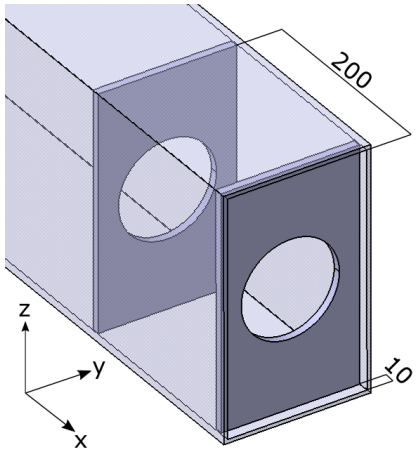

Figure 5.23: Strengthening plates in the beam, with distances from the end section expressed in millimeters

The other critical point of the analysis on the initial structure concerns screws and flanges which do not meet their verifications. This problem and some solutions had been introduced in Sec. 5.8, while, in this section, the details of the chosen changes are reported. Materials of flanges and screws, such as the number of screws, are still the same. The new screw metric is M16. The washer for M16 has the following relevant dimensions, represented in Fig. 3.5:

$$\begin{cases} d_1 = 17mm \\ d_2 = 28mm \\ h = 2.5mm \end{cases} \tag{5.9}$$

The distance between the center hole and plate edge must be raised, due to the increased diameters of the screws, so c augments from $15mm$ to $20mm$. These changes lead to an increase in flanges sizes, in particular:

$$\begin{cases} B_{flange} = 230mm \\ H_{flange} = 330mm \end{cases} \tag{5.10}$$

Finally, the thickness of the thicker flange is increased from $16mm$ to $20mm$, in order to raise the margins of safety for bearing and shear tear out.
The remaining parts have not changed.

5.11 Analysis of the improved structure

At this point, the FE model is updated to account for the newly designed geometry, described in Sec. 5.10.
In Fig. 5.24, the model summary of the carried-out analysis is reported.
The mesh seed on all the edges of the plates is 10 mm and the global edge length is equal to 5 mm.

M O D E L S U M M A R Y

ENTRY NAME	NUMBER OF ENTRIES
CBAR	10
CQUAD4	31169
CTRIA3	392
FORCE	3
GRID	32106
LOAD	1
MAT1	2
MDLPRM	1
MOMENT	1
PARAM	2
PBAR	1
PSHELL	5
RBE2	373
SPC1	2
SPCADD	1

Figure 5.24: Model summary

5.11.1 Checks on FE model

In this section, the checks on the finite element model are shown.
First of all, in Fig. 5.25 and Fig. 5.26 can be seen that there is no element distortion, neither tria nor quad.

Test	Number Failed	Worst Case	At Element
Aspect	0	Max=4.1049304	15901
Skew	0	Min=16.01829	15901

Figure 5.25: Tria verification summary

Test	Total Failed	Worst Case	At Element
Aspect	0	Max=3.0331461	15403
Warp	0	Max=2.7690126E-07	6205
Skew	0	Min=40.244663	15296
Taper	0	Max=0.49928522	965

Figure 5.26: Quad verification summary

Boundaries, duplicates, normals and node equivalencing have been controlled for each group of the analysis.

The output of the Nastran "Grid Point Weight Generator", in Fig. 5.27, has been used to check the mass of the model. The GPWG calculates masses, centers of gravity and inertias of the mathematical model of the structure. It is divided into six discrete sections. The MO matrix represents the rigid body mass properties of the structure, the first 3x3 matrix contains the directional masses of the system on the principal diagonal [15]. The S matrix is a transformation matrix from the principle mass axes to the basic direction.

Principle mass axes are axes that have no coupling between the translational mass components. For real structures there is no coupling in the translational mass terms in the inertia matrix, so the S matrix must be the identity matrix. The third section is the one reporting the center of gravity relative to the reference point in the principal mass axes system. The $I(S)$ matrix is the inertia matrix of the system about the CoG [12]. The $I(Q)$ matrix contains the principal moments of inertia, so, by definition, it has not extra diagonal terms. Q is the transformation matrix relating the system moments of inertia about the CoG to the principal moments of inertia.
A finite element model may have directional mass properties, that is, the mass may differ in each of the three coordinate directions. This is not the case, so mass values shall be the same for axes X, Y and Z, and the center of gravity shall be unique.
On FE model mass has been increased by a maturity margin of 10%. In Table 5.4, masses of FEM and CAD are compared.

```
      O U T P U T   F R O M   G R I D   P O I N T   W E I G H T   G E N E R A T O R
                                  REFERENCE POINT =        0
                                            M O
*  1.006674E+02  0.000000E+00  0.000000E+00  0.000000E+00  3.810687E-09 -3.252337E+01 *
*  0.000000E+00  1.006674E+02  0.000000E+00 -3.810687E-09  0.000000E+00 -1.749971E+01 *
*  0.000000E+00  0.000000E+00  1.006674E+02  3.252337E+01  1.749971E+01  0.000000E+00 *
*  0.000000E+00 -3.810687E-09  3.252337E+01  4.203159E+01 -1.872469E+00 -8.198590E-07 *
*  3.810687E-09  0.000000E+00  1.749971E+01 -1.872469E+00  1.449728E+01  6.491494E-07 *
* -3.252337E+01 -1.749971E+01  0.000000E+00 -8.198590E-07  6.491494E-07  5.479008E+01 *
                                            S
                    *  1.000000E+00  0.000000E+00  0.000000E+00 *
                    *  0.000000E+00  1.000000E+00  0.000000E+00 *
                    *  0.000000E+00  0.000000E+00  1.000000E+00 *
          DIRECTION
    MASS AXIS SYSTEM (S)      MASS              X-C.G.        Y-C.G.        Z-C.G.
            X              1.006674E+02      0.000000E+00  3.230773E-01  3.785421E-11
            Y              1.006674E+02     -1.738368E-01  0.000000E+00  3.785421E-11
            Z              1.006674E+02     -1.738368E-01  3.230773E-01  0.000000E+00
                                            I(S)
                    *  3.152402E+01  7.526227E+00  8.205214E-07 *
                    *  7.526227E+00  1.145518E+01 -6.503806E-07 *
                    *  8.205214E-07 -6.503806E-07  4.124042E+01 *
                                            I(Q)
                    *  3.403287E+01                             *
                    *                8.946330E+00               *
                    *                             4.124042E+01 *
                                            Q
                    *  9.486791E-01  3.162402E-01  0.000000E+00 *
                    * -3.162402E-01  9.486791E-01  0.000000E+00 *
                    *  0.000000E+00  0.000000E+00  1.000000E+00 *
```

Figure 5.27: Mass property check

Source	Mass $[kg]$
CAD	92.1
FEM	100.7

Table 5.4: Comparison between CAD and FEM masses

The multi-level strain energy check procedure allows detecting modeling errors. Computations are performed at various set levels: G-set, N-set, F-set and A-set. At each level, a matrix is computed. These checks can be useful for determining both the location and the cause of errors. The results in Fig. 5.28 demonstrate that constraints prevent rigid-body motion, so the model is properly constrained to ground.

*** USER INFORMATION MESSAGE 7570 (GPWG1S)
RESULTS OF RIGID BODY CHECKS OF MATRIX KGG (G-SET) FOLLOW:
PRINT RESULTS IN ALL SIX DIRECTIONS AGAINST THE LIMIT OF 1.699010E+00

DIRECTION	STRAIN ENERGY	PASS/FAIL
1	7.016957E-05	PASS
2	6.918889E-05	PASS
3	3.090852E-04	PASS
4	2.602701E-04	PASS
5	2.960015E-05	PASS
6	1.366951E-06	PASS

*** USER INFORMATION MESSAGE 7570 (GPWG1S)
RESULTS OF RIGID BODY CHECKS OF MATRIX KNN (N-SET) FOLLOW:
PRINT RESULTS IN ALL SIX DIRECTIONS AGAINST THE LIMIT OF 7.951998E+00

DIRECTION	STRAIN ENERGY	PASS/FAIL
1	6.982498E-05	PASS
2	8.030701E-05	PASS
3	3.035534E-04	PASS
4	2.628245E-04	PASS
5	2.861740E-05	PASS
6	6.410638E-07	PASS

*** USER INFORMATION MESSAGE 7570 (GPWG1S)
RESULTS OF RIGID BODY CHECKS OF MATRIX KFF (F-SET) FOLLOW:
PRINT RESULTS IN ALL SIX DIRECTIONS AGAINST THE LIMIT OF 7.951998E+00

DIRECTION	STRAIN ENERGY	PASS/FAIL
1	3.389014E+10	FAIL
2	2.362378E+10	FAIL
3	8.872704E+09	FAIL
4	3.674454E+08	FAIL
5	1.182392E+10	FAIL
6	9.266159E+09	FAIL

*** USER INFORMATION MESSAGE 7570 (GPWG1S)
RESULTS OF RIGID BODY CHECKS OF MATRIX KAA1 (A-SET) FOLLOW:
PRINT RESULTS IN ALL SIX DIRECTIONS AGAINST THE LIMIT OF 7.951998E+00

DIRECTION	STRAIN ENERGY	PASS/FAIL
1	3.389014E+10	FAIL
2	2.362378E+10	FAIL
3	8.872704E+09	FAIL
4	3.674454E+08	FAIL
5	1.182392E+10	FAIL
6	9.266159E+09	FAIL

Figure 5.28: Strain energy model check

As can be seen in Fig. 5.29, SPCFORCE resultant is equal in modulus and opposite to OLOAD resultant. T1, T2 and T3 are the translations along X, Y and Z axes, and R1, R2 and R3 are the rotations around these axes of the reference system.

OLOAD RESULTANT

SUBCASE/ DAREA ID	LOAD TYPE	T1	T2	T3	R1	R2	R3
1	FX	-5.272878E+03	----	----	----	-4.837069E+03	8.752977E+03
	FY	----	0.000000E+00	----	0.000000E+00	----	0.000000E+00
	FZ	----	----	-8.665504E+03	-1.412314E+04	-5.067588E-06	----
	MX	----	----	----	0.000000E+00	----	----
	MY	----	----	----	----	-4.659750E+03	----
	MZ	----	----	----	----	----	0.000000E+00
	TOTALS	-5.272878E+03	0.000000E+00	-8.665504E+03	-1.412314E+04	-9.496819E+03	8.752977E+03

SPCFORCE RESULTANT

SUBCASE/ DAREA ID	LOAD TYPE	T1	T2	T3	R1	R2	R3
1	FX	5.272878E+03	----	----	----	-4.236381E+02	2.052386E+03
	FY	----	-3.520017E-08	----	1.297698E+03	----	-5.103750E+03
	FZ	----	----	8.665504E+03	4.738689E+02	9.922002E+03	----
	MX	----	----	----	1.235157E+04	----	----
	MY	----	----	----	----	-1.545153E+00	----
	MZ	----	----	----	----	----	-5.701613E+03
	TOTALS	5.272878E+03	-3.520017E-08	8.665504E+03	1.412314E+04	9.496819E+03	-8.752977E+03

Figure 5.29: OLOAD and SPCFORCE resultants

The value of epsilon reported in Fig. 5.30 is lower than 10^{-8} so the problem is numerically stable.

LOAD SEQ. NO.	EPSILON	EXTERNAL WORK
1	-1.4975927E-12	5.9429310E+01

Figure 5.30: Epsilon check

5.11.2 Resistance analysis of a fillet weld

In this section, the analysis of the weldings is done. A coordinate system is defined for each fillet weld, in such a way that its axes are aligned with the stresses $\sigma_{\perp}$, $\tau_{\parallel}$ and $\tau_{\perp}$. Each fillet weld is characterized by the letter C followed by a number and each coordinate system is characterized by CID followed by a number.
In all the fillet welds that are going to be verified, the side z of the isosceles triangle in Fig. 5.31, is $5mm$ and α is 90°, as a consequence, the effective throat thickness a is equal to $3.5mm$.

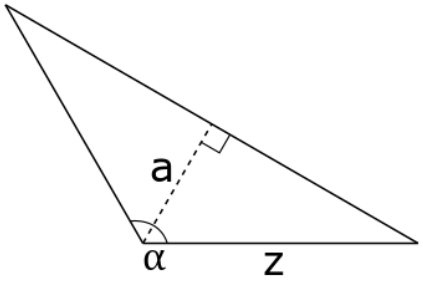

Figure 5.31: Relevant characteristics of a fillet weld

The first analyzed welding is the one that connects the flange to the beam with the axis aligned to the Y-axis. These are four fillet welds of T joints. Fillet welds, coordinate systems and stresses of this welding are reported in Fig. 5.32.
The second welding to be analyzed is the one between the thinner flange and the beam with axis aligned to the X-axis. Fillet welds and reference systems are reported in Fig. 5.33. In this case, the joints of fillet welds C5 and C6 are T joints, while the ones of C7 and C8 are lap joints, but this does not change the verification method. The coordinate systems are the same as the previous welding because the fillet welds are oriented in the same directions. The global reference frame is reported in pink in these figures.
In Table 5.5, the relevant values of the verifications of the first two weldings are reported. Each fillet weld is associated to its length and coordinate systems, then forces and stresses in the three principal directions are written, and finally, the values of the success criteria, explained in Eq. (5.5), can be found.

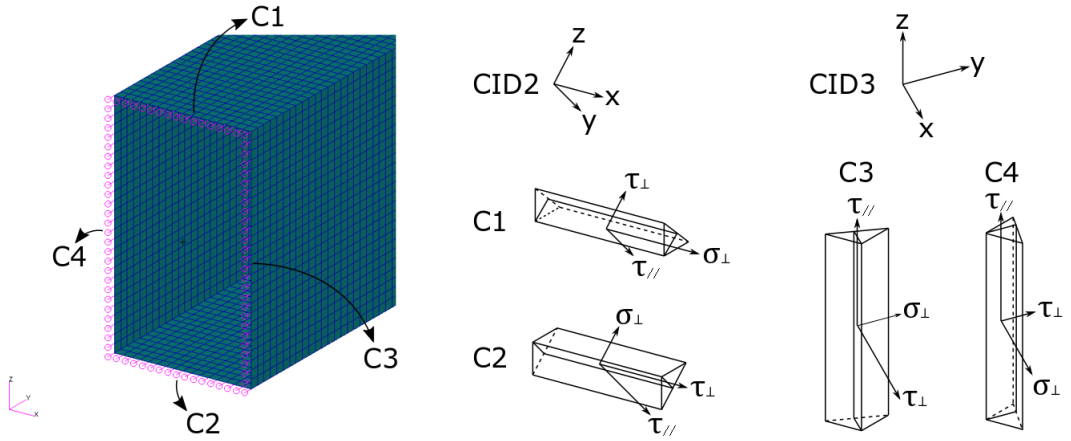

(a) Four fillet welds done with MPCs

(b) CIDs and scheme of fillet welds and stresses on their throat section

Figure 5.32: Fillet welds and coordinate systems of the welding between the thicker flange and beam with axis aligned to Y-axis

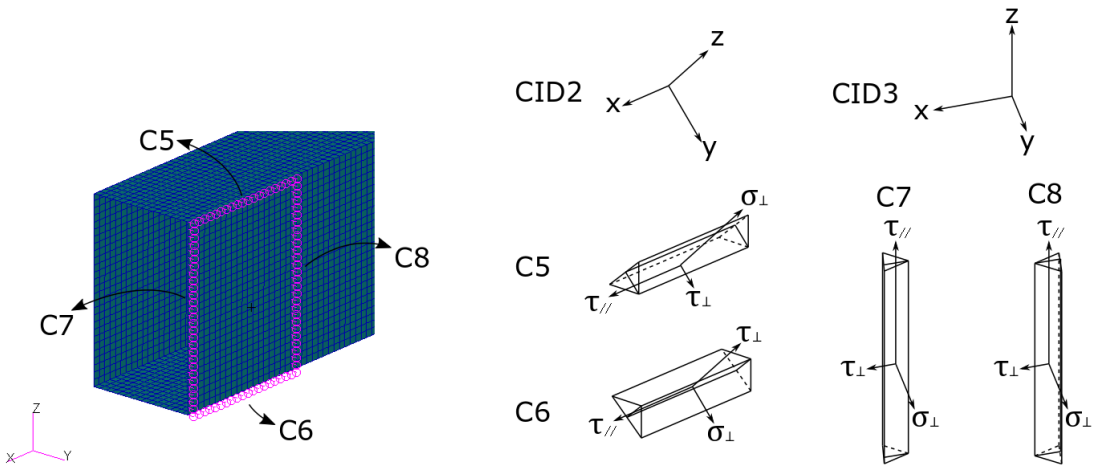

(a) Four fillet welds done with MPCs

(b) CIDs and scheme of fillet welds and stresses on their throat section

Figure 5.33: Fillet welds and coordinate systems of the welding between the thinner flange and beam with axis aligned to X-axis

Table 5.5: Verification results of fillet welds from C1 to C8

Fillet weld	$l\,[mm]$	Coord ID	Forces $[N]$	Stresses $[MPa]$	Success criteria $[MPa]$
C1	146	CID 2	$F_{\sigma_\perp} = 1700$ $F_{\tau_\parallel} = 1470$ $F_{\tau_\perp} = 1790$	$\sigma_\perp = 3.5$ $\tau_\parallel = 4.5$ $\tau_\perp = 5.5$	$12.7 \leq 453.3$ $3.5 \leq 367.2$
C2	146	CID 2	$F_{\sigma_\perp} = 3360$ $F_{\tau_\parallel} = 1240$ $F_{\tau_\perp} = 1080$	$\sigma_\perp = 6.8$ $\tau_\parallel = 3.8$ $\tau_\perp = 3.3$	$11.1 \leq 453.3$ $6.8 \leq 367.2$
C3	246	CID 3	$F_{\sigma_\perp} = 947$ $F_{\tau_\parallel} = 1170$ $F_{\tau_\perp} = 771$	$\sigma_\perp = 1.1$ $\tau_\parallel = 2.1$ $\tau_\perp = 1.4$	$4.5 \leq 453.3$ $1.1 \leq 367.2$
C4	246	CID 3	$F_{\sigma_\perp} = 1230$ $F_{\tau_\parallel} = 1480$ $F_{\tau_\perp} = 1170$	$\sigma_\perp = 1.5$ $\tau_\parallel = 2.6$ $\tau_\perp = 2.1$	$6.0 \leq 453.3$ $1.5 \leq 367.2$
C5	286	CID 2	$F_{\sigma_\perp} = 3140$ $F_{\tau_\parallel} = 2680$ $F_{\tau_\perp} = 1370$	$\sigma_\perp = 3.2$ $\tau_\parallel = 4.1$ $\tau_\perp = 2.1$	$8.5 \leq 453.3$ $3.2 \leq 367.2$
C6	286	CID 2	$F_{\sigma_\perp} = 1260$ $F_{\tau_\parallel} = 1350$ $F_{\tau_\perp} = 1240$	$\sigma_\perp = 1.3$ $\tau_\parallel = 2.1$ $\tau_\perp = 1.9$	$5.0 \leq 453.3$ $1.3 \leq 367.2$
C7	246	CID 3	$F_{\sigma_\perp} = 800$ $F_{\tau_\parallel} = 1020$ $F_{\tau_\perp} = 269$	$\sigma_\perp = 0.9$ $\tau_\parallel = 1.8$ $\tau_\perp = 0.5$	$3.4 \leq 453.3$ $0.9 \leq 367.2$
C8	246	CID 3	$F_{\sigma_\perp} = 1810$ $F_{\tau_\parallel} = 969$ $F_{\tau_\perp} = 969$	$\sigma_\perp = 2.1$ $\tau_\parallel = 1.7$ $\tau_\perp = 1.7$	$4.7 \leq 453.3$ $2.1 \leq 367.2$

At this point, the design resistance of the filled welds of the strengthening plates is done. The eight fillet welds from C9 to C16 and their coordinate systems are reported in Fig. 5.34. The weldings of the plates are all tee joints. The stresses of vertical fillet welds are oriented as CID3, one of the coordinate systems used in the previous weldings, while horizontal filled welds have the new reference frame CID4 for stresses. The results of success criteria and relevant values of these weldings can be found in Table 5.6.

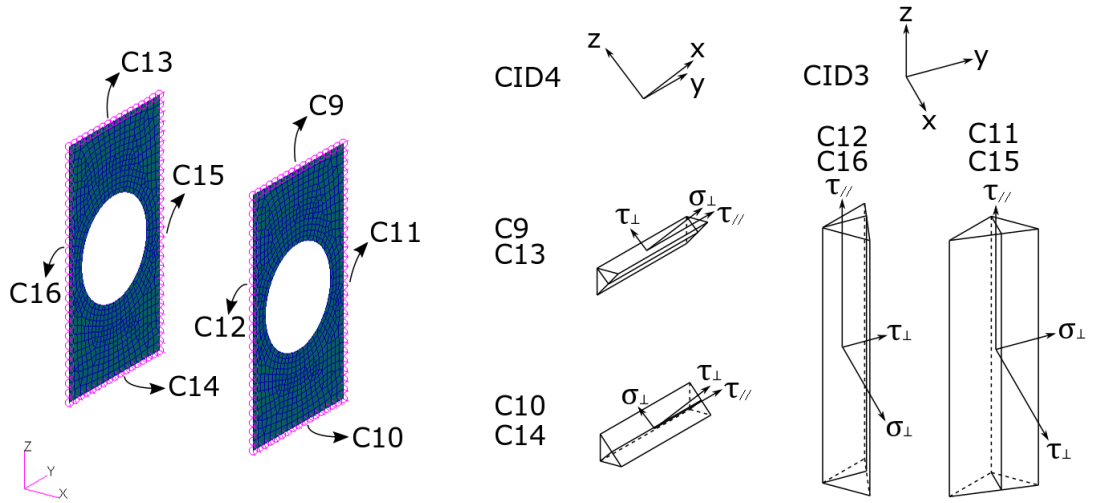

(a) Eight fillet welds done with MPCs

(b) CIDs and scheme of fillet welds and stresses on their throat section

Figure 5.34: Fillet welds and coordinate systems of the welding between the plates and beam with axis aligned to X-axis

Table 5.6: Verification results of fillet welds from C9 to C16

Fillet weld	$l\,[mm]$	Coord ID	Forces $[N]$	Stresses $[MPa]$	Success criteria $[MPa]$
C9	142	CID 4	$F_{\sigma_\perp} = 917$ $F_{\tau_\parallel} = 1670$ $F_{\tau_\perp} = 339$	$\sigma_\perp = 1.9$ $\tau_\parallel = 5.3$ $\tau_\perp = 1.1$	$9.5 \leq 453.3$ $1.9 \leq 367.2$
C10	142	CID 4	$F_{\sigma_\perp} = 378$ $F_{\tau_\parallel} = 895$ $F_{\tau_\perp} = 318$	$\sigma_\perp = 0.8$ $\tau_\parallel = 2.8$ $\tau_\perp = 1.0$	$5.2 \leq 453.3$ $0.8 \leq 367.2$
C11	242	CID 3	$F_{\sigma_\perp} = 471$ $F_{\tau_\parallel} = 1240$ $F_{\tau_\perp} = 428$	$\sigma_\perp = 0.6$ $\tau_\parallel = 2.2$ $\tau_\perp = 0.8$	$4.1 \leq 453.3$ $0.6 \leq 367.2$
C12	242	CID 3	$F_{\sigma_\perp} = 90$ $F_{\tau_\parallel} = 1480$ $F_{\tau_\perp} = 174$	$\sigma_\perp = 0.1$ $\tau_\parallel = 2.7$ $\tau_\perp = 0.3$	$4.7 \leq 453.3$ $0.1 \leq 367.2$
C13	142	CID 4	$F_{\sigma_\perp} = 399$ $F_{\tau_\parallel} = 272$ $F_{\tau_\perp} = 252$	$\sigma_\perp = 0.8$ $\tau_\parallel = 0.9$ $\tau_\perp = 0.8$	$2.2 \leq 453.3$ $0.8 \leq 367.2$
C14	142	CID 4	$F_{\sigma_\perp} = 650$ $F_{\tau_\parallel} = 670$ $F_{\tau_\perp} = 146$	$\sigma_\perp = 1.4$ $\tau_\parallel = 2.1$ $\tau_\perp = 0.5$	$4.0 \leq 453.3$ $1.4 \leq 367.2$
C15	242	CID 3	$F_{\sigma_\perp} = 582$ $F_{\tau_\parallel} = 921$ $F_{\tau_\perp} = 420$	$\sigma_\perp = 0.7$ $\tau_\parallel = 1.7$ $\tau_\perp = 0.8$	$3.2 \leq 453.3$ $0.7 \leq 367.2$
C16	242	CID 3	$F_{\sigma_\perp} = 150$ $F_{\tau_\parallel} = 816$ $F_{\tau_\perp} = 104$	$\sigma_\perp = 0.2$ $\tau_\parallel = 1.5$ $\tau_\perp = 0.2$	$2.6 \leq 453.3$ $0.2 \leq 367.2$

5.11.3 Screws and flange verifications

The changes explained in Sec. 5.9 and Sec. 5.11 lead to the results in Table 5.7. Screws maintain their integrity and there is no pull-out. Shear tear out and bearing are verified. Finally, there is no joint separation and also, no sliding because, even if a few margins of safety are negative, the global sliding is 7.69. In this updated structure, the new Flange B and its screws are verified.

Table 5.7: Final results of verifications on Flange B

			Tension	SV Screw		Pull Out		Joint sep.	Sliding	Shear tear out		Bearing
# Screw ID	V [N]	P [N]	$\sigma_{id}\,[MPa]$	SV_u	SV_y	MS_{po_s}	MS_{po_f}	MS_{js}	MS_{sl}	MS_{u_sto}	MS_{y_sto}	MS_b
15909	2793	4907	857	0.48	0.36	1.12	0.24	7.78	1.92	9.77	9.00	3.92
15910	7271	4082	865	0.45	0.35	1.13	0.25	9.55	0.15	3.14	2.84	0.89
15911	8465	-3162	868	0.86	0.86	1.14	0.25	FALSE	0.17	2.55	2.30	0.62
15912	6287	3765	862	0.46	0.35	1.13	0.25	10.44	0.34	3.78	3.44	1.19
15913	10767	-3892	877	0.81	0.83	1.13	0.25	FALSE	-0.07	1.79	1.59	0.28
15914	9439	3602	871	0.42	0.33	1.13	0.25	10.95	-0.11	2.19	1.96	0.46
15915	12908	-6128	888	0.74	0.79	1.11	0.24	FALSE	-0.19	1.33	1.16	0.07
15916	4817	1727	857	0.48	0.37	1.15	0.26	23.93	0.83	5.25	4.80	1.85
15917	8271	-2518	866	0.86	0.86	1.14	0.25	FALSE	0.18	2.64	2.38	0.66
15918	4431	-6841	861	0.90	0.88	1.11	0.23	FALSE	1.41	5.79	5.30	2.10

5.11.4 Stress analysis

In this section, the stresses on the final configuration are exposed. As written in Sec. 5.9, the stress is calculated using von Mises criterion and fringe and range are the same as the previous analysis.
In Fig. 5.35, the stress analysis of the structure is reported and the scale factor for deformations is 0.1. The integration of the two plates has strengthened the beam with the axis aligned to the X-axis because they help to counteract the torsion on the beam. A detail of this end section is reported in Fig. 5.36, without the plates to see the inner part of the beam. The red regions, present in Fig. 5.19, are not so stressed now. The addition of the two plates has distributed the stresses, avoiding concentrations. In Fig. 5.37, a detail of these plates is reported. The most stressed area is the one around holes, but the yield and ultimate margins of safety are positive, in particular:

$$\begin{cases} MoS_y = 1.49 \cdot 10^{-1} \\ MoS_u = 2.38 \cdot 10^{-1} \end{cases} \tag{5.11}$$

The flanges are reported in Fig. 5.38. The plates have improved also the results on the thinner flange, in fact, the most stressed point is on a hole and it was verified through screws and flanges verification in Sec. 5.11.3.
There is still a small part around a node of the beam very stressed, as can be seen in Fig. 5.39. The margins of safety are:

$$\begin{cases} MoS_y = -6.82 \cdot 10^{-2} \\ MoS_u = 3.94 \cdot 10^{-3} \end{cases} \tag{5.12}$$

The yield margin of safety is negative, but the exceeding magnitude is very small, as also the red area. In addition, this region is an edge on which an MPC is connected. The multi-point constraints, as explained in Sec. 5.4, are infinitely rigid links, so they are useful to

model certain connections, but they do not describe a real situation, so their use may cause unrealistic stress concentrations. This is demonstrated by the welding verification. Remember that it is done on the higher stress on the MPCs composing the fillet weld. The results are written in Table 5.5, in particular, the fillet weld including the MPC under consideration is C5 and its stress is much lower than the one on the beam ($1.27 \cdot 10^8 Pa$). Taking into account these reasons, in the first part of the analysis, it does not worth adding material to solve a calculation error.

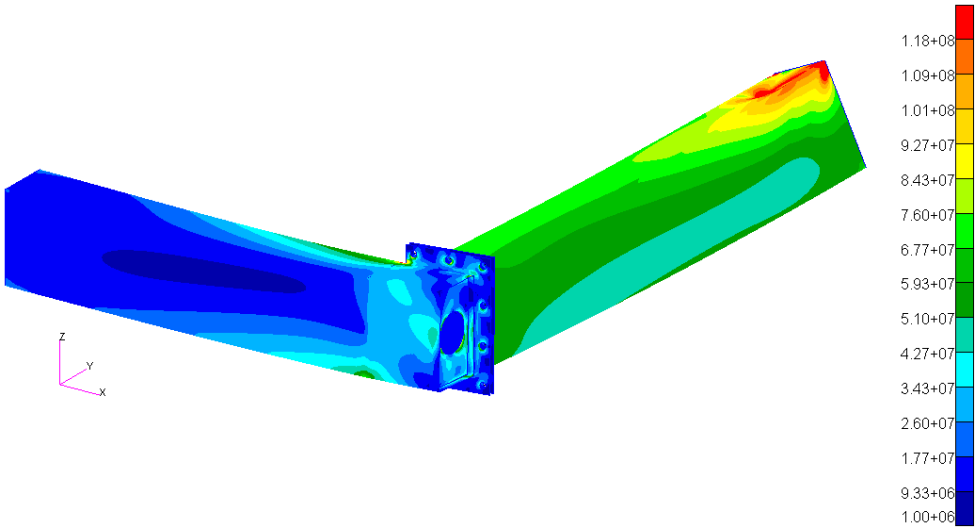

Figure 5.35: Results of the updated structural analysis reporting deformation and von Mises stress in pascal

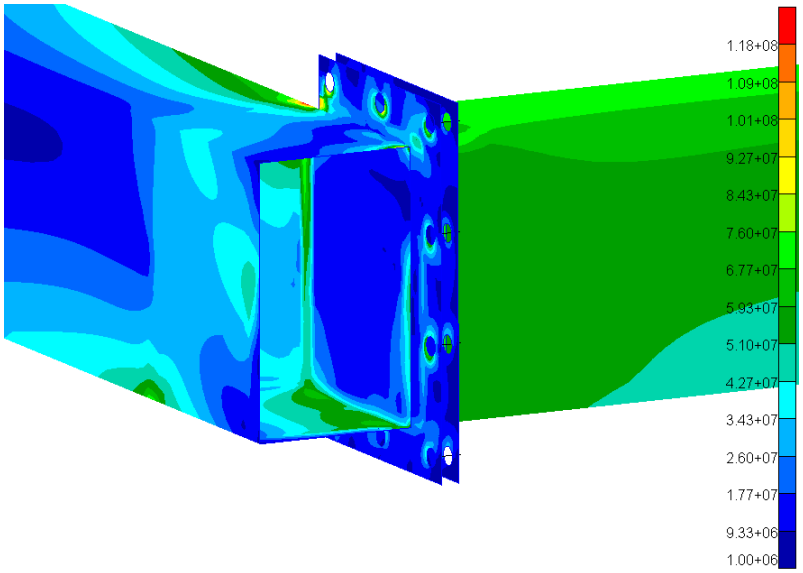

Figure 5.36: Detail of the analysis on the corner of the structure, reporting von Mises stress in pascal. The strengthening plates have been erased to see the internal part of the beam

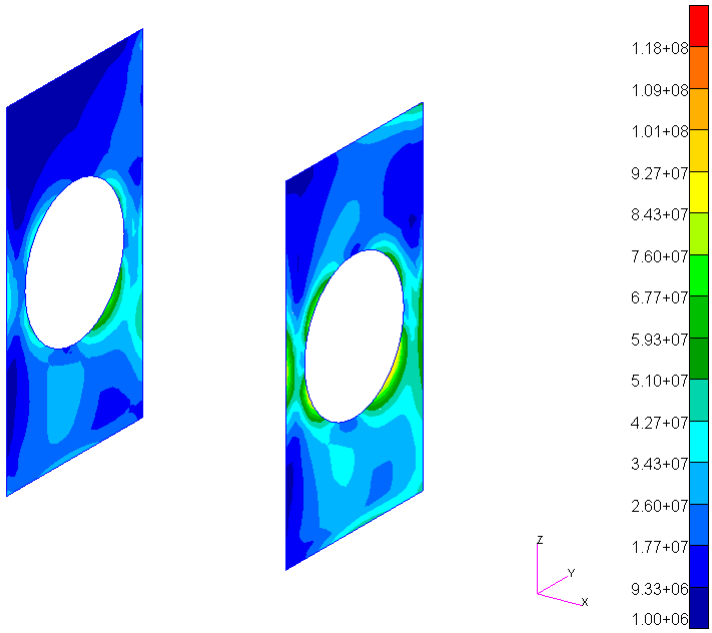

Figure 5.37: Von Mises stress expressed in pascal on the two strengthening plates

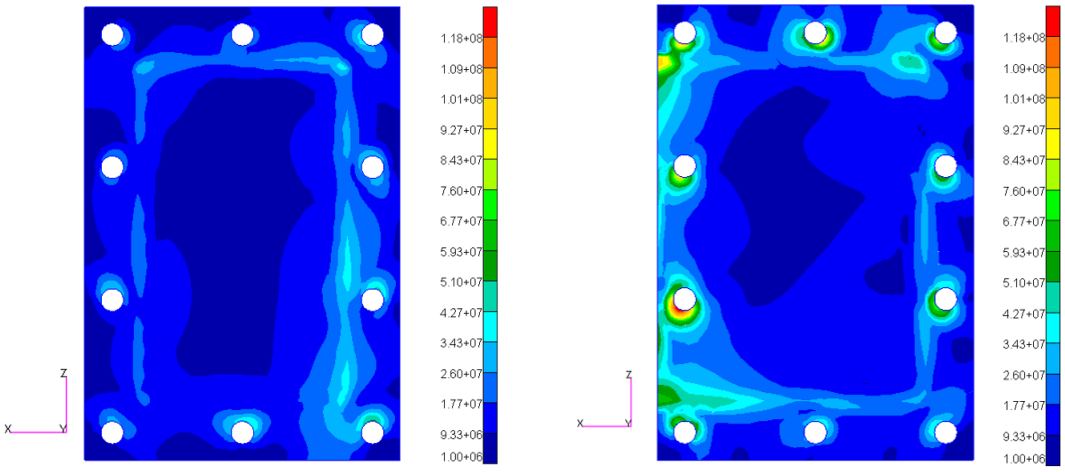

(a) Flange with thickness $t = 20mm$ **(b)** Flange with thickness $t = 12mm$

Figure 5.38: Von Mises stresses expressed in pascal on updated flanges

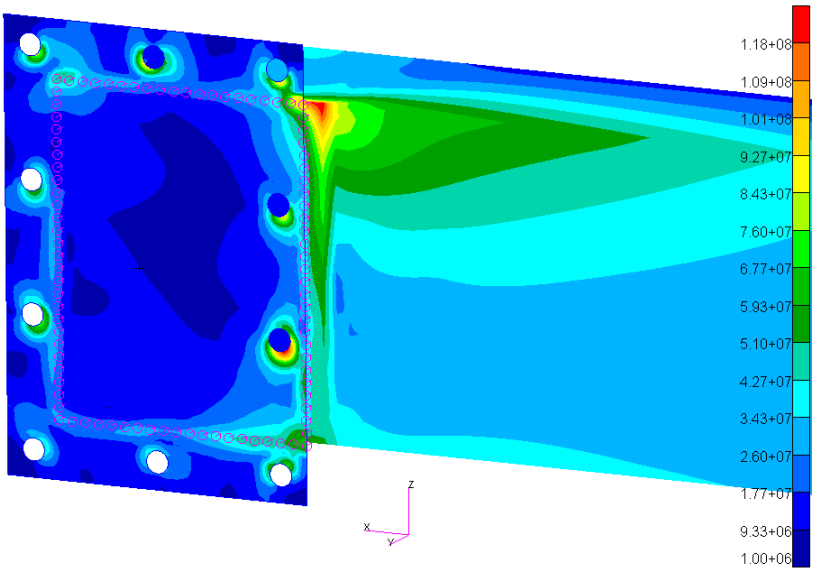

Figure 5.39: Detail of the beam with axis aligned to X-axis, reporting von Mises stress in pascal

After the study of this critical part of the main frame, the updated trolley is illustrated in Fig. 5.40. It is reported only the trolley with Bridge 3 because all the changes are done on the main frame, so the rotation frames have not been modified. All the open end sections of the beams must be closed with plastic removable covers, in blue in figure, to avoid entering of dust, in order to accomplish with a cleanliness requirement.

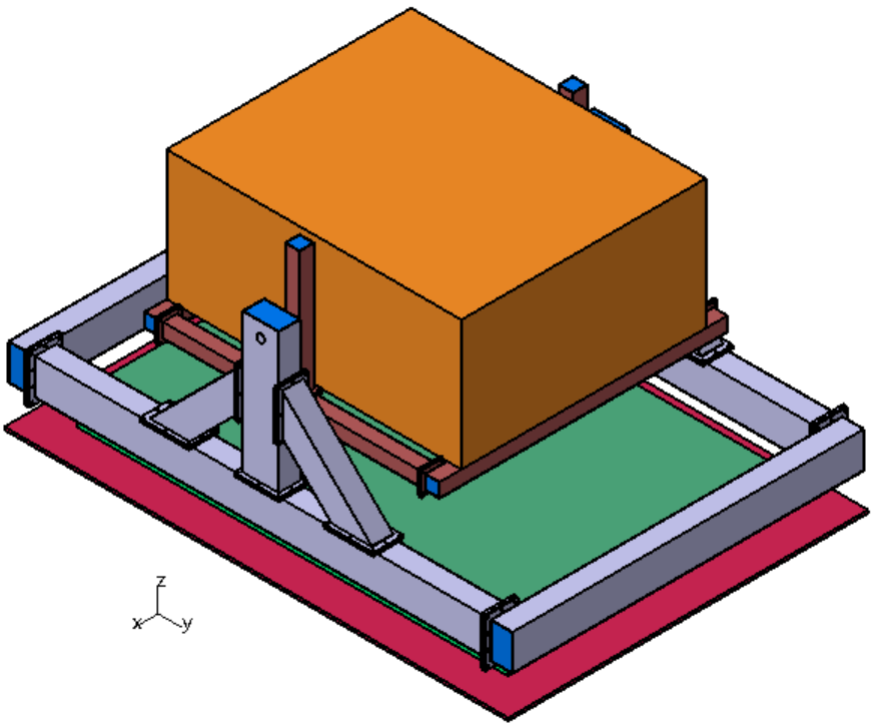

Figure 5.40: Updated trolley with Bridge 3

Chapter 6

Conclusion

In the present thesis, the design of a multipurpose modular trolley of an MGSE for spatial application has been presented.
In the second chapter different configurations of the main frame of the trolley have been discussed and the beams of the selected one have been sized.
In the third chapter, screw verifications, based on *Criteria for preloaded bolts* (NASA), are explained together with flanges verifications, and their preliminary sizing on the main frame has been done. This sizing is the first step toward a more detailed design phase based on finite element simulations.
Subsequently, three types of rotating frames, each one presenting special features to better suit customers' needs, have been dimensioned. In this case, screws, flanges and also shafts have been sized. All the main components of the trolley are linked via flange couplings made by screws, which are removable connections. The advantage of a modular trolley is that, based on the same initial structure, several trolleys of different sizes can be realized in order to support various payloads of disparate dimensions and masses and to satisfy different requirements of the encumbrance of the trolleys.
In the last part of this thesis, starting from the CAD model, the structural analysis of the corner of the main frame has been done. The FEA allows to notice critical points and to improve the structure, in fact, the design has been changed and the trolley has been strengthened where it was stressed the most. In particular, there were concentrations of stresses in some screws and parts of the flanges, so some features needed to be changed. It has been noted that the addition, into the internal part of a beam, of thin plates with section perpendicular to the axis of the beam, helps to counteract torsion, as well as strengthening the beam.

A possible extension of this work is the addition of elements that permit to sustain, stabilize, move and lift the trolley, such as castor wheels, adjustable jacks, hoisting points, handles and forklift interface.
The rotating frame needs further components like the interface with the payload and balancing masses. Another part that has to be developed is the rotation mechanism, that has the aim of rotating the bridge, and so the payload, about Y-axis. The main components of this mechanism shall be a shaft, that has been sized in Sec. 4.4, a bearing, that allows the rotation of the shaft around its axis and keeps it in position, a gearbox, that couples the rotations of the bridge to the rotations of the last main component, the crank handle, which ensures a manually driven and continuous rotation.
As said in Sec. 5.9, the analysis done in this thesis aims to study the corner of the main frame, especially the connection between the beams, so the behavior of regions far from

it is not taken into account and meaningful. As a consequence, it is necessary to do a structural analysis also in other critical parts of the trolley and, at the end of the design, of the entire trolley, in order to demonstrate that all the structural checks are verified.

Bibliography

[1] *E. F. Bruhn, Analysis and design of flight vehicles structures, 1973*

[2] *M. Cannarozzi, A. M. Tarantino, Meccanica dei materiali e delle strutture: lucidi delle lezioni Vol 1, 2002*

[3] *CEN Technical Committee 250 "Structural Eurocodes", European Standard EN 1993, Eurocode 3: Design of steel structures, 2005*

[4] *E. Cueto, D. Gonzalez, An introduction to structural mechanics for architects, 2018*

[5] *E. Chirone, S. Tornincasa, Disegno tecnico industriale Vol.2, 2000*

[6] *L. Corradi dell'Acqua, Meccanica delle strutture: il comportamento dei mezzi continui, 1992*

[7] *EADS Astrium, Generic System MGSE Specification, 2009*

[8] *Endurasim, The concise guide to Nastran rigid elements, 2008*

[9] *A. Harish, What is convergence in Finite Element Analysis?, 2020*

[10] *MSC Software Corporation, MSC.Nastran 2001, Getting Started with MSC.Nastran User's Guide, 2001*

[11] *MSC Software Corporation, Patran 2008 r1, Reference Manual Part 3: Finite Element Modeling, 2018*

[12] *NASA, The Nastran theoretical manual (Level 16.0), 1976*

[13] *NASA, Criteria for preloaded bolts (NSTS 08307), 1998*

[14] *Robert D. Cook, Finite element modeling for stress analysis, 1995*

[15] *Siemens, NX Nastran User's Guide, 2014*

[16] *A. E. Stockwell, A Verification Procedure for MSC/NASTRAN Finite Element Models, 1995*

[17] *A. Strozzi, Costruzione di macchine, 1998*

[18] *Tales Alenia Space, Specification for mechanical ground support equipement used for spacecraft AIT activities, 2014*

[19] *R. Vescovini, Lecture notes of the course "Spacecraft Structures", 2018*

Consulted websites

[20] *Autodesk Knowledge Network. Available:* https://knowledge.autodesk.com/support/nastran

[21] *Bigboltnut. Available:* https://www.bigboltnut.com/technical-spec/12.9.pdf

[22] *Concordia University. Available:* https://www.concordia.ca

[23] *Hauge Fastners, Bolting Property Class. Available:* https://www.haguefasteners.co.uk/bolting-property-classes-8-8-10-9-12-9-14-9/

[24] *Inoxmare. Available:* https://www.inoxmare.com/home/1.html

[25] *Jam Building Products, Stainless Steel Material Properties. Available:* http://www.powah.hk/download/technology/Stainless_Steel_Material_Properties.pdf

[26] *Matweb. Available:* http://www.matweb.com/index.aspx

[27] *Metrication. Available:* http://www.metrication.com/engineering/threads.html

[28] *MSC Nastran Beginner. Available:* http://mscnastrannovice.blogspot.com

[29] *Penn Engineering, Four Ways To Tackle Threaded Inserts For Plastics. Available:* https://www.pemnet.com/fastening-products/four-ways-to-tackle-threaded-inserts-for-plastics/

[30] *Schäfer Peters GmbH. Available:* https://www.schaefer-peters.com/uploads/tx_kkdownloader/Technical-Information_S_P_05.pdf

[31] *University of Rochester. Available:* http://www2.me.rochester.edu